UNIVERSITY OF OKLAHOMA

GRADUATE COLLEGE

FERROCENE-MODIFIED LINEAR POLY(ETHYLENIMINE) BIOELECTRODE MATERIALS FOR USE IN GLUCOSE/O_2 BIOFUEL CELLS

A DISSERTATION

SUBMITTED TO THE GRADUATE FACULTY

in partial fulfillment of the requirements for the

Degree of

DOCTOR OF PHILOSOPHY

By

DAVID P. HICKEY
Norman, Oklahoma
2014

FERROCENE-MODIFIED LINEAR POLY(ETHYLENIMINE)
BIOELECTRODE MATERIALS FOR USE IN GLUCOSE/O_2 BIOFUEL CELLS

A DISSERTATION APPROVED FOR THE
DEPARTMENT OF CHEMISTRY AND BIOCHEMISTRY

BY

Dr. Daniel T. Glatzhofer (Chair)

Dr. David W. Schmidtke

Dr. Kenneth M. Nicholas

Dr. Robert H. Cichewicz

Dr. Robert Thomson

Acknowledgements

I would like to take this opportunity to thank everyone that has helped me throughout my academic career. First, I would like to thank my amazing fiancé, **Stephanie**. Her love and support has provided a constant source of inspiration, and has given me the confidence to expand my intellectual horizons. Thanks to my family, **Mom**, **Dad**, **Katie**, **Jack**, **Kevin**, and **Cameron**, for instilling in me an enthusiasm for life, and for teaching me that I can do anything I put my mind to.

I would like to thank my fantastic research advisory committee; **Dr. Glatzhofer**, **Dr. Cichewicz**, **Dr. Nicholas**, **Dr. Schmidtke**, and **Dr. Thomson**, for their guidance and support throughout this endeavor. I would especially like to thank **Dr. Glatzhofer** for his never-ending patience and for always believing in me. I would also like to give a special thanks to **Dr. Schmidtke** for his collaborative guidance throughout the biofuel cell project.

I would like to give special thanks to **Matt Meredith** for his mentorship, for brining me into the Glatzhofer lab, and for providing the foundation of research on which my work is built.

Additionally, I would like to thank **Shelley Minteer** for allowing me to work in her lab, as well as **Fabien Giroud**, **Mike Minson**, **Jie Chen**, and **Jared DeLuca** for their collaborative work.

Finally, I would like to thank all of my friends and colleagues in the Glatzhofer lab; **Matt Meredith**, **Rahul Kadam**, **Sachin Chavan**, **Farid Ismail**, **Will Hastings**, **Nick Godman**, **Dan Bamper**, **Jordan Redemann**, and **Abby Halmes**.

Table of Contents

Acknowledgements **iv**

Abstract **xii**

1 Introduction **1**
1.1 Introduction to Biofuel Cells and Power Consumption 1
1.2 Enzymatic Biofuel Cells 5
1.3 Fuel Cell Conventions and Nomenclature 9
1.4 Choice of Redox Mediator 12
1.5 Project Background 16
1.6 Project Goals 21

2 $FcMe_4-C_3$−LPEI/GOx Bioanode Characterization **23**
2.1 Introduction 23
2.2 Experimental 27
2.2.1 Chemicals and Solutions 27
2.2.2 Synthesis of 1,1'-*bis*-(Dimethylaminomethyl)-Dimethylferrocenes 28
2.2.3 Methylation of 1,1'-*bis*-(Dimethylaminomethyl)-Dimethylferrocenes 29
2.2.4 Reduction of 1,1'-*bis*-(Dimethylaminomethyl)Dimethylferrocene Dimethiodides 29
2.2.5 Synthesis of (3-Bromopropionyl)tetramethylferrocenes 30
2.2.6 Reduction of (3-Bromopropionyl)tetramethylferrocenes 31
2.2.7 Synthesis of $FcMe_4$-C_3-LPEI 31
2.2.8 Electrode Film Preparation 32
2.2.9 Electrochemical Measurements 33
2.2.10 Carbon Felt Electrode Experiments 33
2.3 Results and Discussion 34
2.3.1 Synthesis of $FcMe_4$-C_3-LPEI 34
2.3.2 Effects of Variable Cross-Linking Concentration 36
2.3.3 Effects of pH Variation 43
2.3.4 Carbon Felt Electrode Film Loading 47
2.4 Conclusions 50

3 Enzyme Cascade for Catalyzing Sucrose Oxidation in a Biofuel Cell **52**
3.1 Introduction 52
3.2 Materials and Methods 55
3.2.1 Materials 55
3.2.2 Electrode Fabrication 56
3.2.3 Voltammetric and Amperometric Characterization of FDH, GOX and Inv/FDH/GOx Electrodes 57
3.2.4 UV/Vis Invertase Assay 58

3.2.5 Fuel Cell Bioanode Characterization . . . 59
3.3 Results . . . 59
3.3.1 Sucrose Cascade Characterization . . . 60
3.3.2 Optimization of Temperature and pH . . . 71
3.3.3 Stability of Sucrose Cascade Anode . . . 71
3.3.4 Sucrose Cascade Operation in a Biofuel Cell . . . 73
3.4 Conclusion . . . 75

4 Chloroferrocene-Mediated Enzymatic Biocathode 77
4.1 Introduction . . . 77
4.2 Experimental . . . 82
4.2.1 Chemicals and Solutions . . . 82
4.2.2 Synthesis of Chloroferrocene . . . 82
4.2.3 Synthesis of (3-Bromopropionyl)chloroferrocene . . . 83
4.2.4 Synthesis of (3-Bromopropyl)chloroferrocene . . . 83
4.2.5 Synthesis of FcCl-C_3-LPEI . . . 84
4.2.6 Electrode Film Preparation . . . 85
4.2.7 Electrochemical Measurements . . . 86
4.3 Results and Discussion . . . 87
4.3.1 Synthesis and Characterization of Chloroferrocene-Modified LPEI 87
4.3.2 Effects of Variable Cross-Linking . . . 90
4.3.3 Effects of Laccase Loading . . . 93
4.3.4 O_2 Diffusion through Biocathode Films . . . 98
4.3.5 Effects of Film Loading on Carbon Felt Electrodes . . . 100
4.3.6 FcCl-C_3-LPEI/Laccase in a Ferrocene-Mediated Biofuel Cell . . . 102
4.4 Conclusion . . . 107

5 Conclusions and Future Directions 108
5.1 Conclusions . . . 108
5.2 Future Work . . . 110

BIBLIOGRAPHY 114

A NMR Data 124

List of Tables

1.1 All redox potentials are vs SCE and were taken at pH 7.0 unless otherwise noted.[1,2] 11
1.2 Summary of previously reported redox-mediated bioanodes and biocathodes. J_{max} refers to the use of GOx for anodes and laccase for cathodes. . 16

2.1 Effects of variable cross-linking on the electrochemical and apparent enzyme kinetics of $FcMe_4$-C_3-LPEI/GOx films. Experiments were performed using a 2 M PBS buffer, pH = 7.4, at 25 °C . Error is reported as ± standard deviation is reported, where $n = 3$. 43

3.1 Comparison of the amperometric responses of different enzyme-modified electrodes in the presence of variable substrate mixtures. 70
3.2 Comparison of sucrose/oxygen biofuel cells composed of an air-breathing Pt cathode with one of three different Inv/FDH/GOx Anodes: (1) C8-LPEI Film with Inv in solution, (2) $FcMe_4$-C_3-LPEI film without Inv, (3) $FcMe_4$-C_3-LPEI. 75

4.1 Summary of $FcMe_4$-C_3-LPEI/GOx - FcCl-C_3-LPEI/laccase glucose/O_2 BFC results. BFCs were prepared on 0.5 cm^2 carbon felt with 40 wt% laccase and 50 mol% EGDGE in the cathode, and 32 wt% GOx and 14 mol% EGDGE at the anode. Experiments were performed using 0.05 M citrate buffer, pH = 5.2. 105

List of Figures

1.1 Graphical comparison of the power outputs (W) of various types of fuel cells.[3] . . . 3
1.2 Graph of power consumption of various electronic devices. Adapted from Romero.[4] . . . 4
1.3 A visual approximation of the three different groups of redox enzymes as described by Heller *et al.*[5] . . . 6
1.4 Reaction scheme of the oxidation of glucose and the reduction of O_2. The reaction potentials shown are the thermodynamic reaction potentials vs SCE at pH = 7.[6] . . . 8
1.5 Schematic of a glucose/O_2 BFC that utilizes GOx and laccase as enzymatic catalysts. . . . 11
1.6 Visual approximation (A) and the simplified mechanistic diagram (B) of the electron transfer process that occurs in a redox polymer on a glucose bioanode. Glucose is oxidized by glucose oxidase (GOx) and electrons are transferred to the electrode surface through redox mediators (R) on a polymer backbone through a self-exchange mechanism. . . . 13
1.7 Schematic of the assembly of a glucose bioanode, using Fc-C_3-LPEI cross-linked with EGDGE in the presence of GOx onto a 3 mm glassy carbon electrode. . . . 17
1.8 Illustration of the protonation state of LPEI at pH $\geq$9, 4 - 8, and $\leq$3.[7] . . . 18
1.9 Molecular drawings of: A.) Fc-C_3-LPEI, B.) $FcMe_2$-C_3-LPEI, and C.) $FcMe_4$-C_3-LPEI (top) and CVs of their corresponding cross-linked films (bottom) performed in 2 M PBS, pH 7.4, 25 °C at 0.05 V/sec vs SCE. . . . 19
1.10 Power curve for fuel cells with PVP-Os/laccase as the cathode and either Fc-C_3-LPEI/GOx (solid line), $FcMe_2$-C_3-LPEI/GOx (dotted line), or $FcMe_4$-C_3-LPEI/GOx (dashed line) as the anode.[8,9] . . . 20

2.1 Diagram of the tetramethylferrocene-modified LPEI polymer ($FcMe_4$-C_3-LPEI) characterized in this work. . . . 25
2.2 Synthetic scheme for tetramethylferrocenes (**1**). . . . 34
2.3 Synthetic scheme for (3-bromopropyl)tetramethylferrocenes, as reported by Meredith *et al.*[9] . . . 36
2.4 Synthetic scheme for the synthesis of $FcMe_4$-C_3-LPEI used in this work. . . . 37
2.5 Plot of $E_{1/2}$ versus the degree of cross-linking of $FcMe_4$-C_3-LPEI/GOx (32 wt%) with EGDGE. Data set was determined from CVs that were run at 0.05 V/sec on 3 mm glassy carbon electrodes using 2 M PBS, pH 7.4, 25 °C. All potentials are vs. SCE, and error bars represent one standard deviation, $n = 3$. . . . 38

2.6 Plot of $E_{1/2}$ of $FcMe_4-C_3-$LPEI/GOx versus hydrodynamic (Stokes) radius of the counteranion. $E_{1/2}$ was determined by performing CVs of $FcMe_4-C_3-$LPEI/GOx films in electrolytes containing anions of varying size; sodium salts of (smallest to largest) NO_3^-, Cl^-, Br^-, I^-, $H_2PO_4^-$, and BF_4^- were used as electrolytes at 25°C. All potentials are vs. SCE, and error bars represent one standard deviation. 39
2.7 Schematic highlighting the shift in redox potential of ferrocene in the presence of an ammonium ion. 40
2.8 Plot of relative electron diffusion coefficient ($cD_e^{1/2}$) as a function of the extent of film cross-linking. Data set was determined from CVs that were run at 0.05 V/sec in 2 M PBS, pH 7.4, 25 °C. $cD_e^{1/2}$ was calculated using the Randles-Sivcek equation from CVs. All potentials are vs. SCE, and error bars represent one standard deviation, $n = 3$. 41
2.9 CVs of $FcMe_4-C_3-$LPEI/GOx films at varying pH (yellow = pH 8.0, orange = pH 7.0, grey = pH 6.0, light blue = pH 5.0, dark blue = pH 4.0) (top) and a plot of $E_{1/2}$ and $cD_e^{1/2}$ as a function of pH; both calculated from CVs of $FcMe_4-C_3-$LPEI/GOx (32 wt%) cross-linked with EGDGE (14 mol%) at varying pH (bottom) using 0.05 M phosphate buffer at 25 °C. Error bars represent one standard deviation from the average, $n = 4$. 44
2.10 Illustration of $FcMe_4$-C_3-LPEI film swelling as a function of pH and its effect on redox potential. 45
2.11 Plot of $E_{1/2}$ of Fc-C_3-LPEI in solution versus pH. $E_{1/2}$ values were determined from CVs of Fc-C_3-LPEI using 0.05 M phosphate at 25 °C at varying pHs with a scan rate of 0.05 V/sec. Phosphoric acid was added to reach the desired pH. Potentials are versus SCE. 47
2.12 Current density response of $FcMe_4$-C_3-LPEI/GOx (32 wt%) films to 100 mM glucose at varying pH. Films were cross-linked with EGDGE (14 mol%), and responses using 0.05 M phosphate were determined by constant potential amperometrically at 25 °C. Error bars represent one standard deviation, $n = 4$. 48
2.13 Current density response of $FcMe_4$-C_3-LPEI/GOx (32 wt%) films in 100 mM glucose at varying film solution loadings. 49

3.1 Chemical structure of 3-(tetramethylferrocenyl)propyl-modified LPEI - ($FcMe_4$-C_3-LPEI). 54
3.2 Simplified outline of the enzymatic pathway used to extract electrons from sucrose by hydrolyzing it to fructose and glucose, and then electroenzymatically oxidizing fructose and glucose to ketofructose and gluconolactone, respectively. 60
3.3 Representative cyclic voltammograms of (A) GOx-modified electrodes in the absence and presence of 100 mM glucose, (B) FDH-modified electrodes in the absence and presence of 100 mM fructose, and (C) Inv/FDH/GOx-modified electrodes in the absence and presence of 100 mM sucrose. . . . 61
3.4 Amperometric response for FDH-modied and GOx-modified electrodes in increasing concentrations of fructose and glucose respectively. 63

3.5 Calibration curves for Inv/FDH-modified electrodes and Inv/GOx-modified electrodes. 64
3.6 Absorbance change at $\lambda = 410$ nm of a PAHBAH solution in presence of different concentration of sucrose first incubated for 15 min at 25 °C in presence of immobilized invertase in a C_8-LPEI hydrogel film. The dashed line represents the fitted Hill function. 66
3.7 Amperometric responses for Inv/FDH-modified electrodes (dashed line), Inv/GOx-modified electrodes (dotted line), and Inv/FDH/GOx-modified electrodes (solid line) in 100 mM sucrose solution ($t_{injection} = 400$ sec). All films were coated onto 1 cm^2 Toray paper electrodes. Experiments were performed using 0.05 M citrate buffer, pH 5.5, at 25 °C. 67
3.8 Amperometric response for Inv/FDH-modified electrodes (solid line), Inv/-GOx-modified electrodes (dashed line) in a mixture of 100 mM fructose, 100 mM glucose solution ($t_{injection} = 400$ sec). All films were coated onto 1 cm^2 Toray paper electrodes. Experiments were performed using 0.05 M citrate buffer, pH 5.5, at 25 °C. 68
3.9 Amperometric responses recorded at + 0.05 V (vs. SCE) above E_{ipa} of C_8-LPEI-modied electrodes without enzymes and with the Inv/FDH/GOx enzymes cascade. 69
3.10 (A) Amperometric response recorded after 2 h for Inv/FDH/GOx-modified electrodes in 100 mM sucrose solution at different temperatures. (B) Amperometric response recorded after 2 h for Inv/FDH/GOx-modified electrodes in 100 mM sucrose solution at different pH solutions. 72
3.11 (A) Amperometric responses recorded for FDH-modified electrodes using 100 mM fructose solution, day 1 and day 6. (B) Amperometric responses recorded for GOx-modified electrodes using 100 mM glucose solution, day 1 and day 6. (C) Amperometric responses recorded for Inv/FDH/GOx-modified electrodes using 100 mM fructose solution, day 1 and day 2. . . . 73
3.12 Representative polarization and power curves obtained from a FDH/GOx-modified electrode using 100 mM sucrose in absence, and in presence of, invertase in solution. 74

4.1 Crystal structure of laccase from *Trametes versicolor* in its oxidized form, obtained from PDB (top), and its proposed mechanism for the reduction of O_2 to H_2O, adopted from Solomon *et al.*[10] 79
4.2 Molecular diagram of FcCl-C_3-LPEI (top) and schematic diagram of a glucose/O_2 biofuel cell using a $FcMe_4$-C_3-LPEI/GOx anode and a FcCl-C_3-LPEI/laccase cathode(bottom). 81
4.3 Synthetic scheme of FcCl-C_3-LPEI. 87
4.4 CV comparison of $FcMe_4$-C_3-LPEI (A), Fc-C_3-LPEI (B) and FcCl-C_3-LPEI (C). Experiments were performed using a 0.05 M citrate buffer (pH 5.5) at 0.05 V/sec. and 25 °C 88
4.5 Example of constant potential amperometric experiment used to determine J_{max} of FcCl-C_3-LPEI/laccase. 89

4.6 Values of J_{max} for FcCl-C_3-LPEI/laccase as a function of the concentration of cross-linker . . . 90
4.7 Plots showing the effect of EGDGE concentration on $E_{1/2}$ (top) and $cD_e^{1/2}$ (bottom) of FcCl-C_3-LPEI/laccase films . . . 92
4.8 Graph of J_{max} for variable laccase loadings in FcCl-C_3-LPEI/laccase films 94
4.9 Effects of laccase loading on $E_{1/2}$ (top) and $cD_e^{1/2}$ (bottom) on FcCl-C_3-LPEI/laccase films . . . 96
4.10 Schematic of possible FcCl-C_3-LPEI/laccase model to account for the decrease in electron diffusion with increased laccase loading . . . 97
4.11 Levich plot showing the effects of O_2 diffusion on the maximum catalytic current density of FcCl-C_3-LPEI/laccase electrodes . . . 99
4.12 Effects of variable FcCl-C_3-LPEI/laccase film loading on the maximum catalytic current density . . . 101
4.13 Overlaid pH profiles of FcCl-C_3-LPEI/laccase and $FcMe_4$-C_3-LPEI/GOx 103
4.14 Power curves and current density curves comparing $FcMe_4$-C_3-LPEI/GOx - FcCl-C_3-LPEI/laccase BFCs using different electrode materials . . . 104
4.15 Representative power and current density curves comparing the output of $FcMe_4$-C_3-LPEI/GOx - FcCl-C_3-LPEI/laccase BFCs at 25 °C and 37 °C 106

A.1 1,1'-*bis*-(Dimethylaminomethyl)-Dimethylferrocenes . . . 125
A.2 1,1'-*bis*-(Dimethylaminomethyl)-Dimethylferrocene Dimethiodide . . . 126
A.3 Tetramethylferrocenes . . . 127
A.4 3-(Bromopropyl)tetramethylferrocenes . . . 128
A.5 $FcMe_4$-C_3-LPEI . . . 129
A.6 Chloroferrocene . . . 130
A.7 (3-Bromopropyl)chloroferrocene . . . 131
A.8 FcCl-C_3-LPEI . . . 132

Abstract

Tetramethylferrocene-modified linear(polyethylenimine) ($FcMe_4$-C_3-LPEI) was cross-linked with ethylene glycol diglycidyl ether (EGDGE) in the presence of glucose oxidase (GOx) on carbon electrodes to form enzymatic redox hydrogels. These films have a direct practical application as enzymatic bioanodes, and as potential glucose biosensors. The amperometric response of $FcMe_4$-C_3-LPEI/GOx films to glucose was optimized by varying the amount of EGDGE, pH, and electrode material. The electrochemical potential varies with the amount of EGDGE used to cross-link the film, from 0.068 V to 0.122 V using 4 mol% to 32 mol% EGDGE respectively. A similar trend occurs with varying pH from 0.073 V at pH 4.0 to 0.118 at pH 8.0. A mathematical model was developed to account for this unique change in redox potential as a function of both pH and cross-linker concentration. Upon optimizing the degree of cross-linking and enzyme loading, current densities of 1.034 mA/cm^2 with 3 mm glassy carbon electrodes and 15.1 mA/cm^2 with 0.5×0.5 cm carbon felt electrodes were achieved at 0.13 V vs SCE in 2 M PBS at 25 °C. Additionally, $FcMe_4$-C_3-LPEI is used to demonstrate a seperate bioanode that is capable of extracting four electrons from a single molecule of sucrose by way of a three-enzyme cascade.

Invertase, fructose dehydrogenase and glucose oxidase were immobilized in a $FcMe_4$-C_3-LPEI hydrogel onto the surface of a carbon electrode. Fuel sources were generated in the polymer film by (1) hydrolyzing sucrose into fructose and glucose, and then (2) electroenzymatically oxidizing fructose and glucose to produce a current response. A previously unreported synergistic effect is observed between glucose oxidase and fructose

dehydrogenase, that resulted in a limiting catalytic current density that was considerably higher than expected. The newly described enzyme cascade generated 302 μA/cm^2 at 25 °C and 602 μA/cm^2 at 37 °C, and when poised against an air breathing platinum cathode in a biofuel cell, the multienzyme-containing film generated 42 μW/cm^2 at 0.17 mV with a maximum current density of 344 μA/cm^2 in 100 mM sucrose at 25 °C. This was the first example of an enzymatic biofuel cell that utilizes both fructose and glucose as oxidation fuel sources.

Finally, a novel chloroferrocene-modified redox polymer (FcCl-C_3-LPEI) was synthesized, and shown to have a redox potential that is 0.1 V higher than its unchlorinated counterpart. This new redox polymer was used to immobilize the enzyme, laccase, to form an enzymatic biocathode (FcCl-C_3-LPEI/laccase) capable of catalyzing the reduction of O_2 to H_2O. FcCl-C_3-LPEI/laccase was capable of generating a maximum catalytic current density of 0.304 mA/cm^2 on a 5 mm rotating disk electrode, and 3.54 mA/cm^2 on a 0.5 $\times$ 0.5 cm carbon felt electrode at a potential of 0.42 V and at 25 °C . The FcCl-C_3-LPEI/laccase biocathode was poised against an optimized $FcMe_4$-C_3-LPEI/GOx bioanode to prepare a glucose/O_2 biofuel cell able to achieve 636 μW/cm^2 with a maximum current density of 3.43 mA/cm^2 at 0.26 V and at 37 °C . This is the first report of a biofuel cell to be mediated by ferrocene at both the anode and the cathode.

Chapter 1

Introduction

1.1 Introduction to Biofuel Cells and Power Consumption

A biofuel cell, in the broadest sense, is defined as any device that can convert chemical energy into electrical energy by the use of a biochemical pathway.[3] The first demonstration of electrochemical power conversion through the metabolism of a living organism was done by Potter *et al.* in 1911, who was able to generate 3.5 V by feeding glucose solutions to bakers yeast that had been deposited on platinum electrodes.[11] However, the idea of a biofuel cell was not thoroughly investigated until the beginning of the 1950's, when it was studied as a means of recycling waste created during space flights to generate electrical energy.[12,13] Recently there has been an expansion in the interest in biofuel cells (BFCs) as a potential environmentally friendly means of generating electricity through renewable sources. BFCs provide several unique advantages over their traditional metal counterparts. Traditional fuel cells require harshly acidic conditions and temperatures that exceed 100 °C, but because BFCs are dependent on biological components, BFCs typically operate at or near physiological pH and temperature. Another distinct advantage of BFCs is that the enzymes that are used to catalyze the anodic and cathodic reactions are typically only capable of binding to a very narrow group of substrates. This high substrate specificity limits the possibility of catalytic poisoning and circumvents the necessity to partition the anode and cathode. The abilities of BFCs to operate at physiological conditions and in a compartmentless cell, allows for their possible use

as implantable power sources.

BFCs can be broken down into two subsets, microbial fuel cells and enzymatic fuel cells. Microbial fuel cells (MFCs) take advantage of existing metabolic pathways inside living microorganisms, such as yeast or *E. coli*, to break down sugar into carbon dioxide (CO_2), protons (H^+) and electrons (e^-).[14] MFCs are a very promising new field of research, however the remainder of this manuscript will be focused primarily on enzymatic biofuel cells. For more information on recent developments in MFC technology, Logan *et al.* have written some excellent reviews in both the methodology and applications of MBFs.[15,16]

Enzymatic biofuel cells (EFCs) operate in a manner similar to MFCs except, instead of using the entire metabolic pathway of an organism to convert sugar into CO_2, an isolated enzyme is immobilized onto an electrode surface to catalyze a single redox reaction at the anode or the cathode. EFCs make use of a class of enzymes, called oxidoreductases, that are capable of catalyzing the oxidation of small sugars at the anode or the reduction of molecular oxygen at the cathode via a reversible redox couple at the enzymes active site. Enzymes are often immobilized onto an electrode to allow for greater rates of electron transfer. While both types of BFCs provide a safe way of extracting energy from renewable sources, their shortcoming lies in their inability to generate large amounts of power.

Traditional fuel cells generate power ranging from a few watts to several hundreds of megawatts, whereas BFCs to date have only been shown to produce a few hundred microwatts.[17–19] The difference between the power output of traditional fuel cells and BFCs has been disaffectionately labeled as the "credibility gap", shown in **Figure 1.1**.[3]

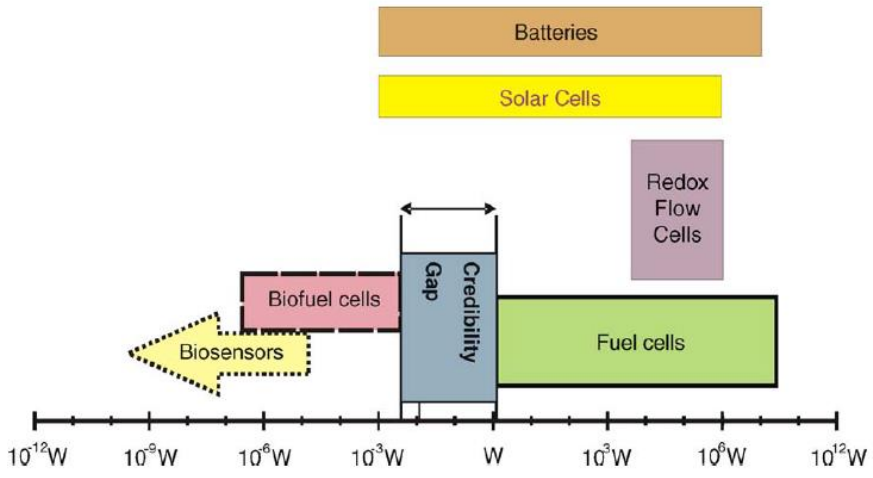

Figure **1.1**: Graphical comparison of the power outputs (W) of various types of fuel cells.[3]

To highlight this problem, Calabrese-Barton *et al.* calculated that the maximum current density for a theoretical monolayer of an enzyme on a 100 nm^2 area electrode with an activity of 500 e^-/sec would be $\sim$ 80 $\mu A/cm^2$, which is considerably lower than the current required to sufficiently power most electronics.[20,21] While Barton's calculation is based on theoretical optimum conditions, it effectively highlights the need to develop more efficient 3D networks to allow for higher enzyme loading densities and thus larger maximum current densities. Using similar assumptions about maximum enzyme activity, Barton estimated that BFCs will need to be able to produce current densities ranging from 1 mA to 10 mA to bridge this so-called "credibility gap" of power generation.[20]

Figure 1.2 illustrates some of the power consumption needs for a wide range of battery-operated electronics. The minimum power required to operate an average laptop

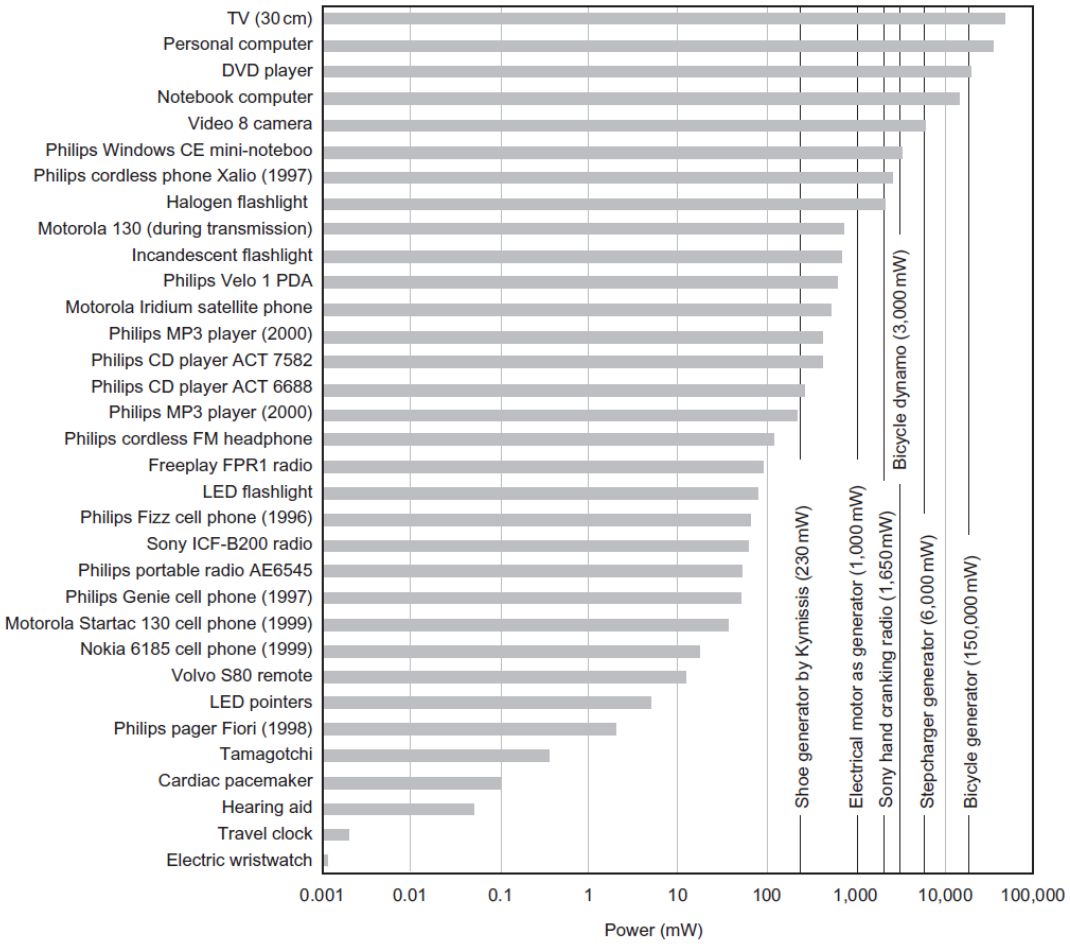

Figure **1.2**: Graph of power consumption of various electronic devices. Adapted from Romero.[4]

is 25-75 W. A modern smartphone requires a minimum of 0.5 W to operate and as much as 10 W to stream video.[4] Given that most BFCs are capable of producing less than 200 μW/cm^2, a modern cell phone would require a BFC that is $\geq$5.2 m^2 to operate. However, small biomedical devices such as pacemakers or hearing aids require much less power to function (as little as 100 μW or 50 μW, respectively), and are therefore seen as the natural electronic niche for BFCs to power.[4]

1.2 Enzymatic Biofuel Cells

In a fuel cell of any type, there are three essential components: an anode, a cathode, and an electrolyte. The anode catalyzes the oxidation of a fuel source, the cathode catalyzes the reduction of an oxidant, and the electrolyte is an ionic medium that allows for the buildup of an electrochemical potential to occur between the anode and the cathode. In a traditional fuel cell, precious metals such as platinum, are used to catalyze both the anodic and cathodic reactions, and an ion-exchange membrane is required to partition the harshly oxidizing environment of the anode from the reducing environment of the cathode, as well as to prevent fuel crossover that leads to catalytic poisoning.[22] Enzymatic biofuel cells use enzymes to catalyze one or both the anode and cathode reaction. Additionally, they do not require a partition between due to their ability to operate in very mild and selective conditions.

As mentioned in **Section** 1.1, EFCs make use of a class of enzymes, called oxidoreductases, that are capable of catalyzing the oxidation of small sugars *via* a reversible redox couple at the enzyme's active site. Oxidoreductases can be broken down into three different groups based on the nature of the redox component of their active site, as shown in **Figure 1.3**.[5]

The first group of enzymes has a weakly bound cofactor, such as nicotinamide adenine dinucleotide (NAD), that can easily diffuse away from the enzyme to act as an external electron carrier.[3,5] Several methods have been developed in which the NAD cofactor has been covalently immobilized onto an electrode surface and the enzyme is reconstituted at the electrode.[23] However, these methods suffer from instability caused by dissociation

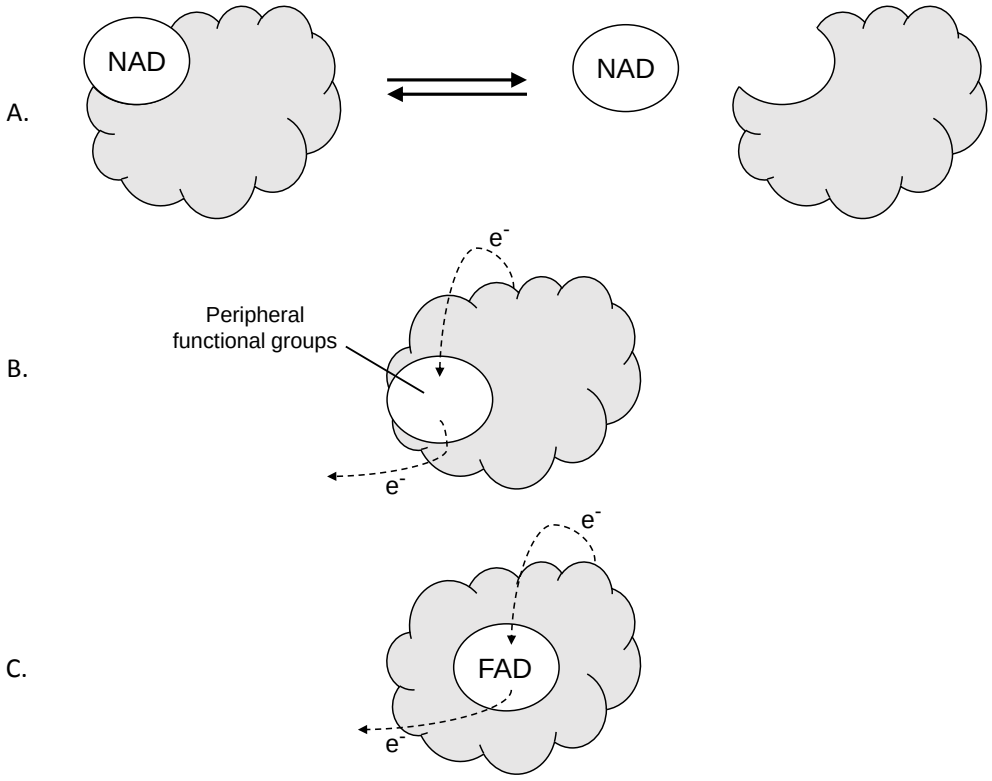

Figure **1.3**: A visual approximation of the three different groups of redox enzymes as described by Heller *et al.*[5]

of the surface-reconstituted enzyme.[24]

The second group of redox enzymes contains a redox cofactor, typically heme or a copper center that is located near the periphery of the enzyme shell. This allows for electron transfer to occur through direct contact with an external electron acceptor, thus making enzymes of this group ideally suited for direct communication with electrodes.[5,25] Recent work has been done to take advantage of this electrochemical communication, however efficient electron transfer at the enzyme-electrode interface is highly dependent on the proper orientation of the enzymes active site.[26–28] Additionally, the theoretical efficiency of the direct electron transfer method is limited because only a single unit layer of enzyme can be used.

The third group of enzymes are large glycoproteins that contain a flavin adenine dinucleotide (FAD) cofactor that is tightly bound in the deep interior of the enzyme.[5] These enzymes most likely transfer electrons through a tunneling event from the FAD active site to one of several points on the enzyme surface. As a result, direct electron transfer (DET) in these enzymes has shown to be highly inefficient or impossible. While there are a handful of publications that claimed to have achieved DET using FAD-dependent enzymes with various nanoparticles, the enzymes at the electrode surface in these studies were shown to be completely denatured due to the large electrochemical potential used, and thus FAD was diffusing from the enzyme to catalyze a small amount of substrate oxidation.[23,29–31]

The choice of enzymes used in a BFC is highly dependent on the substrate to be used as a fuel source. Several substrates such as glucose, fructose, ethanol, and pyruvate have been studied as possible fuel sources for BFCs.[19,32,33] However, glucose has received

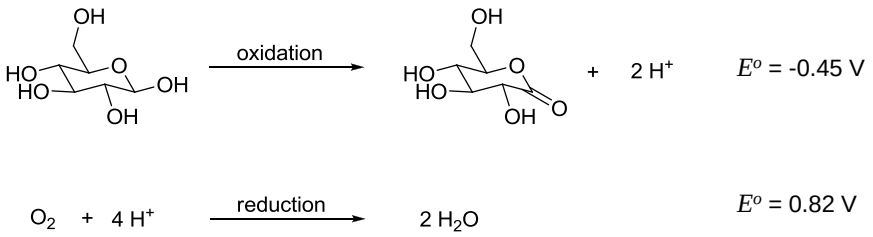

Figure **1.4**: Reaction scheme of the oxidation of glucose and the reduction of O_2. The reaction potentials shown are the thermodynamic reaction potentials vs SCE at pH = 7.[6]

the greatest attention as a substrate because of its relatively high concentrations in the human body (∼5.6 mM in blood plasma).[31] In glucose/O_2 BFCs, the C1-hydroxyl group of glucose is enzymatically oxidized to form gluconolactone which spontaneously hydrolyzes in water to form gluconate at the anode while O_2 is reduced to H_2O at the cathode, as shown in **Figure 1.4**.[6]

The preferred enzymes for the catalytic reduction of O_2 are of a family of blue copper oxidases, laccase and bilirubin oxidase. Laccase is active at pH 5 and is shown to be inhibited by halide ions, while bilirubin oxidase is active at pH 7 and is tolerant of Cl^-[34] However, laccase is commonly preferred because of its high turnover rates. Laccase is a blue copper oxidase that contains a three-copper cluster (type 2/3, T-2/3 cluster) coordinated to histidine ligands at its active site with an additional type 1 (T-1) copper center that aids in electron transfer near the enzyme surface.[6] The T-1 Cu center is adjacent to a hydrophobic pocket through which organic substrates can be bound and oxidized to provide electrons for the reduction of O_2 at the T-2/3 Cu cluster.[6] The location of the T-1 Cu allows laccase to facilitate DET with an electrode surface, and

recent work has shown that anthracene-modified carbon nanotubes (CNTs) can be used to immobilize and orient laccase to generate 1.84 mA/cm^2 as a biocathode.[35] Laccase has several characteristics that make it preferable to platinum catalysts.[19] Apart from a higher activity at near-physiological conditions, laccase also reduces O_2 at a significantly lower overpotential than platinum (η = -0.3 V for laccase vs -0.65 V for Pt).[19]

Enzymatic oxidation of glucose in a BFC is almost exclusively accomplished with GOx. While there has been some work utilizing glucose dehydrogenase (GDH) as an alternative, the resulting current densities were very low when used in a BFC.[36] The widespread use of GOx in bioanodes is owed to its high turnover rate, its ability to operate optimally at physiological pH, and its relatively high stability. The turnover frequency for the oxidation of glucose for FAD-dependent GOx at 25 °C is 1900 s^{-1} compared to 75 s^{-1} for NAD-dependent glucose dehydrogenase (GDH).[37,38] GOx falls into the third group of enzymes described above. It oxidizes the C-1 hydroxyl group of glucose while using O_2 as an electron acceptor. Its active site contains an FAD cofactor that is buried deep within the enzyme, therefore finding a means of achieving efficient electron transfer is a primary challenge for its use in a BFC.

1.3 Fuel Cell Conventions and Nomenclature

When describing the characteristics of a fuel cell, convention is to report the power output in terms of either an absolute power (mW), an area-dependent power density (mW/cm^2) or a volume-dependent power density (mW/cm^3). However, it should be emphasized at the outset that the power of a fuel cell is a function of both the electro-

chemical potential cell potential, E°_{cell} (V), and the current produced at the rate limiting electrode, J_{max} (mA/cm^2), such that,

$$P = E^{\circ}_{cell} \times J_{max} \tag{1.1}$$

where E°_{cell} is equal to the difference in the peak reduction potential of the cathode reaction (E°_{ipc}) and the peak oxidation potential of the anode reaction (E°_{ipa}),

$$E^{\circ}_{cell} = E^{\circ}_{ipc}(cathode) - E^{\circ}_{ipa}(anode) \tag{1.2}$$

The electrochemical potential corresponds to the thermodynamic driving force behind the fuel cell while the current relates to the speed at which the limiting reaction takes place, and both are necessary to do work in the form of electrical power. In order to increase the power output of a fuel cell, there must be an increase in either the E°_{cell} or an increase in J_{max}. However, most fuel cell applications involve powering an electrical circuit that requires a minimum voltage to operate (conventionally in increments of 1.5 V).[4] Therefore, the power output largely becomes a function of the maximum current that can be generated once the minimum potential threshold has been reached.

For a biofuel cell in which glucose is oxidized to gluconolactone at the anode (E° = -0.69 V vs SCE), and O_2 is reduced to H_2O at the cathode (E° = 0.82 V vs SCE), the thermodynamic cell potential is 1.51 V. However, the use of an enzymatic catalyst induces an electrochemical overpotential, η, which is defined as the difference between the experimentally observed potential and the theoretical thermodynamic potential. Therefore, a glucose/O_2 biofuel cell that uses glucose oxidase (GOx) to catalyze the oxidation

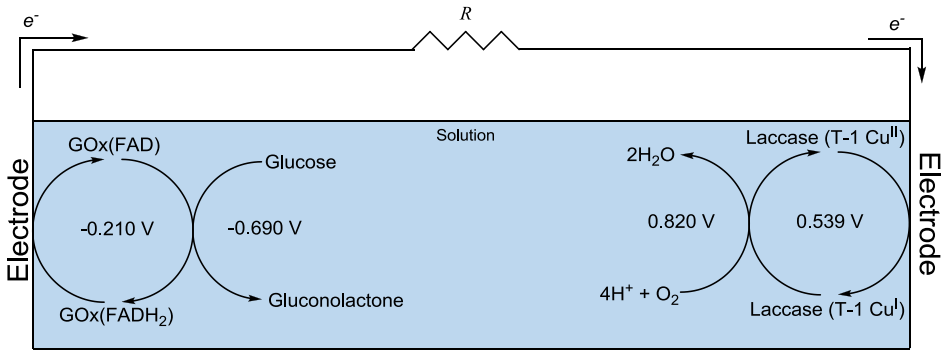

Figure **1.5**: Schematic of a glucose/O_2 BFC that utilizes GOx and laccase as enzymatic catalysts.

Redox Species	$E_{1/2}$
glucose/gluconolactone	-0.690
NAD^+/NADH	-0.570
FAD/$FADH_2$	-0.210
$K_3Fe(CN)_6/K_2Fe(CN)_6$	0.119
quinone/hydroquinone	0.220
ferrocene^{2+}/ferrocene^{3+}	0.405
$ABTS^{-2}/ABTS^{\cdot-}$	0.440
T-1 Cu(II)/Cu(I)	0.539
O_2/H_2O	0.820

Table **1.1**: All redox potentials are vs SCE and were taken at pH 7.0 unless otherwise noted.[1,2]

of glucose (E° (FAD/FADH) = -0.21 V vs SCE), and uses laccase to catalyze the complete reduction of O_2 to H_2O (E° (T-1 Cu(I)/Cu(II)) = 0.539 V vs SCE), as shown in **Figure 1.5**, has a cell potential of E°_{cell} = 0.75 V.[6] Redox potentials for the active sites of GOx, laccase, glucose, and O_2 are given in **Table 1.1**. With the thermodynamic potential of the cell fixed by the enzymatic overpotentials, much of the focus in BFC development is centered on maximizing the current density that can be achieved near the thermodynamic cell potential.

1.4 Choice of Redox Mediator

The maximum current density of a BFC is dependent on the apparent $Jmax$ of the rate limiting electrode, which is most often limited by electron diffusion. To enhance the electron transfer rates of both laccase and GOx, organic and organometallic redox compounds have been employed as electron relays in hydrogel polymer networks.[39] Polymers can be partially substituted with a redox moiety and cross-linked onto the surface of an electrode in the presence of an enzyme to facilitate both enzyme immobilization and enhanced electron transfer. Upon cross-linking, the redox sites are thought to be in close enough radial proximity to the enzyme to intercept electrons and funnel them to the electrode surface through a mechanism of self-exchange shown in **Figure 1.6**.[5,40–42] In addition to enhancing the electron transfer between enzyme and electrode, redox polymers allow for a three-dimensional network in which to immobilize the enzyme. Therefore, an enzymatic electrode film can contain multiple layers of enzyme which in turn significantly increases the theoretical current density that can be generated.

Redox mediators have been incorporated into enzymatic electrode films either by coimmobilization with the enzyme or by use of a redox polymer for the enzyme immobilization. During co-immobilization, the mediator is non-covalently trapped near the enzyme as the film is cross-linked around it. A common organic redox species that has been used to mediate the electron transfer of laccase is 2,2'-azino-bis(3-ethylbenzothiazoline-6-sulfonate) diammonium salt (ABTS). ABTS and laccase are co-immobilized in either a polypyrrole matrix or in a compressed graphene pellet as a biocathode.[1,43,44] Studies of ABTS/laccase systems that are performed on traditional glassy carbon electrodes have

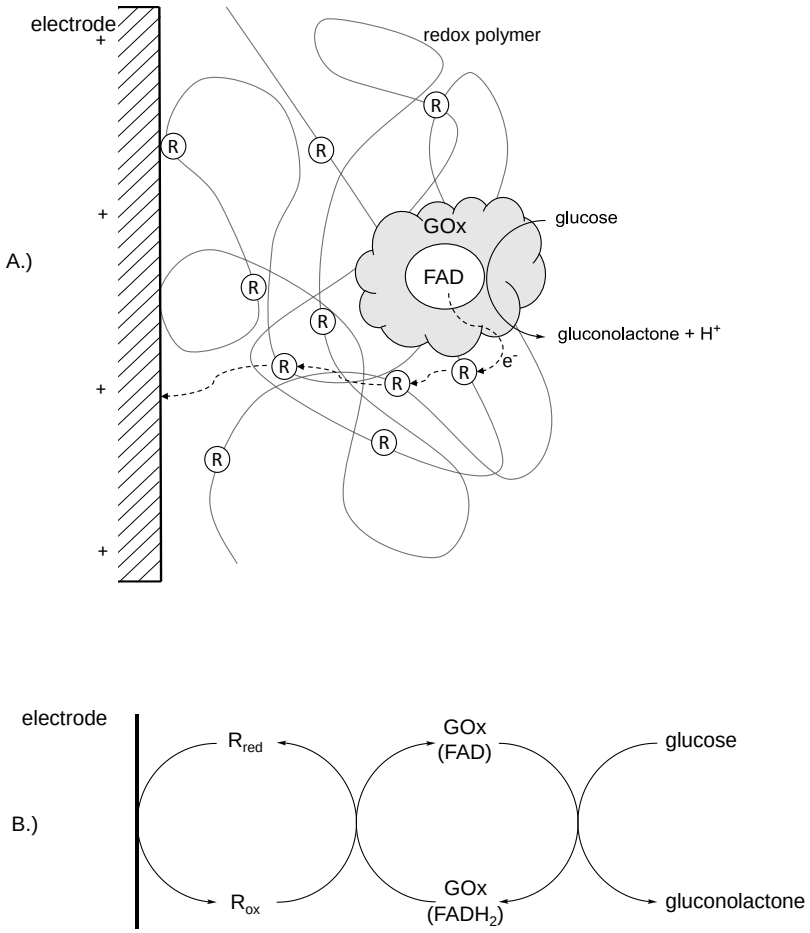

Figure **1.6**: Visual approximation (A) and the simplified mechanistic diagram (B) of the electron transfer process that occurs in a redox polymer on a glucose bioanode. Glucose is oxidized by glucose oxidase (GOx) and electrons are transferred to the electrode surface through redox mediators (R) on a polymer backbone through a self-exchange mechanism.

achieved current densities as high as 2.5 mA/cm^2 at 25 °C.[43] While ABTS provides a small reductive overpotential with laccase (η = -0.11 V), it cannot easily be covalently immobilized into a polymer film and therefore ABTS/laccase biocathodes tend to suffer from activity loss due to ABTS leaching into solution.[1,45] Additionally, the polymers matrices required to immobilize ABTS significantly inhibit the diffusion of oxygen to laccase.

There has been some recent work utilizing quinones as redox mediators with GOx in a bioanode.[46–48] Reuillard *et al.* report a system in which the GOx and naphthoquinone are ground together with multi-walled carbon nanotubes (MWCNTs) to form an aqueous paste. This paste is compressed to form an electrode pellet (5 mm diameter, 4 mm height).[46] While the electrodes are constructed using a seemingly crude method, they have reported J_{max} values of 600 μA/cm^2 at 25 °C and can retain 50% of their current density through 5 days of continuous use.[46]

The most widely studied redox mediators were originally designed by Heller *et al.* throughout the 1990's; they consist of poly(vinyl pyridine) (PVP) or poly(vinyl imidazole) (PVI) that has been covalently modified with [Os(bpy)$_2$Cl$_2$].[5,40,49] By varying the bipyridine (bpy) ligands on the osmium center, the electrochemical potential of the redox moiety can be increased or decreased to fit the desired application.[50] This allows for a significant reduction in the overpotential caused by the redox mediator, and therefore allows the redox films to be applied to either the anode or the cathode with only a slight modification to the preparation.

Mao *et al.* were able to prepare a bioanode film using [Os(N,N'-dimethyl-2,2'-biimidazole)$_3$] attached to PVP via a 12-carbon tether with GOx to generate 1150

μA/cm^2 at 37 °C in 15 mM glucose,[51] while Soukharev *et al.* utilized PVP-[Os(4,4'-dimethyl-2,2'-bipyridine)$_2$(4-aminomethyl-4'-methyl-2,2'-bipyridine)] with laccase to prepare a biocathode capable of producing 1000 μA/cm^2 at 37 °C while oxygen was bubbled through the solution.[17]

Recently there has been a resurgence in the use of ferrocene as a redox mediator.[8,52–55] Ferrocene was discovered in 1951 as one of the first known organometallic compounds, and it was used as one of the earliest BFC mediators.[56,57] Its popularity as a mediator comes from its ability to both achieve high rates of electron transfer and be readily functionalized at either of its cyclopentadienyl (C_p) rings.[58]. Additionally, it provides a non-toxic and inexpensive alternative to the use of Os compounds. Recently, Bunte *et al.* reported a ferrocene-mediated bioanode in which a poly(dimethylacrylamide) is substituted with a long-chain ferrocenyl methylamine, and cross-linked to immobilize GOx.[53–55] The reported bioanode was capable of producing 1.2 mA/cm^2 at 37 °C.[54] Despite various reports of high current densities, ferrocene has been limited as a mediator due to its high redox potential (0.40 V vs SCE), which creates a large overpotential with respect to GOx (η = 0.61 V).

A summary of pertinent data from previously reported redox mediators is compiled in **Table 1.2**. Regardless of the type of mediator/redox polymer being used, it is important to realize that, along with control of the electrochemical potential of the redox mediator, a high rate of electron transfer must be maintained to allow for maximum current density. An ideal mediator would induce a small overpotential while being capable of an electron transfer rate that was approximately equal to, or greater than, the turnover rate of the enzyme being used.

Mediator	$E_{1/2}$ **(V)**	J_{max} **(μA/cm^2)**	**Conditions**	**Ref.**
Anode				
Naphthoquinone	-0.16	600	25 °C, 2 M PBS (pH 7), compressed MWCNT pellet electrode (5 mm diameter, 4 mm height)	[46]
PVP-[Os(dm-2,2'-biimidazole)$_3$]	-0.23	1150	37 °C, 0.1 M citrate (pH 5), carbon fiber electrode (7 μm diameter, 2 cm height)	[51]
PDMA-Ferrocene	0.40	1200	37 °C, 2 M PBS (pH 7), 3 mm glassy carbon electrode	[54]
Cathode				
Pt	0.59	900	37 °C, 0.5 M H_2SO_4, Pt fiber electrode (6 μm diameter, 2 cm height)	[17]
PVP-[Os(dm-2,2'-bpy)$_2$((dmamino)$_2$-2,2'-bpy)]	0.89	1000	37 °C, 0.1 M citrate (pH 5), carbon fiber electrode (7 μm diameter, 2 cm height)	[17]
An-MWCNTs (DET)	0.53	2000	37 °C, 0.1 M citrate (pH 4), toray paper electrode (1 cm × 1 cm), highly purified laccase	[35]

Table **1.2**: Summary of previously reported redox-mediated bioanodes and biocathodes. J_{max} refers to the use of GOx for anodes and laccase for cathodes.

1.5 Project Background

Recent studies by Merchant *et al.* have shown that ferrocene could be covalently immobilized onto linear poly(ethylenimine) (LPEI) for use as a redox polymer in a glucose bioanode.[8,59] Propylferrocene-modified LPEI (Fc$-$C$_3-$LPEI) can be cross-linked using a diepoxide, ethyleneglycol diglycidyl ether (EGDGE), in the presence of GOx, onto the surface of a glassy carbon electrode to be used as an amperometric glucose sensor or as a glucose bioanode as shown in **Figure 1.7**.[8,60] LPEI has previously been shown to electrostatically complex to a wide range of biological macromolecules.[61] It is comprised of a linear chain of secondary amines that allows the polymer to be water soluble, and the backbone amines of LPEI are in close enough proximity that the protonation state of any subunit affects the pKa of both the adjacent subunits.[7] In other words, as one repeat

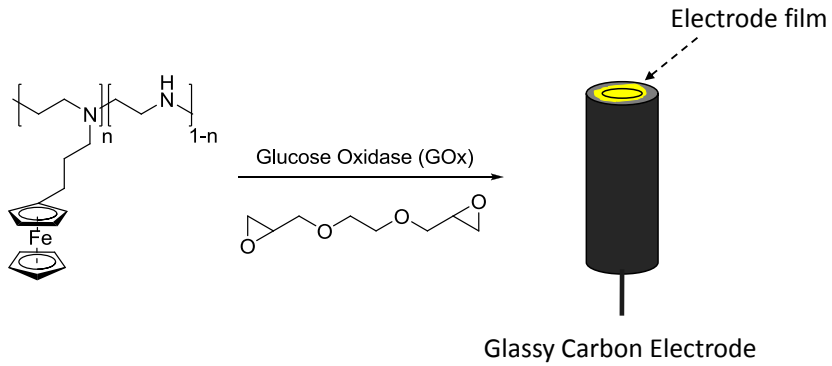

Figure **1.7**: Schematic of the assembly of a glucose bioanode, using Fc-C_3-LPEI cross-linked with EGDGE in the presence of GOx onto a 3 mm glassy carbon electrode.

unit becomes protonated, the pKa of the adjacent units decreases so that only 50% of the backbone amines of LPEI are protonated when dissolved in a neutral aqueous solution (pH 7), as illustrated in **Figure 1.8**.[7] This self-buffering property allows a stabilizing effect on enzymes when electrostatically complexed in biosensor and BFC applications. The high propensity for PEI to adopt a protonated state causes cross-linked LPEI films to take in water and become hydrated, which in turn causes the films to swell to several times their original volume and thus provides a means for substrates (glucose, O_2) to easily diffuse through them. In addition to providing the means for swelling and electrostatic complexation, the backbone amines provide a convenient means of polymer modification through nucleophilic substitution.

Recently our group has attempted to use modified ferrocene (Fc) species to affect the redox potential of ferrocene-modified LPEI films in an attempt to lower the oxidative overpotential induced at a glucose bioanode.[8] Several previous studies have shown that the redox potential of ferrocene can be altered by adding substituents to either

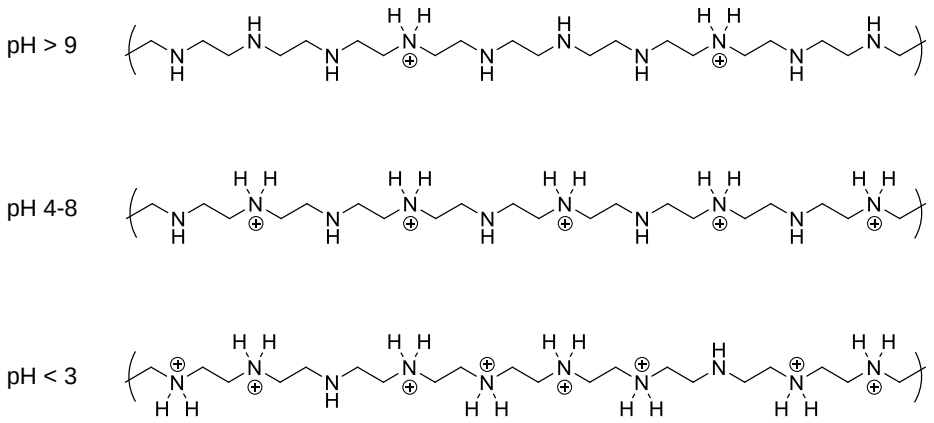

Figure **1.8**: Illustration of the protonation state of LPEI at pH ≥9, 4 - 8, and ≤3.[7]

of its C_p rings.[62–64] As ferrocene is oxidized to the ferrocenium cation, the presence of electron releasing substituents on the C_p rings on Fc acts to stabilize the cation Fe center and thus lower the potential required for the oxidation to occur.[65,66] Emilia *et al.* showed that the incorporation of one methyl group was shown to lower the $E_{1/2}$ of ferrocene by 0.05 V, down to 0.35 V vs SCE, while completely methylated ferrocene (decamethylferrocene) resulted in a decrease of $E_{1/2}$ by 0.57 V down to -0.17 V vs SCE.[62,64] By comparing cross-linked films of 3-propylferrocene-modified LPEI (Fc-C_3-LPEI), 3-propyl(dimethylferrocene)-modified LPEI ($FcMe_2$-C_3-LPEI), and 3-propyl(tetramethylferrocene)-modified LPEI ($FcMe_4$-C_3-LPEI), shown in **Figure 1.9**, we have been able to lower the oxidative overpotential of the bioanode by 0.04 V per methyl group.[8,9] This results in an $E_{1/2}$ for $FcMe_4$-C_3-LPEI of 0.120 V vs SCE.

Cross-linked films of Fc-C_3-LPEI, $FcMe_2$-C_3-LPEI, and $FcMe_4$-C_3-LPEI with GOx are able to produce catalytic current densities of 1.01 mA/cm^2, 1.16 mA/cm^2, and 0.741 mA/cm^2 respectively at 25 °C.[8,9] While both Fc-C_3-LPEI and $FcMe_2$-C_3-LPEI films achieve current densities greater than 1 mA/cm^2, $FcMe_4$-C_3-LPEI films exhibit a pre-

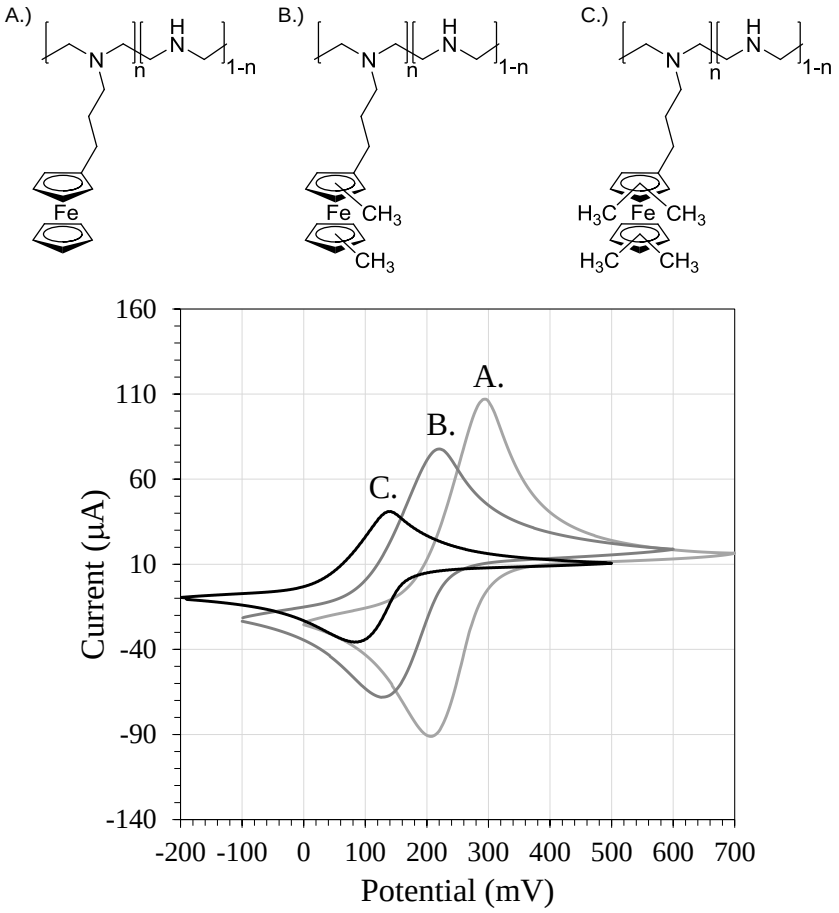

Figure **1.9**: Molecular drawings of: A.) Fc-C_3-LPEI, B.) $FcMe_2$-C_3-LPEI, and C.) $FcMe_4$-C_3-LPEI (top) and CVs of their corresponding cross-linked films (bottom) performed in 2 M PBS, pH 7.4, 25 °C at 0.05 V/sec vs SCE.

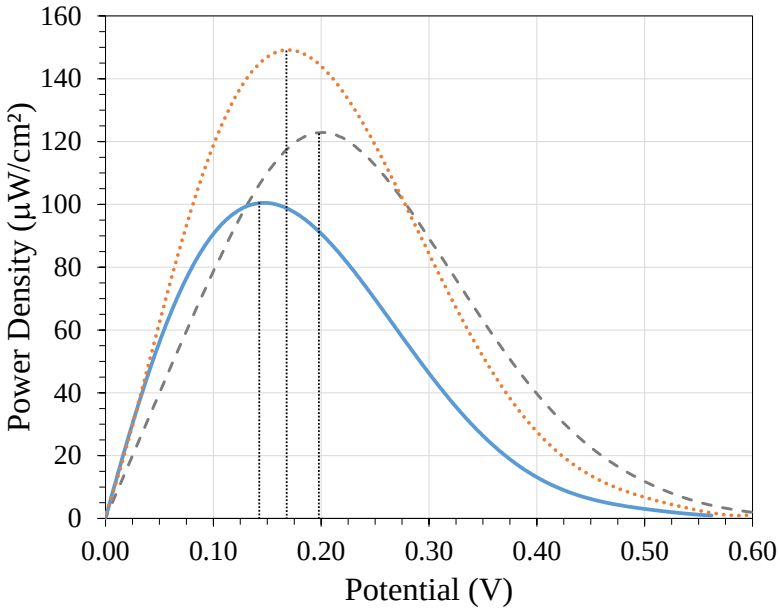

Figure **1.10**: Power curve for fuel cells with PVP-Os/laccase as the cathode and either Fc-C_3-LPEI/GOx (solid line), $FcMe_2$-C_3-LPEI/GOx (dotted line), or $FcMe_4$-C_3-LPEI/GOx (dashed line) as the anode.[8,9]

cipitous decrease in the maximum catalytic current density. BFCs composed of either Fc-C_3-LPEI/GOx, $FcMe_2$-C_3-LPEI/GOx, or $FcMe_4$-C_3-LPEI LPEI/GOx as a bioanode and PVP-Os/laccase as a biocathode, shown in **Figure 1.10**, were capable of generating 100 μW/cm^2, 140 μW/cm^2, and 120 μW/cm^2 respectively.[8,9] As seen in **Figure 1.10**, the difference in peak potential for each of the fuel cells corresponds to the change in potential for each of the polymers. The power increase achieved using $FcMe_2$-C_3-LPEI vs Fc-C_3-LPEI can be largely attributed to the increase in E_{cell}, while the decrease in power when using the tetramethylated ferrocene vs the dimethylated ferrocene (despite the increase in cell potential) highlights the corresponding decrease in catalytic current density for $FcMe_4$-C_3-LPEI/GOx films. This decrease in catalytic current density correlates to a decrease in electron diffusion through films that contain ferrocene species with

higher degrees of methylation.[9] Meredith *et al.* calculated that ≥60% of the decrease can be directly attributed to the increased steric bulk of polymethylated ferrocene.[9] While the loss of power in BFCs was relatively small for cells using $FcMe_4$-C_3-LPEI/GOx, the calculated trend for electron transfer rate indicates that much larger decreases are likely for films that incorporate octamethylferrocene or decamethylferrocene. So in order to continue to utilize ferrocene-methylation as a means of inducing a lower redox potential, strategies must be developed to compensate for the inherent decrease in electron diffusion.

1.6 Project Goals

The aims of the projects presented here are to provide a more thorough characterization of $FcMe_4$-C_3-LPEI/GOx films in an attempt to enhance electron diffusion and increase the maximum catalytic current density. This will be done by optimizing various components of the film such as the degree of cross-linking and the weight percent of GOx incorporated, and investigate the effects of pH and counter-ion. Additionally, we introduce a novel cathodic redox polymer material that is based on chloroferrocene. Chlorferrocene-modified LPEI can be used to immobilize laccase to achieve catalytic current densities that are among the highest reported for an enzymatic cathode. Finally we examine the possibility of incorporating multiple redox enzymes into a single $FcMe_4$-C_3-LPEI film to allow for use of sucrose as a fuel source. The overall goal throughout the work presented in this manuscript is to test and provide strategies to increase the maximum catalytic current and E_{cell} of a glucose/O_2 BFC to overcome the "credibility

gap" outlined in **Section** 1.1.

It should be noted at the outset that, at the time of its writing, much of the contents of this work are either already published in peer reviewed journals or are being prepared for submission. The contents of **Chapter** 3 are published in *ACS Catalysis*[67], and the contents of **Chapters** 2 and 4 are currently being prepared for submission to *Electrochimica Acta* and *Angewandte Chemie Intl. Ed.*, respectively.

Chapter 2

$FcMe_4-C_3$–LPEI/GOx Bioanode Characterization

2.1 Introduction

Redox polymers have been studied extensively since the 1980s for use as molecular actuators, biosensors, in pharmaceutical drug delivery, and in dye-sensitized solar cells.[39,68–75] By modifying just the redox species of the polymer, the physical and electrochemical properties of the entire macromolecule can be altered in a predictable way. This provides a convenient means of fine-tuning the properties of a polymer to fit the needs of a given application. Lately there has been significant interest in the use of redox polymers for *in vivo* glucose biofuel cells (GBFCs).[20,76] Enzymatic GBFCs provide a means of generating power to operate small implantable electronic devices such as pace makers, drug pumps and biosensors.[77] Redox polymers are cross-linked onto an electrode surface in the presence of a redox enzyme to enhance the electron transfer from the enzyme's active site to the electrode surface.[49,74] While there have been an abundance of advances in novel cathode assemblies, there is still much to be desired in new bioanode materials.[70,78]

Recently there has been an expansion of the research done on ferrocene-modified hydrogels for their ability to facilitate high rates of electron transfer when mediating the electroenzymatic oxidation of glucose by GOx.[8,9,28,60,79,80] Ferrocene-modified linear poly(ethylenimine) (LPEI) films have been used to immobilize GOx on the surface of glassy carbon electrodes. The use of such redox films negates the need to control the

orientation of the enzyme, because the ferrocene redox moieties effectively "wire" GOx to the electrode surface. However, the use of a redox mediator induces an electrochemical potential higher than the oxidation potential of GOx that limits the thermodynamic driving force in a biofuel cell.

Our previous work has focused on compensating for this oxidative overpotential by incorporating polymethylated ferrocene redox mediators. The methylation of ferrocene has long been studied as means of increasing solubility, lowering the oxidation potential, and increasing the stability of the corresponding ferrocenium cation.[62,81–84] Methylation of the cyclopentadienyl (Cp) ligands of ferrocene lowers the oxidation potential of the iron center by enhancing the electron releasing character of the Cp ligands to stabilize the positive charge of the ferrocenium cation. The net result is a decrease in the oxidation potential of ferrocene.[9,81]

We previously reported a series of high current density redox polymers based on 3-propylferrocene-substituted LPEI that are capable of assisting in highly efficient electron transfer between GOx and a glassy carbon electrode. By using various degrees of ferrocene-methylation, unmethylated ferrocene- (Fc-C_3-LPEI, $E_{1/2} = 0.26$ V), dimethylferrocene- ($FcMe_2$-C_3-LPEI, $E_{1/2} = 0.21$ V), and tetramethylferrocene- ($FcMe_4$-C_3-LPEI, $E_{1/2} = 0.12$ V) modified LPEI films are able to generate 1.01 mA/cm^2, 1.36 mA/cm^2, and 0.741 mA/cm^2 respectively with GOx in saturating glucose conditions at 25 °C on planar glassy carbon electrodes.[8,9] A diagram of the $FcMe_4$-C_3-LPEI polymer is shown in **Figure 2.1**.

Based on these reports, it becomes apparent that methylation of the ferrocene redox site does result in a lower oxidative overpotential. However, the increased steric bulk on

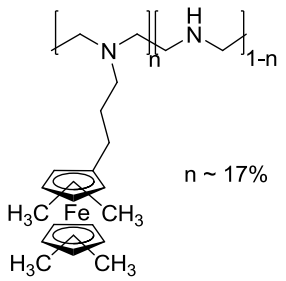

Figure **2.1**: Diagram of the tetramethylferrocene-modified LPEI polymer ($FcMe_4$-C_3-LPEI) characterized in this work.

the tetramethylated redox moiety results in a decrease in the maximum catalytic current density.[9] The nature of this decrease stems from the way that electrons are transferred within the redox film. Redox polymers are thought to conduct electrons by Marcus-type electron transfer, which depends on an outer-shell collisional exchange event between two identical redox species.[72,85,86] The rate of this collision, k_{ET}, is highly dependent on the distance between the centers of the redox species undergoing the exchange, σ, as described in **Equation 2.1**;

$$k_{ET} = A \exp(-\beta\sigma)(\lambda)^{-1/2} \exp(-[(-\Delta G^{\circ} - \lambda)^{1/2} \lambda k T]) \qquad (\mathbf{2.1})$$

where A is a preexponential factor that is constant for systems in which the electron donor and acceptor are identical species, β is the electron transmission coefficient of the electrolyte medium, λ is the reorganization energy required to distort the nuclear configuration of the product state into the geometry of the reactant state, ΔG° is the free energy difference between the reactant and product state in the electron transfer, k is the Boltzman constant, and T is the absolute temperature.[85,87–90] For two systems under identical conditions in which the only variable is the size of the redox species, the

rate of electron transfer is proportional to the exponent of the negative diameter of the redox species;

$$k_{ET} \propto \exp(-\sigma) \tag{2.2}$$

Using a spherical approximation for the molecular volume of a series of methylated ferrocene species, the molecular radii of ferrocene, dimethylferrocene, tetramethylferrocene, and decamethylferrocene can be estimated at 3.63 Å, 3.92 Å, 4.16 Å, and 4.76 Å, respectively.[9,91,92] Assuming a ΔG° of 0.00 V for an electron exchange between identical redox sites, and similar values for λ, k_{ET} for ferrocene, dimethylferrocene, tetramethylferrocene, and decamethylferrocene are calculated to be 2.44×10^7 sec^{-1}, 1.11×10^7 sec^{-1}, 5.61×10^6 sec^{-1}, and 1.03×10^6 sec^{-1} respectively.[93] In other words, each additional methyl group results in a reduction in the rate of electron exchange by $\sim 30\%$ per methyl group added from sterics alone.

In the unmethylated and dimethylated ferrocene-modified GOx films, the apparent rate of electron diffusion appears to be greater than the turnover rate of GOx. However, the increased steric bulk of tetramethylferrocene decreases electron diffusion within the film to the extent that it becomes the rate-limiting step, and thus a lower catalytic current density is observed.[8,9] This trend can be extrapolated outward towards ferrocenes with higher degrees of methylation (such as decamethylferrocene) to show that the maximum catalytic current density of such Fc-LPEI films would be severely limited by slow rates of electron transfer. In moving forward with the use of polymethylated ferrocene-modified LPEI materials for bioanode materials, there is a growing need to compensate for the

inherent decrease in current density associated with using highly methylated ferrocene as well as to develop a better understanding of how such high currents are generated.

The work presented here attempts to present a more complete characterization of $FcMe_4$-C_3-LPEI/GOx films, as such materials are increasingly being applied in biofuel cell research. Additionally, we outline strategies to enhance the maximum current that they can generate. By optimizing enzyme loading and the degree of cross-linking in $FcMe_4-C_3-$LPEI/GOx films, the maximum apparent current density was increased from 0.741 mA/cm^2 shown in previous work to 1.034 mA/cm^2 on 3 mm planar glassy carbon electrodes and 15.10 mA/cm^2 on 0.5×0.5 cm carbon felt electrodes described in this work.[9] The effects of pH, electrolyte, and degree of cross-linking on the electrochemical potential and apparent electron diffusion are reported.

2.2 Experimental

2.2.1 Chemicals and Solutions

Glucose oxidase from *Aspergillus niger* (EC 1.1.3.4, type X-S, 147 units/mg solid, 75% protein) and all chemicals were purchased from Sigma-Aldrich unless otherwise noted and used as received. Ethylene glycol diglycidyl ether (EGDGE) was purchased from Polysciences Inc., Warrington, PA. Stock solutions of 2 M glucose were allowed to mutarotate for 24 hr before use and subsequently kept refrigerated at 4 °C. Carbon felt electrodes (3.18 mm (0.1125 in) thick, 99.0%, Product Number 43199, specific area = 0.6 m^2/sec) were purchased from Alfa Aesar. $FcMe_4$-C_3-LPEI was synthesized as previously reported.[9]

2.2.2 Synthesis of 1,1'-*bis*-(Dimethylaminomethyl)-Dimethylferrocenes

N,N,N',N'-Tetramethylmethanediamine (2.86 g, 28.04 mmol) was added dropwise to a stirring solution of 10:1 glacial acetic acid (20 mL) and phosphoric acid (3 mL) at 0 °C. 1,1'-Dimethylferrocene (2.00 g, 9.34 mmol) was added to the acid solution at 25 °C which was stirred for 24 hours at 100 °C. The reaction mixture was cooled to room temperature and diluted with H_2O (100 mL), and neutralized with NaOH pellets until a pH $\geq$ 9 was reached. The basic solution was extracted four times with diethyl ether (75 mL aliquots). The organic portions were combined and filtered through $MgSO_4$, and the solvent was removed under reduced pressure to yield a mixture of mono- and di-aminomethylated isomers. The product mixture was purified using a column of basic alumina with a 10:1 mixture of diethyl ether/hexanes mixture as the eluent. Two fractions were collected off of the column, and the solvent was removed from each under reduced pressure to yield a mixture of 1-(dimethylaminomethyl)-2,1'-dimethylferrocene, 1-(dimethylaminomethyl)-3,1'-dimethylferrocene, and a mixture of 1,1'-*bis*-(dimethylaminomethyl)-2,2'-dimethylferrocene, 1,1'-*bis*-(dimethylaminomethyl)-2,3'-dimethylferrocene, and 1,1'-*bis*-(dimethylaminomethyl)-3,3'-dimethylferrocene.

The mixture of mono-substituted (dimethylaminomethyl)-dimethylferrocene isomers eluted off the column first as an orange liquid (1.51 g, 5.57 mmol, 60% yield). ^{1}H-NMR (300 MHz, $CDCl_3$): δ 1.86-1.95 (m, 6H, Fc-(C**H**$_3$)$_2$), 2.15 (s, 6H, -N-(C**H**$_3$)$_2$), 3.13-3.34 (m, 2H, Fc-C**H**$_2$-N), 3.80-4.03 (m, 6H, Fe-Cp-**H**).

The mixture of di-substituted *bis*-(dimethylaminomethyl)-dimethylferrocene isomers

eluted off the column second as a slightly darker orange liquid than the mono-substituted product (1.11 g, 3.38 mmol, 36% yield). ^{1}H-NMR (300 MHz, $CDCl_3$): δ1.85-1.95 (overlapping sd, J = 1.5, 6H, Fc-(C**H**$_3$)$_2$), 2.14 (sd, J = 1.5, 12H, -N-(C**H**$_3$)$_3$), 3.09-3.31 (m, 4H, Fc-C**H**$_3$-N), 3.75-3.98 (m, 5H, Fe-Cp-**H**).

2.2.3 Methylation of 1,1'-*bis*-(Dimethylaminomethyl)-Dimethylferrocenes

Iodomethane (0.96 g, 6.76 mmol) was added dropwise to a stirring solution of a mixture of 1,1'-*bis*-(dimethylaminomethyl)-dimethylferrocene isomers (1.112 g, 3.38 mmol) in methanol (20 mL), and the reaction solution was stirred for one hour at 50 °C The solution was cooled to room temperature and triturated with diethyl ether (175 mL). The precipitate was collected and the remaining solvent was removed under reduced pressure to yield a mixture of 1,1'-*bis*-(dimethylaminomethyl)-2,2'-dimethyl ferrocene dimethiodide, 1,1'-*bis*-(dimethylaminomethyl)-2,3'-dimethylferrocene dimethiodide, and 1,1'-*bis*-(dimethylaminomethyl)-3,3'-dimethylferrocene dimethiodide isomers as a brown/yellow powder (1.46 g, 2.39 mmol, 71% yield). ^{1}H-NMR (300 MHz, CD_3OD): δ 1.95-2.15 (m, 6H, Fc-(C**H**$_3$)$_2$), 3.00-3.15 (m, 18H, -N-(C**H**$_3$)$_6$), 4.00-4.85 (m, 10H, Fe-Cp-**H** and Fc-C**H**$_2$-N).

2.2.4 Reduction of 1,1'-*bis*-(Dimethylaminomethyl)Dimethylferrocene Dimethiodides

Sodium borohydride (0.363 g, 9.56 mmol) was added slowly to a stirring solution of *bis*-(dimethylaminomethyl)dimethylferrocene dimethiodide isomers (1.46 g, 2.39 mmol)

in acetonitrile (20 mL), and the reaction mixture was heated to reflux solvent and stirred for 24 hours at 110 °C. The reaction mixture was cooled to room temperature and the solvent was removed under reduced pressure and the dried product was triturated into a stirring solution of hexanes (150 mL). The hexanes solution was concentrated and passed through a plug of basic alumina to remove any remaining $NaBH_4$, and the solvent was removed under reduced pressure to yield a mixture of 1,2,1'2'-tetramethylferrocene, 1,3,1',2'-tetramethylferrocene, and 1,3,1',3'-tetramethylferrocene as an orange liquid (0.375 g, 1.55 mmol, 65% yield). ^{1}H-NMR (300 MHz, $CDCl_3$): δ 1.86-1.94 (overlapping singlets, 12H, Fc-(C**H**$_3$)$_4$), 3.72-3.83 (m, 6H, Fe-Cp-**H**).

From this point on a mixture of tetramethylferrocene isomers was used without distinction, and this mixture is referred to as tetramethylferrocenes. The use of isomerically impure tetramethylferrocene was previously determined to not significantly affect the electrochemical properties of the polymer film.[9]

2.2.5 Synthesis of (3-Bromopropionyl)tetramethylferrocenes

3-Bromopropanoyl chloride (0.85 g, 5.00 mmol) was added to a suspension of aluminum chloride (0.66 g, 5.0 mmol) in CH_2Cl_2 (20 mL) at 0 °C and stirred for one hour. The mixture was added slowly to a stirring solution of tetramethylferrocenes (1.00 g, 4.0 mmol) in CH_2Cl_2 (50 mL) at 0 °C. The resulting purple solution was stirred for 18 hours at room temperature. This solution was diluted with CH_2Cl_2 (20 mL) and poured over an equivalent volume of ice. The product was extracted with CH_2Cl_2 and the organic phase was washed with a saturated aqueous solution of $NaHCO_3$ and brine. The organic portion was filtered over $MgSO_4$ and concentrated under reduced pressure. 0.93

g of crude product mixture was obtained. Attempts to purify this compound resulted in rapid degredation of the product before analysis could be accomplished; therefore, no further analysis was performed prior to the next step in the reaction sequence.

2.2.6 Reduction of (3-Bromopropionyl)tetramethylferrocenes

Borane-*tert*-butylamine complex (0.65 g, 7.40 mmol) in CH_2Cl_2 (10 mL) was added to a suspension of aluminum chloride (0.49 g, 3.70 mmol) in CH_2Cl_2 (20 mL) at 0 °C. After the mixture was stirred for one hour, the 3-(tetramethylferrocenyl)propanoyl bromide product from the previous reaction (0.93 g) in CH_2Cl_2 (10 mL) was added slowly over 15 min. The resulting solution was stirred for 18 hours at room temperature under a slow stream of nitrogen gas. The reaction mixture was hydrolyzed with water for one hour and extracted with CH_2Cl_2. The crude product was purified using a column of flash silica with CH_2Cl_2 as the eluent. The solvent was removed under reduced pressure to afford 3-(bromopropyl)tetramethylferrocenes as a red liquid (0.43 g, 1.20 mmol, 48% yield). ^{1}H-NMR (300 MHz, $CDCl_3$): δ 1.75 - 1.95 (overlapping singlets, 12H, Fc-(C**H**$_3$)$_4$), 1.90 (m, 2H, CH_2-C**H**$_2$-CH_2), 2.05-2.50 (m, 2H, Fc-C**H**$_2$-CH_2), 3.33-3.59 (m, 2H, CH_2-C**H**$_2$-Br), 3.50 - 3.70 (m, 5H, Fe-Cp-**H**).

2.2.7 Synthesis of $FcMe_4$-C_3-LPEI

Tetramethylferrocene-modified linear poly(ethylenimine) (LPEI) was prepared according to a previously reported procedure.[9] LPEI (0.14 g, 3.25 mmol) was dissolved in a mixture of acetonitrile and methanol (10:1, 10 mL) and heated to reflux the solvent. 3-(Bromopropyl)tetramethylferrocenes (0.20 g, 0.60 mmol) in methanol (1 mL) were added

to the refluxing LPEI solution. The reaction mixture was stirred for 24 hours at reflux. The solvent was removed under reduced pressure and the product was extracted using diethyl ether to remove any excess starting material. The final polymer was determined to be ca. 17% substituted by ^{1}H-NMR analysis, which was consistent with the polymer previously described.[9]

2.2.8 Electrode Film Preparation

Glassy carbon (3 mm diameter stationary disc) electrodes were cleaned before use by polishing them successively on three grades of alumina (5, 1, 0.3 μm) and washing thoroughly with Nanopure water after each polishing step. Electrode films were prepared by cross-linking $FcMe_4-C_3-$LPEI in the presence of GOx to form enzymatic redox hydrogels: 14 μL of polymer solution (12 mg/mL $FcMe_4-C_3-$LPEI in DI water), 6 μL of glucose oxidase solution (2-24 mg/mL in DI water), and 0.75 μL of EGDGE solution (1%-30% v/v) were mixed together and 3 μL aliquots were coated onto the glassy carbon electrode surface using an Eppendorf pipette. The mixture was allowed to cure for 18-24 hours under ambient conditions. Films used for variable GOx loading experiments were prepared with 10% vol/vol EGDGE solutions. Films used for variable cross-linking experiments were prepared with 13 mg/mL GOx solutions. The mole percent EGDGE was calculated using the mass-average molar mass of the $FcMe_4-C_3-$LPEI polymer (223.3 g/mol). For experiments on carbon felt electrodes, electrode films were prepared similarly: 224 μL of polymer solution (12 mg/mL $FcMe_4-C_3-$LPEI in DI water), 96 μL of GOx solution (13 mg/mL in DI water), and 12 μL of EGDGE solution (4.26% vol/vol in DI water) were mixed together and 3 - 200 μL aliquots were coated onto carbon felt

electrode surfaces.

It should be noted that the curing conditions of the electrode films were not strictly controlled, and therefore fluctuations in the exact temperature, air flow, and humidity, likely occured. This did not appear to significantly affect the electrochemical performance of the films, with the exception of humidity extremes. Significant decreases in J_{max} were observed when films were cured below 15% humidity or above 50% humidity.

2.2.9 Electrochemical Measurements

Constant potential experiments and cyclic voltammetry were performed with a CH Instruments Model 832 bipotentiostat. Unless otherwise noted, experiments utilizing the potentiostat were conducted using a three-electrode cell configuration with a saturated calomel reference electrode (SCE), and a platinum wire counter electrode with phosphate buffered saline (PBS, 2.0 M, pH 7.4) as the background electrolyte unless otherwise noted. Constant temperature (25 $\pm$ 1 °C) was maintained during the experiments by using a water-jacketed electrochemical cell connected to a circulating water bath. Cyclic voltammetry experiments were performed at a scan rate of 50 mV/sec unless otherwise noted. Constant potential experiments were performed at +0.05 V relative to the peak oxidation potential, E_{ipa}, of each film. Variable pH measurements were performed in 0.05 M sodium phosphate buffer that was tuned to the required pH at 25 °C.

2.2.10 Carbon Felt Electrode Experiments

Carbon felt electrodes were cut into 3 cm $\times$ 0.5 cm strips and were coated with parafin wax so that only a 0.5 cm $\times$ 0.5 cm (0.25 cm^2) area was exposed. Electrodes

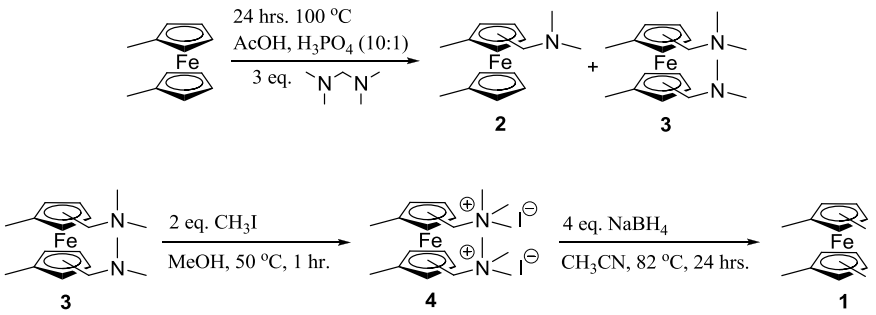

Figure **2.2**: Synthetic scheme for tetramethylferrocenes (**1**).

were coated with various amounts of electrode film solution (3 μL, 5 μL, 10 μL, 20 μL, 50 μL, 100 μL or 150 μL) and allowed to cure for 48 hours at 25 °C prior to use.

2.3 Results and Discussion

2.3.1 Synthesis of $FcMe_4$-C_3-LPEI

Tetramethylferrocene (**1**) was synthesized using a sequence of reactions that was previously described in which 1,1'-dimethylferrocene was reacted with N,N,N',N'-tetramethylmethanediamine in a mixture of acetic and phosphoric acid to afford a mixture of 1,1'-*bis*-dimethylaminomethyl-dimethylferrocene isomers (**3**).[9] The mixture of **3** was methylated with iodomethane to form the *bis*-methylammonium iodide salt (**4**) which was reduced using $NaBH_4$ to a mixture of tetramethylferrocene isomers.[9]

Previous methods for attaching a three-carbon spacer to ferrocene species were accomplished by Friedel-Crafts acylation with 3-chloropropionyl chloride and $AlCl_3$ to give 3-chloropropionylferrocene, which was reduced using trifluoroacetic acid/sodium boro-

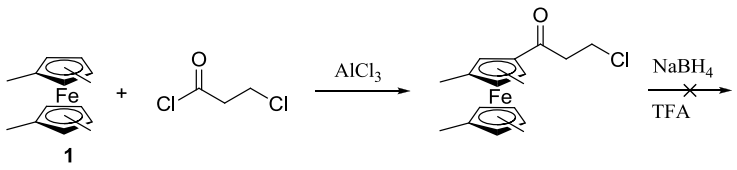

hydride to yield (3-chloropropyl)ferrocene. A Finkelstein reaction was performed using sodium iodide to substitute the ferrocene propylchloride to the corresponding iodide, thus providing a better leaving group during the subsequent attachment to the polymer backbone. However, attempted reduction of (3-chloropropionyl)tetramethylferrocene resulted with an insoluble brown sludge. The apparent degradation of tetramethylferrocene was presumed to be caused by the harsh conditions used for the reduction.

The only published synthetic procedure for (3-bromopropionyl)tetramethylferrocenes (**6**), shown in **Figure 2.3**, involves a Villsmeier-Haack formylation of **1** with $POCl_3$ in DMF to generate tetramethylferrocenecarboxaldehydes, which were used in a Wittig reaction with ethyl bromoacetate and triphenylphosphine to give ethyl 3-tetramethylferrocenylpropenoate. The ferrocenylpropenoate undergoes a two-step reduction with lithium aluminum hydride, then Pd/C and hydrogen gas to give (3-hydroxypropyl)-tetramethylferrocenes. Finally, (3-hydroxypropyl)tetramethylferrocene is reacted with phosphorus tribromide to convert the terminal alcohol into an alkyl bromide. This procedure results in 1.2% yield over five steps.[9]

In an attempt to provide a more efficient route to (3-bromopropyl)tetramethylferrocenes, an alternative synthesis was adapted from Metay *et al.* in which a Friedel-Crafts acylation was performed with 3-bromopropionyl chloride to circumvent the need for halogen exchange, and a mixture of aluminum chloride/*tert*-butylamine-borane is

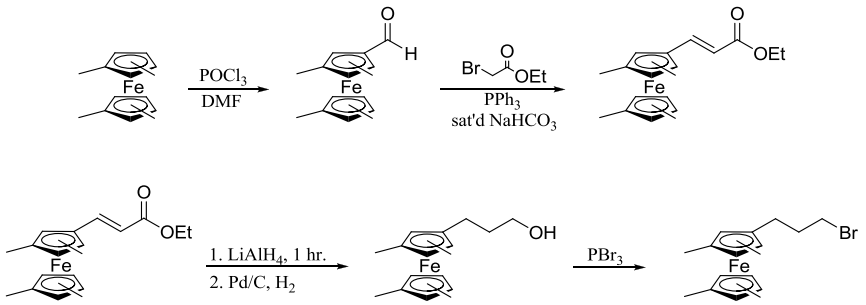

Figure **2.3**: Synthetic scheme for (3-bromopropyl)tetramethylferrocenes, as reported by Meredith *et al.*[9]

used as a much milder reducing agent.[94] Using this synthetic pathway, shown in **Figure 2.4**, (3-bromopropionyl)tetramethylferrocenes (**6**) was produced with a yield of 70% over two steps. The ferrocene moiety was then attached to the backbone of LPEI by nucleophilic substitution to give $FcMe_4$-C_3-LPEI.

2.3.2 Effects of Variable Cross-Linking Concentration

Once an efficient synthetic route to $FcMe_4$-C_3-LPEI was reached, studies of the characteristics of cross-linked $FcMe_4$-C_3-LPEI/GOx films were begun. The degree of cross-linking in analogous osmium-containing redox hydrogels has long been known to affect the electrochemical potential and electron transport characteristics of their corresponding films.[51,95,96] To this point however, an extensive study on the effects of cross-linking on ferrocene-modified LPEI films has not been performed.[96] Cyclic voltammetry was used to determine the peak oxidative (E_{ipa}), peak reductive (E_{ipc}), and half-wave ($E_{1/2}$) potentials of electrode films with varying degrees of cross-linking; the results are shown in **Figure 2.5**. The degree of cross-linking is described in terms of the number of moles

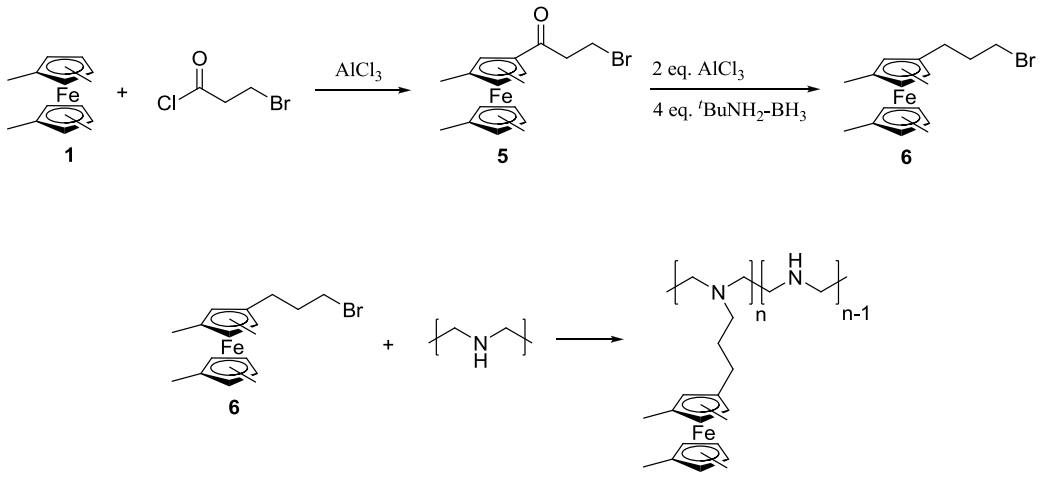

Figure **2.4**: Synthetic scheme for the synthesis of $FcMe_4$-C_3-LPEI used in this work.

EGDGE per number of polymer repeat units. It should be noted that each molecule of EGDGE contains two epoxide rings which react with two amines of the polymer backbone. Therefore, the addition of >50 mol% EGDGE is in excess of the amount required for complete cross-linking of the polymer film. An increase in $E_{1/2}$ is observed for $FcMe_4-C_3-$LPEI/GOx films as they become more cross-linked from 0.07 $\pm$ 0.02 V in films with 4 mol% EGDGE to 0.122 $\pm$ 0.003 V in films with 32 mol% EGDGE.

Electrochemical oxidation of ferrocene within a hydrogel requires the diffusion of counter-ions into the film to maintain electroneutrality, and high degrees of cross-linking in redox hydrogels have been previously shown to correlate to a restriction in counter-ion mobility.[60] So it is conceivable that limitations in counter-ion mobility could induce an electrochemical impedance to account for the shift in redox potential. To determine whether some shift in potential was caused by counter-ion impedance, the redox potential of the $FcMe_4$-C_3-LPEI/GOx films was monitored in series of counter-ions with

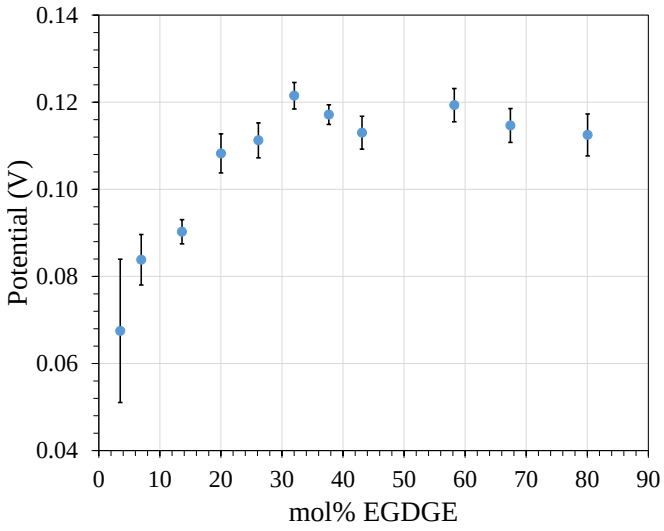

Figure **2.5**: Plot of $E_{1/2}$ versus the degree of cross-linking of $FcMe_4$-C_3-LPEI/GOx (32 wt%) with EGDGE. Data set was determined from CVs that were run at 0.05 V/sec on 3 mm glassy carbon electrodes using 2 M PBS, pH 7.4, 25 °C. All potentials are vs. SCE, and error bars represent one standard deviation, $n = 3$.

varying Stokes radii. The Stokes radius refers to the effective hydrated radius of an ion and therefore accounts for ion size as well as solvent coordination effects.[97] However, examination of anionic Stokes radius versus $E_{1/2}$ of the ferrocene mediator, shown in **Figure 2.6**, indicates that counter-ion mobility is not a limiting factor.[98] If counter-ion impedance were causing a shift in $E_{1/2}$, it would be expected that a larger anionic Stokes radius should exacerbate any impedance effects and cause an increase in $E_{1/2}$. **Figure 2.6** shows a slight inverse correlation between $E_{1/2}$ and anionic radius. However, changing anionic radius only shifts $E_{1/2}$ by a maximum of 10 mV. This small shift in potential indicates that the counterion size has little effect on $E_{1/2}$ of the mediator.

Previous work done by Benito *et al.* has shown that large changes in ferrocene redox potential can be accounted for by their proximity to ammonium cations. The redox potential of ferrocene increases in the presence of protonated amines due to electrostatic

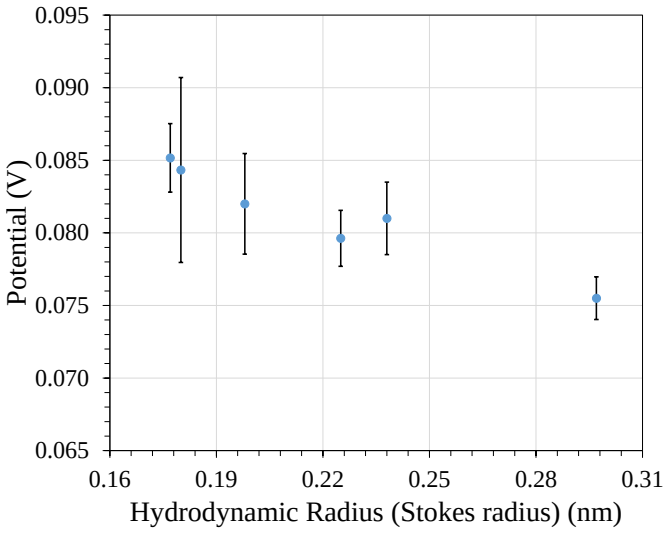

Figure **2.6**: Plot of $E_{1/2}$ of $FcMe_4{-}C_3{-}$LPEI/GOx versus hydrodynamic (Stokes) radius of the counteranion. $E_{1/2}$ was determined by performing CVs of $FcMe_4{-}C_3{-}$LPEI/GOx films in electrolytes containing anions of varying size; sodium salts of (smallest to largest) NO_3^-, Cl^-, Br^-, I^-, $H_2PO_4^-$, and BF_4^- were used as electrolytes at 25°C. All potentials are vs. SCE, and error bars represent one standard deviation.

repulsion between the two cations as shown in **Figure 2.7** (where $E_+ > E_\circ$).

The difference in these two potentials is inversely proportional to the distance between the iron center of ferrocene and the nitrogen atom of the amine such that,

$$\Delta E = \frac{z_a z_b e^2 N_A}{4\pi\varepsilon_o\varepsilon F}\frac{1}{jn}\sum_j\sum_i\frac{1}{r_{ji}} \tag{2.3}$$

where ΔE is the difference in potentials between ferrocene near protonated amines (E_+) and ferrocene near the corresponding unprotonated amines ($E_\circ$), z_a is the charge of oxidized ferrocene, z_b is the charge of a protonated amine, ε is the macroscopic permittivity of the medium, and r_{ji} is the average distance between all ferrocene redox centers (j) and all protonated amine sites (i).[99] If we assume that $E_\circ$ for the ferrocene moieties in $FcMe_4$-C_3-LPEI/GOx films is approximately equivalent across the range of cross-linking

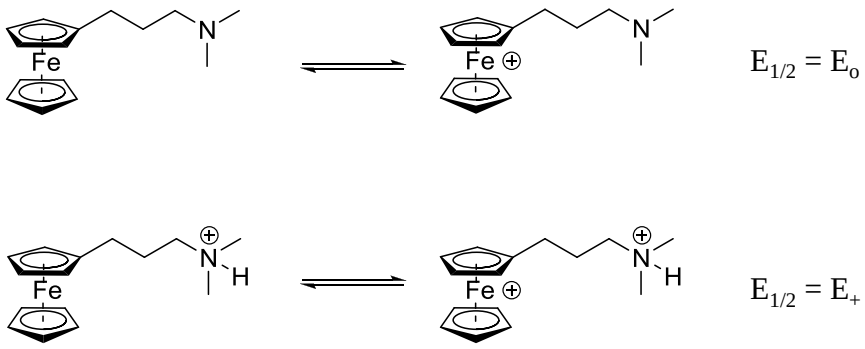

Figure **2.7**: Schematic highlighting the shift in redox potential of ferrocene in the presence of an ammonium ion.

states studied, then the change in redox potential can be entirely attributed to fluctuations in the average distance between ferrocene centers and protonated ammonium sites on the LPEI backbone, as described by the proportionality, $E_{1/2} \propto \frac{1}{r_{ji}}$. Limitations in film swelling associated with increasing degrees of cross-linking leads to an increase in r_{ji} and thus may lead to an electrostatic repulsion between protonated sites on the polymer backbone and the oxidized form of the ferrocene mediator. This repulsion increases the electrochemical potential necessary to facilitate the oxidation of ferrocene. These findings are consistent with previous observations of osmium-mediated redox polymers.[95,96]

Enzyme-modified electroactive polymer films can be described in terms of an apparent electron diffusion coefficient (D_e) which can be calculated using chronocoulometry, chronoamperometry, step potentiometry or cyclic voltammetry if the concentration of the redox species or the film thickness is known.[51,100–102] However, the determination of these values is complicated because redox hydrogels can swell up to several times their original volume upon oxidation of the electroactive species.[96] The diffusion coefficient

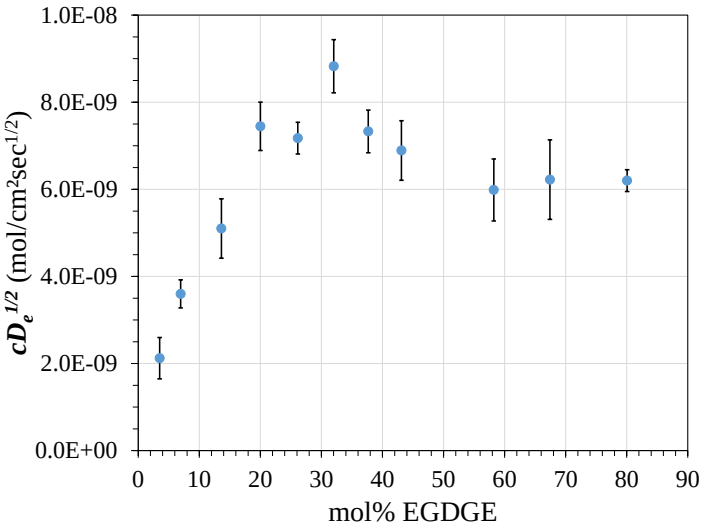

Figure **2.8**: Plot of relative electron diffusion coefficient ($cD_e^{1/2}$) as a function of the extent of film cross-linking. Data set was determined from CVs that were run at 0.05 V/sec in 2 M PBS, pH 7.4, 25 °C. $cD_e^{1/2}$ was calculated using the Randles-Sivcek equation from CVs. All potentials are vs. SCE, and error bars represent one standard deviation, $n = 3$.

in these cases is reported as a relative electron diffusion ($cD_e^{1/2}$) in terms of the concentration of the redox species (c). Calculation of $cD_e^{1/2}$ was done with cyclic voltammetry using the Randles-Sivcek equation;

$$cD_e^{1/2} = \frac{i_p(RT)^{1/2}}{0.4463nF^{3/2}A\nu^{1/2}} \tag{2.4}$$

where i_p is the peak anodic current, R is the gas constant, T is the absolute temperature, n is the number of electrons transferred in a single redox process, F is Faraday's constant, A is the electrode surface area, and ν is the scan rate in V/sec. A plot of $cD_e^{1/2}$ versus degree of cross-linking is shown in **Figure 2.8**.[102–104]

The relative electron diffusion coefficient increases from $2.1 \times 10^{-9} \pm 0.5 \times 10^{-9}$ mol/cm^{2}sec$^{1/2}$ for films with 4 mol% EGDGE to $8.8 \times 10^{-9} \pm 0.6 \times 10^{-9}$ mol/cm^{2}sec$^{1/2}$

in films with 32 mol% EGDGE. However, $cD_e^{1/2}$ decreases to $6.9 \times 10^{-9} \pm 0.7 \times 10^{-9}$ mol/cm^{2}sec$^{1/2}$ for films with 43 mol% EGDGE. Previous studies of ferrocene-modified LPEI hydrogels have shown that the degree of cross-linking is inversely proportional to the extent of oxidative swelling exhibited by a film.[60] This decrease in swelling results in a smaller average intersite distance and a higher local redox mediator concentration and thus $cD_e^{1/2}$ increases. Several reports also show that limited swelling capability of the film, caused by higher degrees of cross-linking, restricts segmental motion of the electroactive ferrocene species to the extent that some ferrocene moieties become electrochemically isolated.[60,95] In films containing greater than 32 mol% EGDGE, restriction of segmental motion of the ferrocene-containing side chains becomes more significant than increased effective ferrocene concentration. The overall result is a decrease in $cD_e^{1/2}$ of films prepared with more than 32 mol% EGDGE.

The maximum current densities (J_{max}) and Michaelis constants (K_m) for $FcMe_4$-C_3-LPEI/GOx films with variable amounts of EGDGE were calculated from constant-potential calibration curves; the results are compiled in Table **2.1**. The apparent J_{max} reaches a maximum of 1043 ± 39 μA/cm^2 with 14 mol% EGDGE and generally decreases with higher EGDGE concentrations. K_m does not significantly change as a function of EGDGE concentration, which indicates that any conformational restrictions induced by higher degrees of cross-linking do not affect the apparent binding affinity of glucose to GOx. There is a lack of apparent correlation between $cD_e^{1/2}$ and J_{max}, which suggests that electron diffusion is not the limiting step, but rather a decrease in substrate diffusion is likely limiting J_{max} in films with higher EGDGE concentration. Because the overall goal is to increase the current generated in the presence of glucose (ie increase J_{max}),

mol% EGDGE	$E_{1/2}$ vs SCE (V)	$cD_e^{1/2}$ (mol/cm^{2}sec$^{1/2}$)	J_{max} (μA/cm^2)	K_m
4	0.068 ± 0.016	$2.1 \times 10^{-9} \pm 0.5 \times 10^{-9}$	571 ± 133	11.0 ± 0.9
7	0.084 ± 0.006	$3.6 \times 10^{-9} \pm 0.3 \times 10^{-9}$	669 ± 83	10.2 ± 0.7
14	0.090 ± 0.003	$5.1 \times 10^{-9} \pm 0.7 \times 10^{-9}$	1043 ± 39	11.0 ± 1.0
20	0.108 ± 0.004	$7.4 \times 10^{-9} \pm 0.6 \times 10^{-9}$	635 ± 91	11.9 ± 0.5
26	0.111 ± 0.004	$7.2 \times 10^{-9} \pm 0.4 \times 10^{-9}$	519 ± 94	13.0 ± 3.0
32	0.122 ± 0.003	$8.8 \times 10^{-9} \pm 0.6 \times 10^{-9}$	770 ± 87	12.2 ± 0.4
38	0.117 ± 0.002	$7.3 \times 10^{-9} \pm 0.5 \times 10^{-9}$	539 ± 22	12.0 ± 1.0
43	0.113 ± 0.004	$6.9 \times 10^{-9} \pm 0.7 \times 10^{-9}$	366 ± 80	11.0 ± 2.0
58	0.119 ± 0.004	$6.0 \times 10^{-9} \pm 0.7 \times 10^{-9}$	344 ± 29	10.0 ± 1.0
80	0.113 ± 0.005	$6.2 \times 10^{-9} \pm 0.3 \times 10^{-9}$	272 ± 19	8.0 ± 2.0

Table **2.1**: Effects of variable cross-linking on the electrochemical and apparent enzyme kinetics of $FcMe_4$-C_3-LPEI/GOx films. Experiments were performed using a 2 M PBS buffer, pH = 7.4, at 25 °C . Error is reported as ± standard deviation is reported, where $n = 3$.

the use of 14 mol% EGDGE resulted in the optimum amount of cross-linking and was used throughout the remainder of this work.

2.3.3 Effects of pH Variation

The effects of pH variation on $cD_e^{1/2}$ and on $E_{1/2}$ were determined using CV data; the results are shown in **Figure 2.9**. No net change in $cD_e^{1/2}$ is observed as the pH is varied from 4.0 to 8.0. However, $E_{1/2}$ decreases linearly from 0.118 ± 0.003 V at pH 8.0 to 0.073 ± 0.004 V at pH 4.0.

This result is counter to what might be expected for ferrocene-modified amine polymers for the electrostatic considerations described by *Benito et al.*.[99] As discussed earlier, previous studies on similar model compounds have shown that coulombic interactions between ferrocene and a cationic ammonium species causes an increase in $E_{1/2}$ of the ferrocene species, such that $E_{1/2} \propto \frac{1}{r_{ij}}$. For the model compound studied previously, it was shown that a lower pH results in an increase in the frequency of protonated ammo-

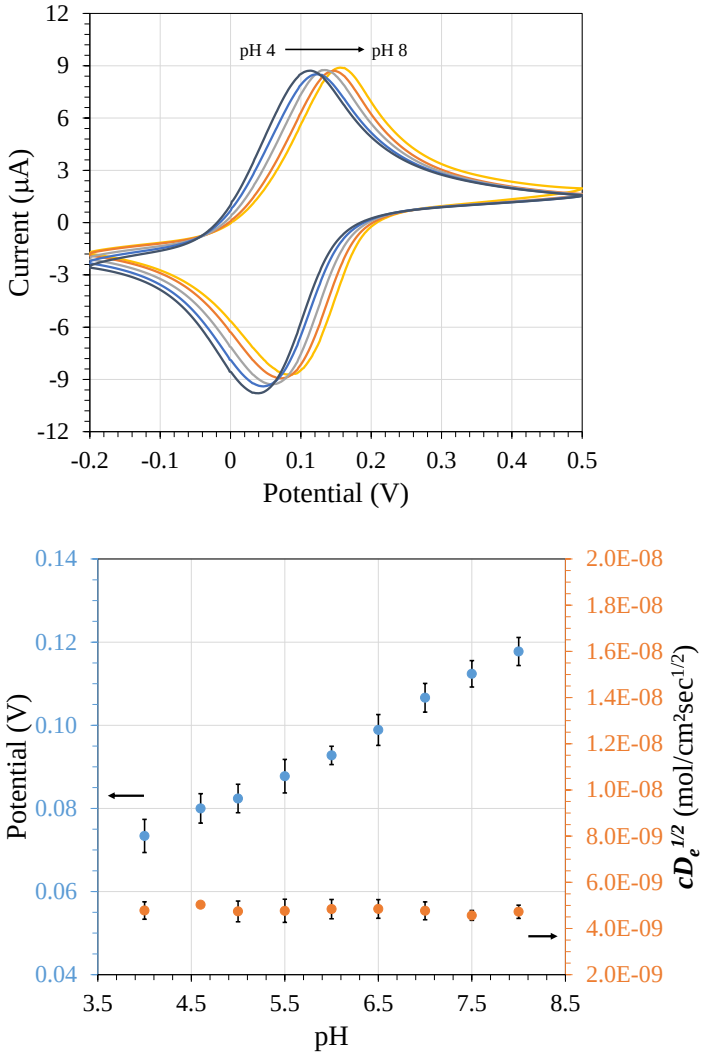

Figure **2.9**: CVs of $FcMe_4{-}C_3{-}$LPEI/GOx films at varying pH (yellow = pH 8.0, orange = pH 7.0, grey = pH 6.0, light blue = pH 5.0, dark blue = pH 4.0) (top) and a plot of $E_{1/2}$ and $cD_e^{1/2}$ as a function of pH; both calculated from CVs of $FcMe_4{-}C_3{-}$LPEI/GOx (32 wt%) cross-linked with EGDGE (14 mol%) at varying pH (bottom) using 0.05 M phosphate buffer at 25 °C. Error bars represent one standard deviation from the average, $n = 4$.

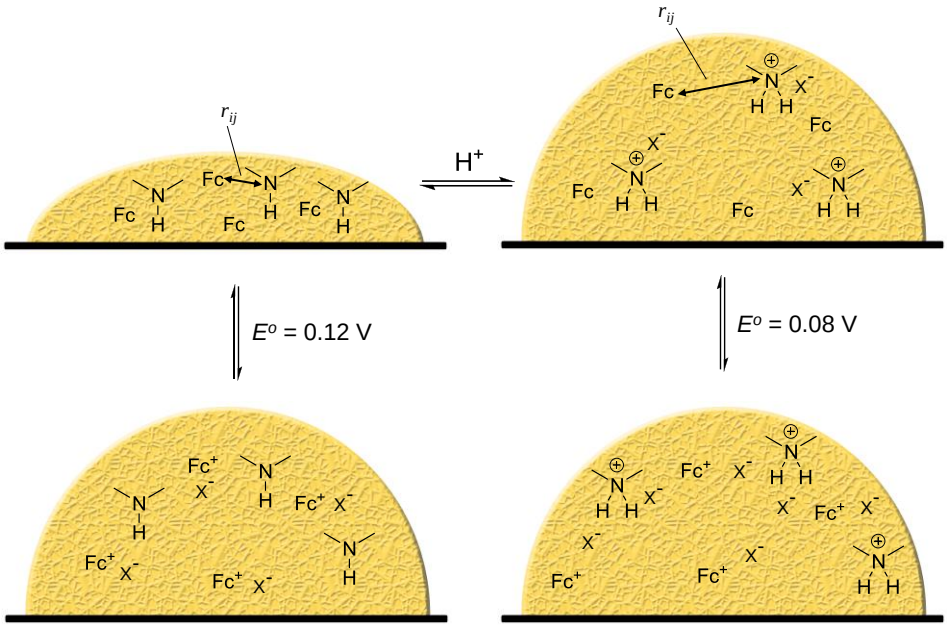

Figure **2.10**: Illustration of $FcMe_4$-C_3-LPEI film swelling as a function of pH and its effect on redox potential.

nium species, and therefore resulted in an increase in the redox potential of the ferrocene species.[99] In the $FcMe_4$-C_3-LPEI/GOx films studied in this work, we see that a decrease in the pH results in a lower redox potential, however this is not necessarily mutually exclusive to the findings reported on the model compounds.

It has been shown for similar ferrocene-modified LPEI hydrogels that at low pH, LPEI swells to several times its original volume.[60] As pH decreases, and more of the backbone amines of LPEI become protonated, swelling is caused by an influx of counter-ions to maintain electroneutrality.[95,96] The observed decrease in $E_{1/2}$ at lower pH indicates that hydrogel swelling allows for an increase in r_{ji} such that the electrostatic repulsion between neighboring cationic species is smaller in the swollen film than it is in the condensed film, as illustrated in **Figure 2.10**.

While it may seem to be mathematically contradictory for Equation **2.3** to result in an apparent negative ΔE, this is possible because LPEI is a self-buffering system in which a significant portion of the backbone is protonated even at a neutral pH. Therefore, the observed ΔE is not actually negative but rather approaches an absolute minimum value that corresponds to a chemical environment in which the ferrocene moiety experiences no coulombic impedance.

Further evidence for this model can be drawn from a solution study of $E_{1/2}$ of an analogous polymer with variable pH. $FcMe_4$-C_3-LPEI undergoes rapid thermal oxidation and subsequent decomposition when in solution at the low pH required for this study. Therefore, an analogous polymer was used for which the ferrocene moieties were unmethylated, Fc-C_3-LPEI, that is less prone to oxidative decomposition. When in the solution phase, the polymer is approximately homogeneous and the induced electrostatic interactions negligible. The polymer therefore behaves similarly to the model compounds described by Benito *et al.*, so that the ferrocene redox potential increases at lower pH, as shown in **Figure 2.11**.[99]

The effect of pH on apparent enzyme activity was determined by measuring the current response of electrode films at various pHs in near saturating glucose conditions; the results are shown in **Figure 2.12**. Current response of $FcMe_4$-C_3-LPEI/GOx films to 100 mM glucose increases rapidly between pH 4.0 and 6.5 and does not change between pH 6.5 and pH 8.0 with current densities ranging from 71 $\pm$ 19 $\mu A/cm^2$ at pH 4.0 to 560 $\pm$ 100 $\mu A/cm^2$ at pH 6.5. Maximum apparent enzyme activity is observed above a threshold pH at 6.5. However, GOx is increasingly inhibited as the pH is lowered beyond this threshold. The inhibition does appear to be completely reversible. Previous work

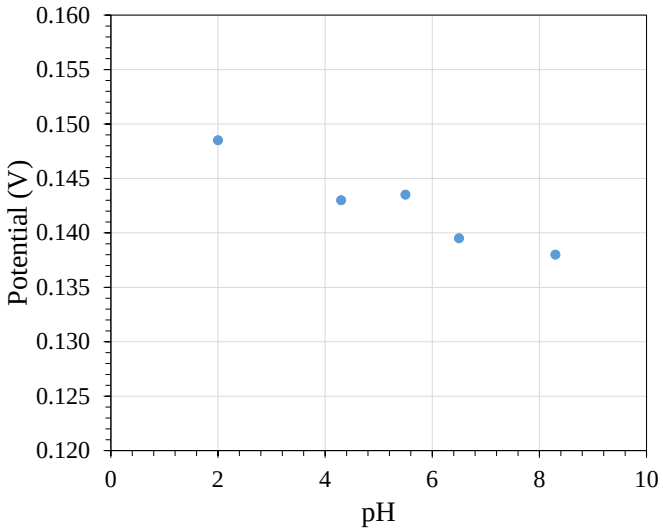

Figure **2.11**: Plot of $E_{1/2}$ of Fc-C_3-LPEI in solution versus pH. $E_{1/2}$ values were determined from CVs of Fc-C_3-LPEI using 0.05 M phosphate at 25 °C at varying pHs with a scan rate of 0.05 V/sec. Phosphoric acid was added to reach the desired pH. Potentials are versus SCE.

by Saveant has shown that the mediated pH profile of GOx can vary slightly with the use of different ferrocene mediators. However, the findings here are consistent with the pH range described in previous reports.[105]

2.3.4 Carbon Felt Electrode Film Loading

Carbon felt electrodes (CFE) have been studied previously for uses in environmental treatment and catalysis due to their high porosity and surface area.[106–108] However, its use as a fuel cell material has been limited.[109,110] Previous characterization of CFEs has shown them to have specific surface areas as high as 22700 m^{-1} with a porosity of 0.98.[111] In addition to a large surface area, the highly porous 3D structure allows for significantly higher polymer loading capacity per gross geometric area. Apparent and calculated current density responses of $FcMe_4$-C_3-LPEI/GOx films to 100 mM glucose

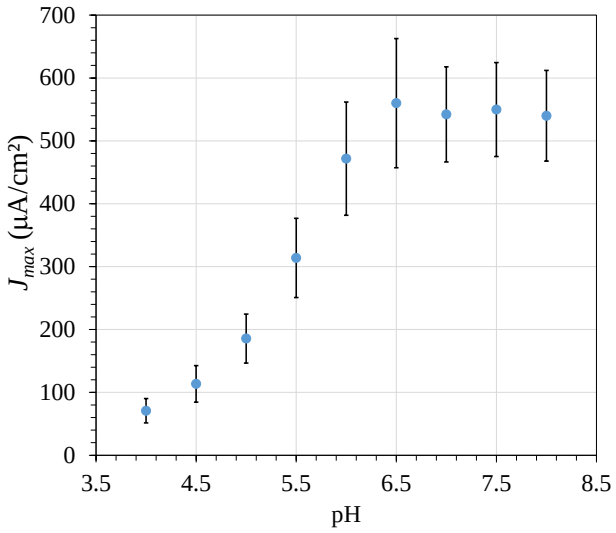

Figure **2.12**: Current density response of $FcMe_4$-C_3-LPEI/GOx (32 wt%) films to 100 mM glucose at varying pH. Films were cross-linked with EGDGE (14 mol%), and responses using 0.05 M phosphate were determined by constant potential amperometrically at 25 °C. Error bars represent one standard deviation, $n = 4$.

at various film loading volumes is shown in **Figure 2.13**.

Apparent J_{max} increases as a function of $FeMe_4$-C_3-LPEI/GOx film solution loading density from 1.4 ± 0.3 mA/cm^2 with 3 μL/cm^2 of film solution to 15.1 ± 0.8 mA/cm^2 with 150 μL/cm^2 of film solution. Film loading was eventually limited by the physical saturation of the carbon felt material, and solution loading greater than 150 μL resulted in the loss of solution to dripping from the electrode before having a chance to cure.

When using high-surface area electrodes it is often desirable to examine the maximum current response with respect to the true electrode surface area as well as the apparent electrode area to determine scaling efficiency of the materials being used. This is done by simply dividing the current generated by the microscopic surface area of the CFEs rather than the apparent geometric area. However, upon coating CFEs with $FcMe_4$-C_3-LPEI/GOx films, it was apparent that the felt was not completely absorbing the

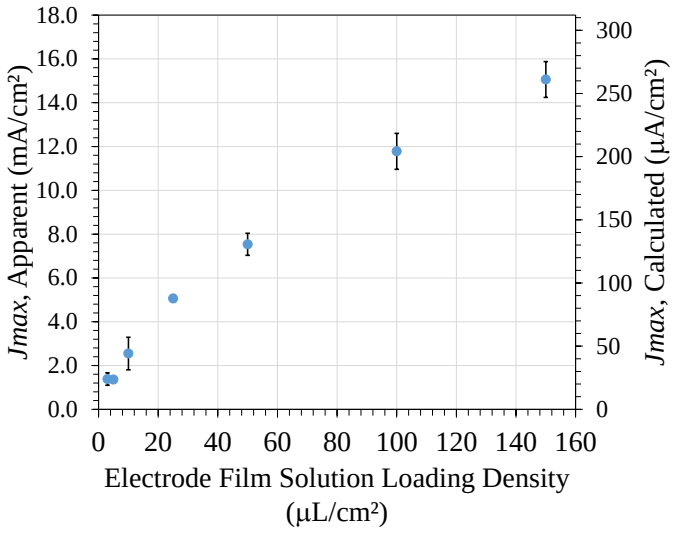

Figure **2.13**: Current density response of $FcMe_4$-C_3-LPEI/GOx (32 wt%) films in 100 mM glucose at varying film solution loadings. Films were cross-linked with EGDGE (14 mol%), and responses were determined using 2 M PBS, pH 7.4 at 25 °C by constant potential amperometry. Error bars represent one standard deviation, $n = 3$.

aqueous polymer solution and that only a fraction of the actual surface area was being utilized. Therefore, the specific area of the CFEs was not useful in determining the real J_{max}. To determine the coated surface area of the CFEs, the Randles-Sevcik equation was rearranged to solve for the electrode area, A;

$$A = \frac{i_{pa}(RT)^{1/2}}{0.4463nF^{3/2}v^{1/2}cD_e^{1/2}} \qquad (\mathbf{2.5})$$

It was assumed that the electron diffusion kinetics of the $FcMe_4$-C_3-LPEI/GOx films on GCEs and CFEs are approximately equivalent, so that the value of $cD_e^{1/2}$ (determined above) could be used to calculate the average coated surface area of GCEs to be 14.4±0.8 cm^2. The resulting values for calculated J_{max} are shown in **Figure 2.13** (right y-axis). The calculated J_{max} for $FcMe_4$-C_3-LPEI/GOx films is decreased from 1035 ± 97 $\mu A/cm^2$ on GCEs (coated surface area = 0.071 cm^2) to 261 ± 14 $\mu A/cm^2$ on CFEs (coated

surface area = 14.4 cm^2). While this decrease in calculated J_{max} is significant, it is compensated for by the increase in surface area density that the carbon felt network provides. Additionally, this suggests that further improvements in current density are possible through improved coating methods to utilize the entire surface area of CFEs.

2.4 Conclusions

Electrochemical characterization of $FcMe_4-C_3-$LPEI/GOx films was accomplished by varying the amount of cross-linking, amount of GOx, and pH to optimize $cD_e^{1/2}$, counter-ion diffusion, and apparent enzyme activity within the film. By increasing the amount of EGDGE used for cross-linking of $FcMe_4-C_3-$LPEI/GOx films to 14 mol%, we were able to increase J_{max} from the previously reported value of 0.741 mA/cm^2 to 1.035 mA/cm^2 at 25 °C on GCEs.[9] The use of highly porous, three-dimensional CFEs allowed for the film loading densities as high as 150 $\mu L/cm^2$, resulting in current densities as high as 15.1 ± 0.8 mA/cm^2 in 25 °C 100 mM glucose at 0.13 V. Further studies are ongoing to determine the effects of temperature on the $FcMe_4-C_3-$LPEI/GOx films in terms of $cD_e^{1/2}$ and apparent enzyme kinetics, as well as more thorough characterization of CFE kinetics for use in enzymatic biofuel cells.

The optimization of $FcMe_4$-C_3-LPEI/GOx films has allowed the sterically-imposed current density limitations from the additional methyl functionalities, to be overcome. Therefore, the benefits of a lowered redox potential afforded by the addition of methyl groups to ferrocene, outweighs the steric restrictions that the methyl groups induce. Additionally, the use of carbon felt electrodes provides a means to further overcome

current density limitations so that more highly methylated ferrocene species (such as octamethylferrocene or decamethylferrocene) may be used.

Chapter 3

Enzyme Cascade for Catalyzing Sucrose Oxidation in a Biofuel Cell

3.1 Introduction

In the context of a biofuel cell, enzymes provide several advantages over their transition metal counterparts: they have a very high per-molecule activity, the ability to operate near neutral pH, and high substrate specificity. High specificity allows for mixing of the anode and cathode substrates without the possibility of fuel crossover and therefore eliminates the need for an ion-exchange separator membrane (i.e. Nafion), which increases cell resistance as well as cost. However, high substrate specificity also limits the degree of oxidation of possible fuel sources by a single enzyme and the ability to use fuel mixtures without the incorporation of multiple enzymes. The choices for fuels for enzymatic biofuel cells are effectively limited to substrates for which an isolatable redox enzyme exists. The use of only one anodic enzyme also limits the extent of oxidation of the fuel.

Much of the current research on enzymatic biofuel cells utilizes a multi-copper oxidase enzyme or platinum metal at the cathode to reduce molecular oxygen to water[1,18,20,112] and an oxidase or dehydrogenase enzyme at the anode to oxidize a small sugar[20,113] or short-chain alcohol.[20,114,115] Most redox enzymes used at the anode catalyze only a single two-electron oxidation per molecule of substrate and leave the remainder of the substrate unreacted, which limits the efficiency and energy density of the biofuel cell.[116]

Recent research has attempted to catalyze deeper oxidation of substrates through the use of immobilized enzyme cascades.[47,117–119] It was found that multiple enzymes can be immobilized at a single electrode in which the product of one enzymatic reaction can be used as a substrate for a subsequent enzymatic reaction.[114,120,121] Enzyme cascade-based bioanodes allow for deeper substrate oxidation in which multiple pairs of electrons can be extracted from one molecule of substrate, thus a larger current can be generated per molecule.

Several studies of deep substrate oxidation for enzymatic biofuel cells have examined methanol or glycerol as substrates because both can be completely oxidized using only three enzymes.[122,123] Methanol is oxidized to CO_2 using three nicotinamide adenine dinucleotide (NAD)-dependent dehydrogenases to extract six electrons, while glycerol is oxidized to CO_2 using two pyrroloquinoline quinone (PQQ)-dependent dehydrogenases and oxalate oxidase to extract twelve electrons per molecule of substrate.[114,121,124] Only a few studies have focused on larger sugar molecules as the primary substrate for an enzyme cascade-based oxidation.[47,125,126] Despite the prevalence of glucose in single-enzyme biofuel cell research, little work has been done using it as a parent substrate for deep fuel oxidation. This is because the primary oxidative pathway for glucose, glycolysis, contains only one oxidoreductase from which electrons can be transferred. Multiple alternative enzymatic pathways have been used to achieve four and six electron oxidation of glucose, however these methods are hindered by low maximum current densities (30 $\mu A/cm^2$ to 80 $\mu A/cm^2$)[47,125] and require the use of enzymes that are either genetically engineered or are otherwise not commercially available.

An alternative to more complete oxidation of glucose is the use of upstream metabolic

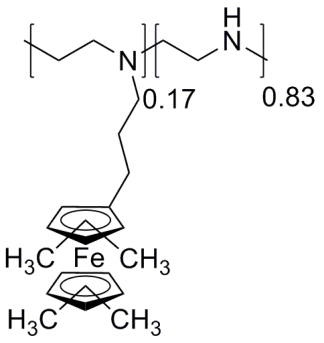

Figure **3.1**: Chemical structure of 3-(tetramethylferrocenyl)propyl-modified LPEI - ($FcMe_4$-C_3-LPEI).

targets such as sucrose. Sucrose is a common sugar (table sugar) and is a disaccharide. Amperometric sucrose biosensors have previously been reported that operate by the indirect detection of sucrose via the oxidation of fructose or glucose.[127,128] Invertase is used to hydrolyze sucrose into glucose and fructose, while either fructose dehydrogenase (FDH) or glucose oxidase (GOx) is used to oxidize fructose or glucose, respectively. This method has been successfully used in the amperometric detection of sucrose; however, the low current densities generated have limited its potential use in biofuel cells.

In the previous chapter, an optimized tetramethylferrocene-modified linear poly(ethylenimine) ($FcMe_4$-C_3-LPEI) was used to immobilize GOx for the two-electron oxidation of glucose. In this work, we demonstrate a high current density bioanode which uses invertase, FDH, and GOx that have been co-immobilized in a $FcMe_4$-C_3-LPEI film to extract four electrons from one molecule of sucrose. Cross-linked films of $FcMe_4$-C_3-LPEI, shown in Figure **3.1**, were used to both immobilize the enzymes and enhance the electrochemical communication between the enzymes and the electrode surface.[9]

The combination of the three enzymes resulted in improvement in the bioelectrode

performance compared to dienzyme (hydrolyase/oxidoreductase) electrodes. To our knowledge, this is the first use of a bioanode that employs glucose and fructose simultaneously as substrates. The effects of pH and temperature on the current density, as well as the stability of the bioanode, are examined.

3.2 Materials and Methods

3.2.1 Materials

Sucrose and D-glucose (anhydrous) were purchased from Macron Chemicals. D-Fructose was obtained from Sigma-Aldrich. Glucose oxidase from *Aspergillus niger* (EC 1.1.3.4, type X-S, 157 U/mg of solid, 75% protein) and invertase glycoprotein from *Saccharomyces cerevisiae* (EC 3.2.1.26, 332.8 U/mg of solid) were purchased from Sigma-Aldrich. Fructose dehydrogenase from *Gluconobacter sp.* (EC 1.1.99.11, Grade III, 169 U/mg of solid) was purchased from Toyobo Enzymes. Ethylene glycol diglycidyl ether (EGDGE) was purchased from Polysciences Inc., Washington, PA. All chemicals used in the synthesis of the redox polymer were purchased from Sigma-Aldrich. All chemicals were used as received unless otherwise noted. Tetramethylferrocenes and octyl-modified linear poly(ethyleneimine) (C_8−LPEI) were synthesized as previously reported.[9,129] $FcMe_4$-C_3-LPEI was synthesized as described in **Chapter** 2. Stock solutions of glucose and fructose were allowed to mutarotate for 24 hours and stored at 4°C. Toray paper electrodes were purchased from Fuel Cell Earth (190 μm thick, non-wet proof, Prod. No. TGP-H-060).

3.2.2 Electrode Fabrication

Electrode film solutions were prepared by combining aqueous solutions of $FcMe_4$-C_3-LPEI (60 μL, 12 mg/mL), enzyme mixture (25.74 μL total), and EGDGE (3.22 μL, 2 μL EGDGE per 45 μL H2O). Enzyme mixture solutions consisted of invertase (8.58 μL, 20 mg/mL), fructose dehydrogenase (8.58 μL, 13 mg/mL), and glucose oxidase (8.58 μL, 13 mg/mL) in 18 MΩcm de-ionized H_2O. Toray paper electrodes were cut into L-shapes. The connecting ends of the electrodes were coated in paraffin wax (so that the exposed geometric electrode area was 1 cm^2) to prevent wicking of the electrolyte solution to the potentiostat lead. The electrode film solutions were mixed together and vortexed for 1 minute until the solution was homogeneous, containing 1.25 mg/mL GOx, 1.25 mg/mL FDH, and 1.9 mg/mL invertase; then 25 μL of this mixture was drop-coated onto the Toray paper electrodes and evenly spread across the exposed electrode area using a plastic pipette tip. The electrodes were allowed to cure open to the atmosphere overnight at 25°C. The cured electrode films contained 15.5 wt% GOx, 15.5 wt% FDH and 24 wt% invertase with respect to the polymer weight.

For films that contained only one (or two) enzymes, the same procedure was used except the omitted component of the enzyme mixture was replaced by 8.58 μL (or 17.16 μL) of 18 MΩcm de-ionized H_2O. This was done to ensure a constant volume and relative concentration of the electrode film solution. Control experiments were performed by substituting for the $FcMe_4-C_3-$LPEI redox polymer with the non-redox active C_8-LPEI.

3.2.3 Voltammetric and Amperometric Characterization of FDH, GOX and Inv/FDH/GOx Electrodes

Electrodes were tested using a conventional three-electrode setup, and the potential was scanned from -0.2 to 0.5 V versus a saturated calomel electrode (SCE) using a platinum mesh counter electrode at 1 mV/s. CV experiments were performed using 3 mm glassy carbon electrodes as the working electrode, all other experiments were performed on 1 cm × 1 cm Toray electrodes. Experiments were performed in 50 mM citrate buffer pH 5.5 (unless otherwise stated) using a VSP Multichannel Analyzer (Biologic), a CH650 (CH Instruments) potentiostat or a DY2100 (Digi Ivy) potentiostat. Each experiment was performed in triplicate using separately constructed electrodes (n = 3). Electrodes were analyzed by allowing them to soak in a 50 mM citrate buffer solution, pH = 5.5, for 5 minutes before performing cyclic voltammetry experiments to determine the oxidation potential for each film as well as to allow them to equilibrate in solution prior to performing amperometry experiments. Amperometric studies were performed by allowing the films to reach a steady state at a potential that is +0.05 V (vs. SCE) above the peak oxidation potential (E_{ipa}) at 25 °C. The solutions were continuously stirred at 400 rpm. The charging current was allowed to dissipate for 400 s, and sequential injections from 1 M substrate solution in 50 mM citrate buffer pH 5.5 were made as current was recorded as a function of time. The substrate concentration in the bulk solution was increased by 0.5 mM (two times), 1 mM (four times), 5 mM (one time), 10 mM (one time), 30 mM (one time), 50 mM (one time) and 100 mM (one time, FDH and GOx experiments only) for determination of Michaelis-Menten kinetics. Inv/GOx film

kinetics were determined by testing the current response to each concentration of sucrose independently to allow steady state to be reached after mutarotation to minimize the effects of enzyme degradation. The substrate concentration was brought to 100 mM for the stability, temperature, pH and efficiency studies. For the stability studies, electrodes were tested once per day for 2 hours per test, and stored in buffer at 4 °C when not being used.

3.2.4 UV/Vis Invertase Assay

Invertase was immobilized at the bottom of a glass vial using C_8-LPEI. Solutions were prepared from C_8-LPEI (60 μL, 12 mg/mL), invertase (25.74 μL total), and EGDGE (3.22 μL, 2 μL EGDGE per 45 μL H_2O). Invertase solutions consisted of invertase (8.58 μL, 20 mg/mL) diluted in 17.16 μL 18 MΩcm de-ionized H_2O. The solution was mixed together and vortexed for 1 minute until the solution was homogeneous; then 25 μL of this mixture was drop-casted directly at the bottom of the vial. A total of 10 films in 10 separate vials were allowed to cure open to the atmosphere overnight at 25 °C. Each film was used to test a single sucrose concentration in the presence of invertase. Sucrose concentrations were 0, 1, 2, 3, 4, 5, 10, 20, 50 and 100 mM.

Aliquots of 450 μL of each sucrose solution was carefully injected into the vial and the solutions were incubated exactly 15 min at 25 °C. After incubation, 5 μL of the solutions were taken from the vials and added to 1495 μL of alkali-PAHBAH reagent, and the mixture was heated to 75 °C for 10 min. After the reaction of the reducing sugars was complete, 125 μL of the solutions were taken and further diluted into a cuvette with 1 cm length pathway with 1375 μL citrate buffer. Finally, the absorbance was read at

λ = 410 nm. The absorbance was reported compared to the starting concentration of sucrose used during the assay.

3.2.5 Fuel Cell Bioanode Characterization

Bioanodes were constructed as described above using 25 μL castings of $FcMe_4$-C_3-LPEI/enzymes on 1 cm × 1 cm Toray electrodes. The cathode consisted of a gas permeable ELAT electrode with 20% Pt on Vulcan XC-72 (E-Tek) pressed against the Naon NRE-212 (Sigma) polymer electrolyte membrane as reported previously.[120] Sucrose was injected during the open circuit potential (OCP) measurements into the bulk electrolyte at t = 600 s to bring the sucrose concentration of the solution to 100 mM. The OCP was allowed to reach steady state for two hours to build-up the concentration of both glucose and fructose. Slow scan polarization (1 mV/s from the measured open circuit potential to 1 mV) was used to obtain polarization and power curves by monitoring current as a function of potential. Controls were performed by omitting invertase into the bioanode or by substituting the $FcMe_4$-C_3-LPEI redox polymer with the C_8-PEI non-redox polymer. It should be noted at the outset that amperometric results are reported as current densities; this value is based on the planar geometric electrode area rather than the true microscopic surface area of the Toray paper.

3.3 Results

The first objective was to determine the function of a sucrose enzyme cascade contained in a single polymer film as a bioanode. Previously, it was shown that ferrocene-modified poly(ethylenimine) films can be used to effectively immobilize and wire GOx

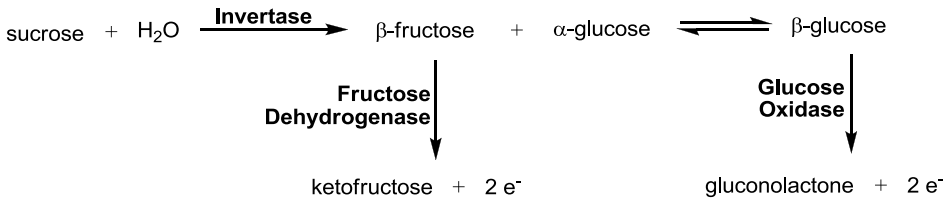

Figure **3.2**: Simplified outline of the enzymatic pathway used to extract electrons from sucrose by hydrolyzing it to fructose and glucose, and then electroenzymatically oxidizing fructose and glucose to ketofructose and gluconolactone, respectively.

onto the surface of an electrode.[8,9,59,130] Immobilization of GOx allows the oxidation of glucose to occur near the electrode surface, while the ferrocene moiety acts as a redox mediator to efficiently shuttle electrons from the flavin adenine dinucleotide (FAD) cofactor of GOx to the electrode surface. A similar approach is used in this work to immobilize three enzymes in a single polymer film; $FcMe_4$-C_3-LPEI was cross-linked with EGDGE in the presence of invertase, GOx, and FDH and coated onto a 1 cm $\times$ 1 cm Toray paper electrode. As illustrated in **Figure 3.2**, invertase is used to hydrolyze sucrose in order to form glucose and fructose, which are subsequently oxidized by GOx and FDH, respectively.

3.3.1 Sucrose Cascade Characterization

Cyclic voltammetry was used to characterize the electrocatalysis of fructose and glucose oxidation as well as the hydrolysis of sucrose by FDH, GOx, and Inv/FDH/GOx-based bioelectrodes, respectively, as shown in **Figure 3.3**. The representative CV for each bioelectrode has the same shape in the absence of substrate which is due solely to the ferrocene redox moiety, however the peak current of the FDH electrode is significantly

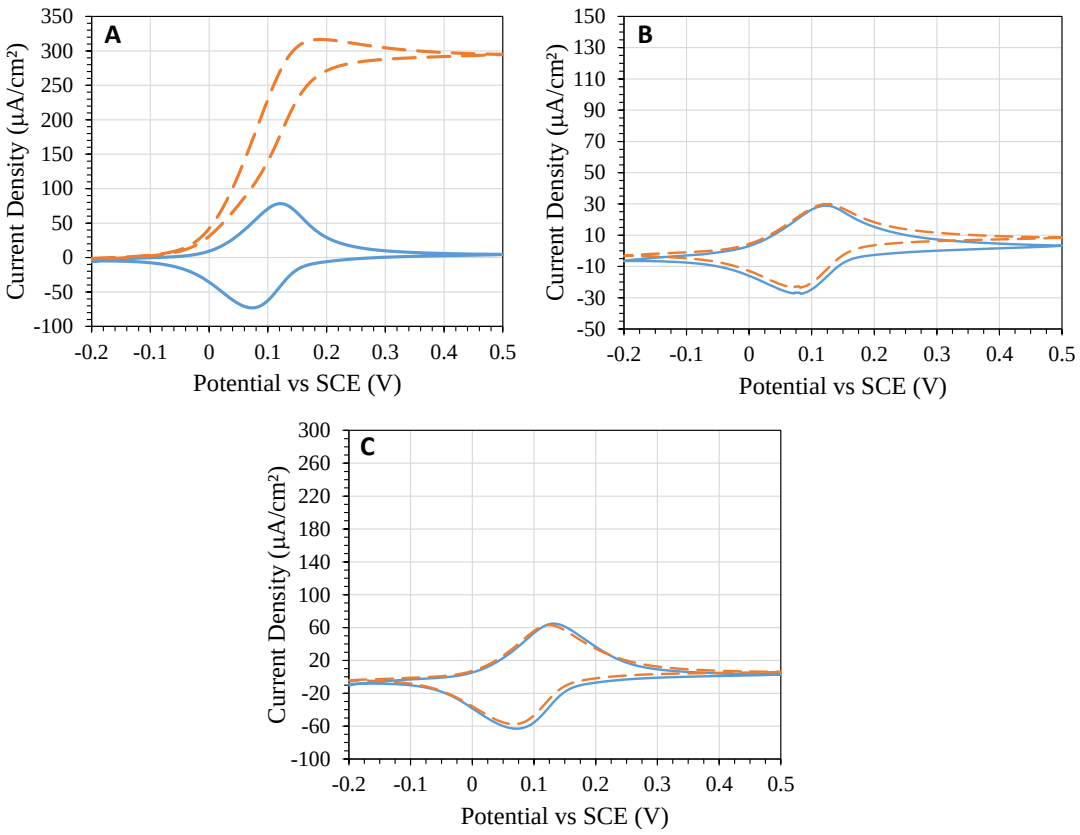

Figure **3.3**: Representative cyclic voltammograms of (A) GOx-modified electrodes in the absence (solid line) and presence (dashed line) of 100 mM glucose, (B) FDH-modified electrodes in the absence (solid line) and presence (dashed line) of 100 mM fructose, and (C) Inv/FDH/GOx-modified electrodes in the absence (solid line) and presence (dashed line) of 100 mM sucrose. Experiments were performed with 3 mm glassy carbon electrodes, and at 25 °C using a 0.05 M citrate buffer, pH 5.5, with a scan rate of 1 mV/s.

lower than that of the GOx or Inv/FDH/GOx electrodes. A visible complex forms between $FcMe_4$-C_3-LPEI and GOx when they are mixed together in solution. This complexation could cause a restriction of the polymer film swelling, thus resulting in a smaller hydrogel volume and a higher effective redox site concentration. In the absence of GOx, the FDH electrode would have a lower peak current due to a decrease in the effective redox site concentration.

Both the FDH and the GOx electrodes show an electrochemical response to the

addition of substrate. However, there is no difference between the CVs of Inv/FDH/GOx films in the presence and absence of sucrose; this is likely due to the low activity of invertase which results in a large amount of time required to produce the two substrates essential for electrooxidation at the electrodes. Additionally, previous studies have shown that invertase can be reversibly inhibited by glucose and fructose via competitive product inhibition; which could be leading to further decrease its activity.[131]

Since observed evidence of enzymatic activity using cyclic voltammetry at the Inv/FDH/GOx electrodes was limited, amperometric measurements were taken to determine kinetics parameters of both oxidoreductases and invertase. Representative amperometric traces of fructose or glucose injections for FDH or GOx-modified electrodes held at 50 mV above the potential of the peak anodic current (E_{ipa}) are shown in **Figure 3.4**, along with the corresponding calibration plots. Fast increases in oxidation current were obtained, and both enzymes displayed a Michaelis-Menten profile. For FDH- and GOx-based electrodes, apparent K_m values were determined to be 7.9 ± 0.5 mM and 18.7 ± 2.3 mM and the currents at enzyme saturation (J_{max}) were 53.2 ± 0.9 $\mu A/cm^2$ and 286.5 ± 11.0 $\mu A/cm^2$, respectively. Since invertase does not involve an electrochemical process during the hydrolysis of sucrose, bienzyme electrodes (Inv/FDH or Inv/GOx) were used to indirectly characterize the kinetic behavior of invertase. **Figure 3.5** presents the amperometric response of Inv/FDH and Inv/GOx-based electrodes to various concentrations of sucrose when held at 50 mV over E_{ipa} of the redox polymer. Unlike for the single oxidoreductase-modified electrodes, the response for Inv/FDH- and Inv/GOx-based electrodes was much slower following the addition of sucrose into the bulk solution. The calibration curves shown in **Figure 3.5** did not display a typical

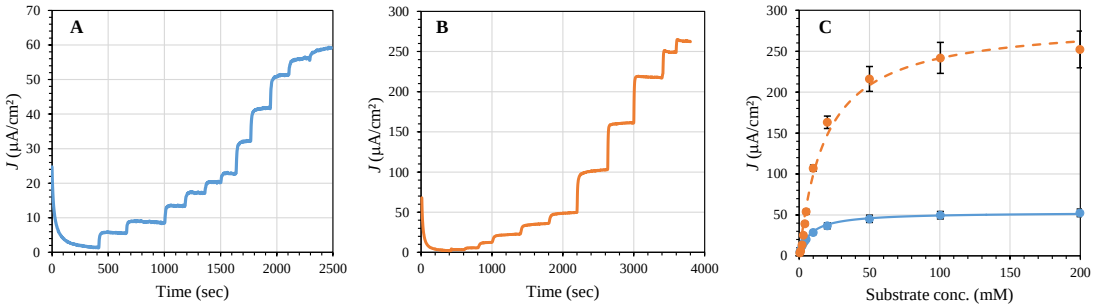

Figure **3.4**: (A)Amperometric response for FDH-modied electrodes in increasing concentrations of fructose (0-200 mM). (B) Amperometric response for GOx-modied electrodes in increasing concentrations of glucose (0-200 mM). (C) Calibration curve for FDH-modified electrodes (solid lines) and GOx-modied electrodes (dashed lines). All films were coated onto 1 cm^2 Toray paper electrodes. Experiments were performed using 50 mM citrate buffer, pH 5.5, at 25 °C (Error bars represent the standard deviation).

Michaelis-Menten response, but rather a sigmoidal response. Deviation of Inv/FDH and Inv/GOx electrodes from Michaelis-Menten behavior indicates that the presence of the invertase in the polymer matrix alters the kinetics of the overall electrode reaction.

The sigmoidal response of both bienzyme electrodes can be mathematically interpreted using the Hill equation.[132] This equation takes into account a possible cooperativity or allosteric interactions in the enzymatic activity with the substrate concentration and is defined as

$$J = J_{initial} + \Delta J \frac{x^n}{K_m + x^n} \tag{3.1}$$

where J_{intial} is the initial current density, ΔJ is the current density variation, x is the sucrose concentration, K_m is the apparent constant and n is the Hill coefficient. In the case of positive cooperativity, the enzyme activity is enhanced as the substrate

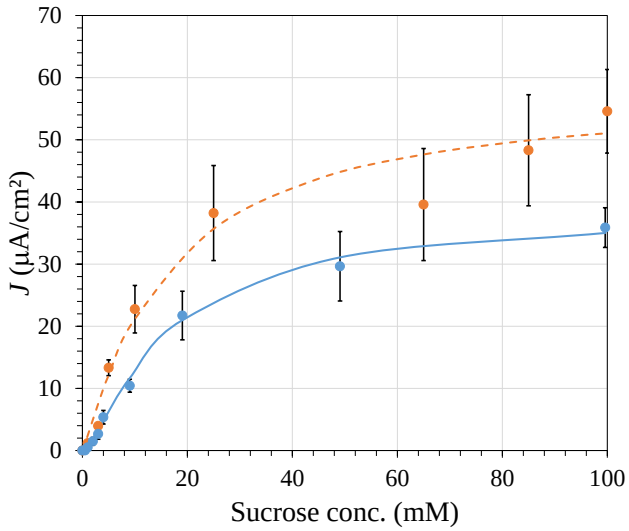

Figure **3.5**: Calibration curves for Inv/FDH-modified electrodes (solid) and Inv/GOx-modified electrodes (dashed); the lines for each represent the fitted Hill function. All films were coated onto 1 cm^2 Toray paper electrodes. Experiments were performed using 50 mM citrate buffer (pH 5.5) at 25 °C. Error bars represent the standard deviation.

concentration increases and its representation is a sigmoidal curve.[132] For negative cooperativity, its activity decreases as the substrate concentration increases. It can be claimed that a positive cooperativity occurs when invertase is an active component of electrode films based on calculated Hill coefficients of $n = 1.33 \pm 0.21$ for Inv/FDH films and $n = 1.12 \pm 0.61$ for Inv/GOx films. However, it remains unclear if this effect comes from the invertase only or from an allosteric behavior when the two enzymes are present. For the Hill coefficient to be interpreted in terms of cooperativity, an enzyme must contain multiple associated binding sites. Invertase has been shown previously to form functioning oligomers in solution,[133] therefore it is reasonable to consider that these oligomers can be present within the polymer matrix. Alternatively, the Hill coefficient can be interpreted in terms of a concerted transition model (or CT model) in which the conformation of the polymer matrix is being affected by reactions of either

of the two redox enzymes.[134] This conformational change would then be favorable for invertase so that the catalytic hydrolysis of sucrose would be slow initially, and then be enhanced as the cascade reaches a minimum activity threshold. These results are congruent with previous findings which indicate that apparent K_m for invertase changes with the concentration of substrate; a concentration threshold must be reached before efficient hydrolysis can take place.[132] UV-Vis assays performed on invertase immobilized in non-redox polymer films, C_8-LPEI, show that there is a slightly sigmoidal response even in the absence of other enzymes (**Figure 3.6**). This result indicates that the cause of the unique kinetics is due to an interfacial or conformational interaction between invertase and the PEI matrix, and that the addition of either FDH or GOx enhances this interaction. However, the exact cause of this result is not fully understood, and experiments are ongoing to determine the exact nature of the cooperativity/allostery of the immobilized cascade system.

Kinetic parameters were analyzed for both bienzyme systems; apparent K_m values were determined to be 18.1 ± 4.2 mM and 16.3 ± 1.1 mM, the currents at enzyme saturation (J_{max}) were 40.2 ± 4.3 $\mu A/cm^2$ and 57.7 ± 2.5 $\mu A/cm^2$ and the relative Hill coefficients (n) were 1.33 ± 0.21 and 1.12 ± 0.61 for Inv/FDH and Inv/GOx electrodes, respectively. Values of J_{max} for Inv/FDH-based electrodes were similar to the current density for the single FDH-based electrodes, and any variation in the J_{max} can be explained by the lower activity of invertase. However, J_{max} for Inv/GOx electrodes was much lower than J_{max} for the GOx electrodes (87% loss). This decrease may to be due to an apparent partial inhibition of GOx by fructose accumulation after sucrose hydrolysis, however this is highly speculative and further studies are ongoing to investigate this

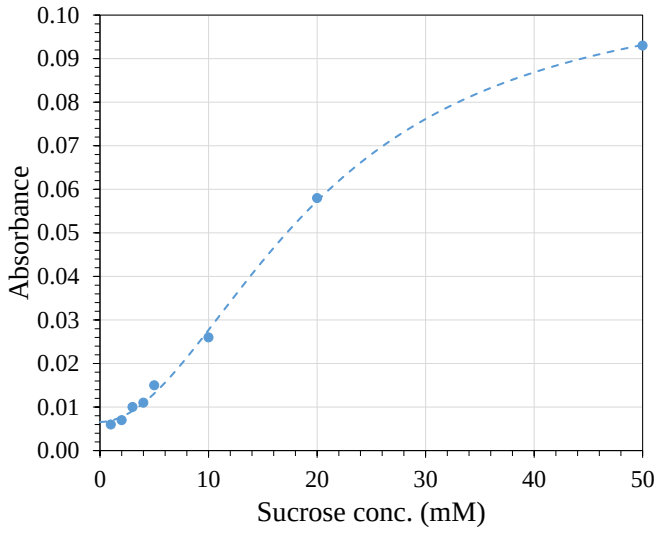

Figure **3.6**: Absorbance change at $\lambda = 410$ nm of a PAHBAH solution in presence of different concentration of sucrose first incubated for 15 min at 25 °C in presence of immobilized invertase in a C_8-LPEI hydrogel film. The dashed line represents the fitted Hill function.

result.

The amperometric response of Inv/FDH/GOx films was compared to films containing invertase and only one redox enzyme (Inv/FDH or Inv/GOx), when 100 mM sucrose was added in solution (injection at $t = 400$ s). The constant-potential amperometric results are shown in **Figure 3.7**. It is known that cross-linked $FcMe_4-C_3-$LPEI films form a hydrogel through which counter ions, substrates, and products can easily diffuse.[9] Previous studies have shown that high substrate diffusion through enzymatic electrode films constructed using $FcMe_4-C_3-$LPEI allows for a single rapid amperometric response to substrate. However, the Inv/FDH/GOx films constructed for this study displayed a current response that occurred in two distinct events: an initial increase of ca. 50 $\mu A/cm^2$ from the sucrose injection over 1000 seconds followed by a much larger subsequent increase that was observed over 5000 seconds. In the case of the Inv/FDH-based

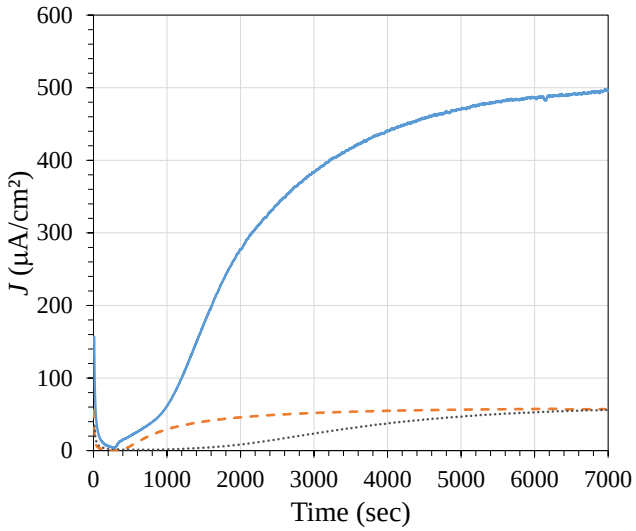

Figure **3.7**: Amperometric responses for Inv/FDH-modified electrodes (dashed line), Inv/GOx-modified electrodes (dotted line), and Inv/FDH/GOx-modified electrodes (solid line) in 100 mM sucrose solution ($t_{injection}$ = 400 sec). All films were coated onto 1 cm^2 Toray paper electrodes. Experiments were performed using 0.05 M citrate buffer, pH 5.5, at 25 °C.

electrodes, the current increased to about 50 $\mu A/cm^2$ after sucrose injection and slowly reached a steady state current over 1500 seconds. For the Inv/GOx-based electrodes, the current increased steadily over 2000 s and stabilized after 2 h incubation. These results indicate that the initial current response in Inv/FDH/GOx electrodes is a result of fructose oxidation, and the delayed current response is caused by the oxidation of glucose. Invertase catalyzes the hydrolysis of sucrose into α-D-fructose and β-D-glucose; and although FDH has a relatively high activity for both forms of fructose, GOx activity for α-glucose is only 0.64% of that for β-D-glucose.[135] Therefore, the delayed increase in current caused by glucose oxidation is likely due to the time required for thermal mutarotation from α-D-glucose to β-D-glucose. It should also be noted that slow current responses indicate the Inv/FDH/GOx film requires a significantly longer amount of time to reach steady state than was expected. The amperometric responses of Inv/FDH/GOx

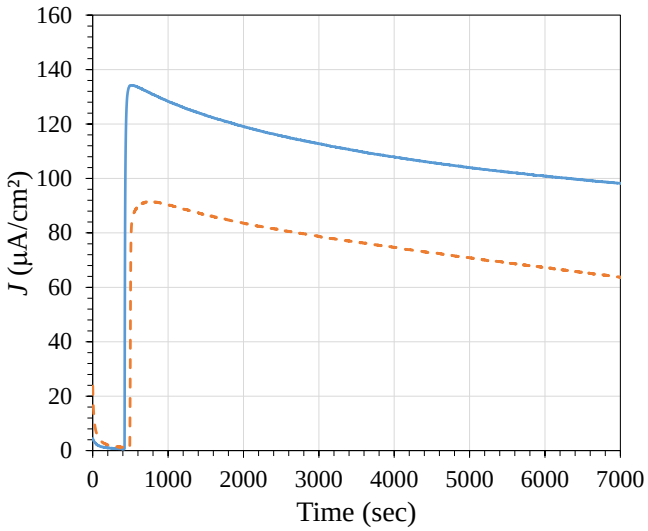

Figure **3.8**: Amperometric response for Inv/FDH-modified electrodes (solid line), Inv/-GOx-modified electrodes (dashed line) in a mixture of 100 mM fructose, 100 mM glucose solution ($t_{injection}$ = 400 sec). All films were coated onto 1 cm^2 Toray paper electrodes. Experiments were performed using 0.05 M citrate buffer, pH 5.5, at 25 °C.

films to injections of a mixture of 100 mM glucose and 100 mM fructose are shown in **Figure 3.8**. Rapid amperometric response time to equivalent amounts of fructose and glucose lead us to reason that the hydrolysis of sucrose by invertase is the rate limiting step in the cascade.

Control experiments were performed by using a non-redox polymer, octyl-modified linear polyethylenimine (C_8−LPEI), was used as the polymer matrix for enzyme immobilization. Constant potential amperometric experiments performed in 100 mM sucrose (**Figure 3.9**) shows the need for use of a redox mediator to help shuttle electrons from the enzymes to the electrode surface. A small amount of current density is obtained in the presence of the three enzyme cascade without a redox mediator which is attributed to the direct electron transfer of the FDH from its active site (pyroloquinoliquinone, PQQ) through the heme c.[136] Similar control experiments show that the polymer does

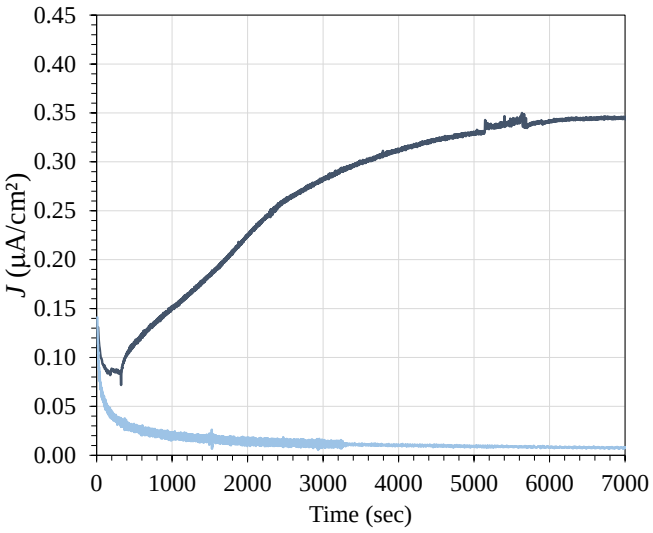

Figure **3.9**: Amperometric responses recorded at + 0.05 V (vs. SCE) above E_{ipa} of C_8-LPEI-modied electrodes without enzymes (light line) and with the Inv/FDH/GOx enzymes cascade (dark line). All films were coated onto 1 cm^2 Toray paper electrodes. Experiments were performed at 25 °C using 0.05 M citrate buffer, pH = 5.5, with the addition of 100 mM sucrose at t = 400 s.

not exhibit any electrochemical response to 100 mM sucrose in the absence of FDH, GOx and invertase.

The effect of substrate composition on the amperometric responses of various films is given in **Table 3.1**. Invertase catalyzes the hydrolysis of sucrose into one molecule of fructose and one molecule of glucose. The overall cascade-electrode current was presumed to be a result of the additive currents from each of the two redox enzymes. Therefore it would be expected that the current response of Inv/FDH/GOx films to 100 mM sucrose should be equal to the sum of the current response of Inv/FDH and Inv/GOx to 100 mM sucrose. However, this is not observed. The amperometric response of films containing both redox enzymes (Inv/FDH/GOx) to sucrose is much higher (351 $\pm$ 99 $\mu A/cm^2$) than the sum of the response of films containing only one of the redox enzymes (54 5 $\mu A/cm^2$ for Inv/FDH; 51 $\pm$ 8 $\mu A/cm^2$ for Inv/GOx). A similar trend is observed when

	J_{max} (μA/cm^2)				
	Inv/FDH/GOx	Inv/FDH	Inv/GOx	GOx	FDH
100 mM sucrose	351 ± 99	54 ± 5	51 ± 8		
100 mM glucose and 100 mM fructose	330 ± 40	100 ± 20	61 ± 7		
100 mM glucose				242 ± 19	
100 mM fructose					50 ± 5

Table **3.1**: Comparison of the amperometric responses of different enzyme-modified electrodes in the presence of variable substrate mixtures. All films were coated onto 1 cm^2 Toray paper electrodes. Experiments were performed at 25 °C using 0.05 M citrate buffer, pH = 5.5.

an equilibrated mixture of 100 mM glucose and 100 mM fructose are added as substrates instead of 100 mM sucrose. This trend indicates that there is a synergistic effect of immobilizing FDH and GOx in the same film.

Single oxidoreductase-based electrodes (GOx and FDH) were made, and amperometric measurements were taken using their respective substrate to try to understand the unexpectedly high current response of Inv/FDH/GOx electrodes. The current response of GOx-based electrodes to glucose (242 ± 19 μA/cm^2) is significantly higher than that of analogous Inv/GOx-based electrodes to either sucrose or a glucose-fructose mixture. Additionally, there is a proportional difference in current response of FDH-based electrodes to fructose (50 ± 5 μA/cm^2) compared with the response of Inv/FDH-based electrodes to either sucrose or a glucose-fructose mixture. This indicates that the observed synergism between FDH and GOx is the result of an apparent product inhibition of Inv caused by the presence of fructose or glucose. When both GOx and FDH are present, fructose and glucose can be rapidly oxidized to prevent Inv inhibition which results in a higher than expected current response from Inv/FDH/GOx-based electrodes.

3.3.2 Optimization of Temperature and pH

The overall activities of Inv/FDH/GOx films were measured amperometrically as a function of both temperature and pH, as shown in **Figure 3.10**. The maximum current responses to sucrose by Inv/FDH/GOx films increase linearly with temperature between 21 °C and 37 °C. These experiments show that a current of 302 ± 57 $\mu A/cm^2$ was obtained at 25 °C, and a current of 602 ± 62 $\mu A/cm^2$ was obtained when the temperature was increased to 37 °C. This increase in current response agrees with the previously reported increase in activity per temperature for each enzyme.[137–139] All of the enzymes used in this study exhibit an increase in activity with an increase in temperature; however, this is not true for the dependence of pH on activity. Previous studies report that both invertase and FDH have a maximum activity for their respective substrates between pH 3.5 4.0 and the activities of both are inhibited by 50% above pH 6.5; however, the maximum activity of GOx is observed at pH 7.4 while maintaining 80% of the maximal activity over the range of pH 5.5-9.0.[26,140,141] A pH profile of the Inv/FDH/GOx electrode film clearly showed that an optimum pH 5.5 allowed for all three enzymes to maintain a reasonable amount of activity.

3.3.3 Stability of Sucrose Cascade Anode

Comparative stability experiments on Inv/FDH/GOx films (**Figure 3.11**) show that both FDH and GOx maintain a reasonable fraction of their maximum current response for up to six days; the amperometric response to fructose decreased from 150 $\mu A/cm^2$ to 75 $\mu A/cm^2$ (50% decrease), while the response to glucose decreased from 500 $\mu A/cm^2$ to 250 $\mu A/cm^2$ (50% decrease) over a six day period. However, the maximum current

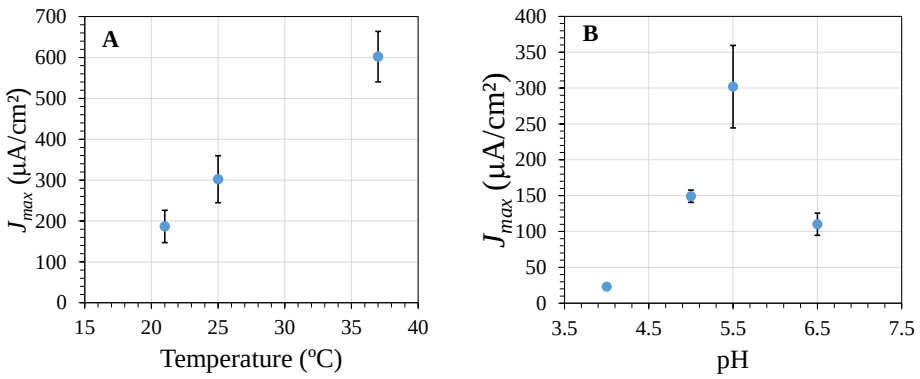

Figure **3.10**: (A) Amperometric response recorded after 2 h for Inv/FDH/GOx-modified electrodes in 100 mM sucrose solution at different temperatures. (B) Amperometric response recorded after 2 h for Inv/FDH/GOx-modified electrodes in 100 mM sucrose solution at different pH solutions. All films were coated onto 1 cm^2 Toray paper electrodes. Experiments were performed using 0.05 M citrate buffer (pH = 5.5 for variable temperature experiments).

response to sucrose decreased from 302 ± 57 $\mu A/cm^2$ to 41 $\mu A/cm^2$ (87% decrease) in only 24 hours. This loss in current response is likely caused by a conformational instability of invertase that occurs, when it is immobilized in $FcMe_4-C_3-$LPEI films, as stability experiments performed with fresh invertase in solution (i.e. not immobilized) result in a decrease from 387 ± 37 $\mu A/cm^2$ to 138 ± 20 $\mu A/cm^2$ (64.5% decrease) over a three day period. It has been shown previously that the polyamine backbone of cross-linked ferrocene-modified LPEI films is significantly protonated in an aqueous buffer at an acidic pH.[60] We hypothesize that the positively charged polymer backbone complexes favorably with the negatively charged surfaces of some enzymes. The occurrence of such a complexation was qualitatively confirmed in this study by a rapid formation of precipitate that occurs when $FcMe_4-C_3-$LPEI is mixed with GOx or FDH; however, no precipitate is observed upon the mixing of $FcMe_4-C_3-$LPEI and invertase. This

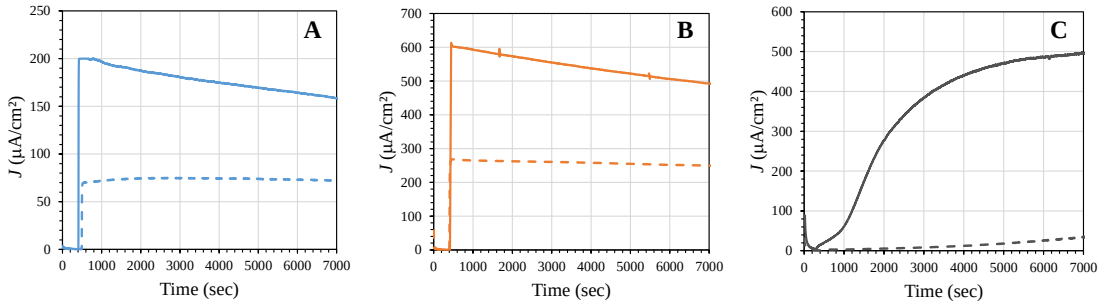

Figure **3.11**: (A) Amperometric responses recorded for FDH-modified electrodes using 100 mM fructose solution, day 1 (solid line) and day 6 (dotted line). (B) Amperometric responses recorded for GOx-modified electrodes using 100 mM glucose solution, day 1 (solid line) and day 6 (dotted line). (C) Amperometric responses recorded for Inv/FDH/GOx-modified electrodes using 100 mM fructose solution, day 1 (solid line) and day 2 (dot line). All films were coated onto 1 cm^2 Toray paper electrodes. Experiments were performed at 25 °C using 0.05 M citrate buffer, pH = 5.5.

lack of precipitate formation with invertase could be an indication that it is not fully incorporated into the polymer film, but rather randomly immobilized between several complexes of $FcMe_4$−C_3−LPEI/FDH and $FcMe_4$−C_3−LPEI/GOx near the surface of the film.

3.3.4 Sucrose Cascade Operation in a Biofuel Cell

To determine the effectiveness of the cascade electrode film in a sucrose/O_2 biofuel cell, $FcMe_4$−C_3−LPEI was used to immobilize invertase, FDH and GOx on a Toray paper electrode as the anode while an air-breathing Pt electrode was used as the cathode. A commercially available air-breathing Pt electrode was chosen as the cathode to ensure that it would not be the limiting electrode in the fuel cell. The resulting power curves are shown in **Figure 3.12**.

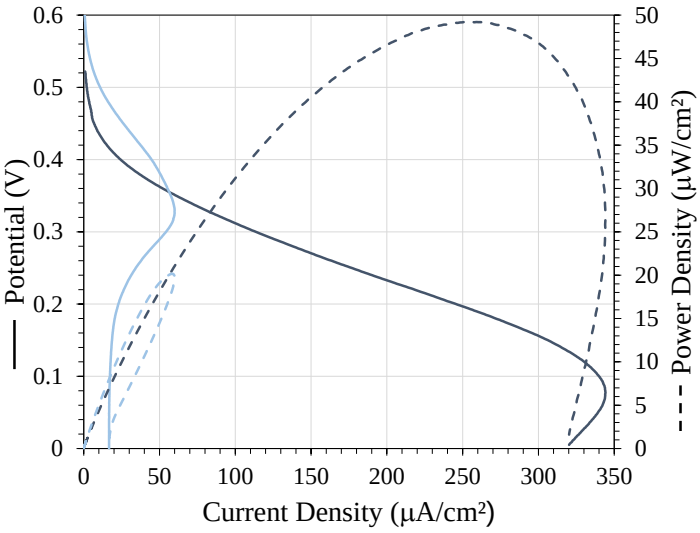

Figure **3.12**: Representative polarization (solid line) and power (dashed line) curves obtained from a FDH/GOx-modified electrode using 100 mM sucrose in absence (light), and in presence of, invertase in solution (dark). All films were coated onto 1 cm^2 Toray paper electrodes. Experiments were performed using 0.05 M citrate buffer at 25 °C with scan rate = 1 mV/sec.

A summary of the fuel cell characteristics is shown in **Table 3.2**. The Inv/FDH/GOx anode was equilibrated in a mixture of 100 mM sucrose for two hours prior to use; this was done to account for the time required for production of an amount of fructose and glucose sufficient enough for oxidation to occur at the anode. The constructed fuel cell was able to generate 42 ± 15 $\mu W/cm^2$ of power at *ca*. 172 mV with a maximum current density (short circuit current density) of 344 ± 25 $\mu A/cm^2$ at 25 °C. A decay in the current density is observed when the potential is approaching short circuit (0 V); this is most likely a result of a buildup of converted substrate within the polymer film decreasing the diffusion of new substrate to be oxidize at the electrode.

A separate bioanode was constructed by omitting the incorporation of invertase into the film. In this case, both maximum current density and power density dropped to 13 ± 3 $\mu A/cm^2$ and 19 ± 1 $\mu W/cm^2$ respectively. C_8−PEI was used in separate experiments

	FDH/GOx + Inv C_8-LPEI	FDH/GOx $FcMe_4$-C_3-LPEI	Inv/FDH/GOx $FcMe_4$-C_3-LPEI
E_{open}	413 ± 1	610 ± 20	518 ± 14
J_{max} (μA/cm^2)	0.57 ± 0.04	13 ± 3	344 ± 25
Max. Power (μW/cm^2)	0.004 ± 0.01	19 ± 1	42 ± 15

Table **3.2**: Comparison of sucrose/oxygen biofuel cells composed of an air-breathing Pt cathode with one of three different Inv/FDH/GOx Anodes: (1) C8-LPEI Film with Inv in solution, (2) $FcMe_4$-C_3-LPEI film without Inv, (3) $FcMe_4$-C_3-LPEI. All films were coated onto 1 cm^2 Toray paper electrodes. Experiments were performed using 0.05 M citrate buffer at 25 °C .

as a mediator-less polymer analogue to determine the effect of the ferrocene redox moiety. The resulting power curve shows significant decrease in both maximum power density (0.04 ± 0.01 μW/cm^2) and maximum current density (0.57 ± 0.04 μA/cm^2) due to insufficient electron transfer from the FDH and GOx active sites to the electrode surface. It has been shown in literature that GOx does not readily exhibit direct electron transfer, but FDH has been shown to exhibit direct electron transfer.[26,142]

3.4 Conclusion

$FcMe_4$-C_3-LPEI can be cross-linked to immobilize invertase, FDH, and GOx onto the surface of an electrode and operate as an enzymatic sucrose cascade. Inv/FDH/GOx-based electrode films exhibit a current response of 302 ± 57 μA/cm^2 in 100 mM sucrose at 25 °C and 602 ± 62 μA/cm^2 when the temperature is increased to 37 °C. When poised against an air-breathing Pt cathode, Inv/FDH/GOx-based sucrose biofuel cells are able to reach a maximum power density of 42 ± 15 μW/cm^2 at ca. 172 mV with a maximum current density of 344 ± 25 μA/cm^2 on a 1 cm^2 Toray paper electrode at 25 °C. FDH/GOx films maintain almost 50% of their amperometric activity for three days when invertase is in solution.

The reduction potential of the cathode is fixed while using a Pt cathode to reduce molecular oxygen, however the oxidation potentials of both GOx and FDH are lower than the oxidation potential of the ferrocene redox mediator. Therefore future work to increase the overall cell voltage must be focused on lowering the oxidative overpotential of the ferrocene redox moiety in the bioanode. Strategies must also be devised to account for the relatively low activity of invertase and for the slow rate of mutarotation of α-glucose in order to achieve higher current densities and thus higher power densities. However, this is one of the first reported sucrose bioanodes and, to our knowledge, the first report of a bioanode that utilizes both glucose and fructose as simultaneous fuel sources. Further examination of the overall kinetics of the cascade is currently underway.

Chapter 4

Chloroferrocene-Mediated Enzymatic Biocathode

4.1 Introduction

Recent advances in enzymatic electrode materials have led to a dramatic increase in both the current and power densities in enzymatic biofuel cells (BFCs). As a result, BFCs have gone from producing 4 μW/cm^2 (90 μA/cm^2 at 0.04 V) in 1999[143], to 281 μW/cm^2 (1.28 mA/cm^2 at 0.29 V) in 2012.[35] However, electrochemical reactions at the cathode are commonly the limiting factor in EFC power output. As mentioned previously, the most commonly used enzymatic cathode catalyst is laccase, which is a member of the blue copper oxidase family of enzymes. Laccase has previously been shown to effectively catalyze the complete reduction of molecular oxygen to H_2O at pH = 5 and at as low as 20 °C.[10] Like many of the enzymatic electrode materials described in previous chapters, laccase is often immobilized onto the surface of an electrode to enhance the rate of electron transfer between the enzyme active site and electrode. Unlike glucose oxidase (GOx) and fructose dehydrogenase (FDH) systems described in **Chapter** 2 and **Chapter** 3 that require a positively charged electrode surface to initiate enzymatic oxidation of various sugars, laccase is capable of catalyzing the reduction of O_2 in a neutral electronic field. In the context of a BFC, laccase provides an electrochemical driving force, and creates the positively charged electrode surface that is necessary for the anodic reaction to complete the electrochemical cell. Therefore, efficient electrochemical communication between the electrode surface and laccase active site, is essential for

providing sufficient driving force in a BFC. Previous attempts to enhance this electron transfer have focused on immobilization of the enzyme on the surface of an electrode with either the use of organometallic osmium complexes as redox mediators, or modified carbon nanotubes to induce direct electron transfer (DET).[17,28,70,144]

Laccase contains four copper centers that comprise its active site. A type 1 (T1) "blue" Cu center is coordinated to a cysteine residue that is located in a hydrophobic pocket near the exterior of the enzyme.[145] The T1-Cu center is electronically coupled to a three, type 2/3 (T2/3), Cu cluster that is bound to the interior of the enzyme by three histidine residues, as shown in **Figure 4.1**.[145] Electroreduction of O_2 occurs through a mechanism in which the T1 Cu acts as an electron shuttle between an external electron source and the T2/3 cluster, while the T2/3 Cu cluster coordinates and reduces O_2 through a peroxide intermediate.[10,145] The result is the four-electron reduction of O_2 to H_2O that is dependent on the efficient electron transfer through the T1 Cu site. The accessibility of the T1 Cu site from the surface of the enzyme allows laccase to undergo direct electron transfer (DET).[145] However, it is necessary to orient laccase so that the T1 Cu center is in close proximity to an electrode surface in order to achieve efficient (DET).

The most effective demonstration of laccase orientation in a DET biocathode was shown by Minson *et al.* who utilized anthracene-modified multi-walled carbon nanotubes to immobilize laccase.[35] The terminal anthracene moieties are able to coordinate with the hydrophobic pocket of the T1 Cu site to allow for current densities as high as 1.84 mA/cm^2 using purified laccase.[28,35] While DET enzymatic biocathodes are capable of generating high current densities without the overpotential of a redox mediator,

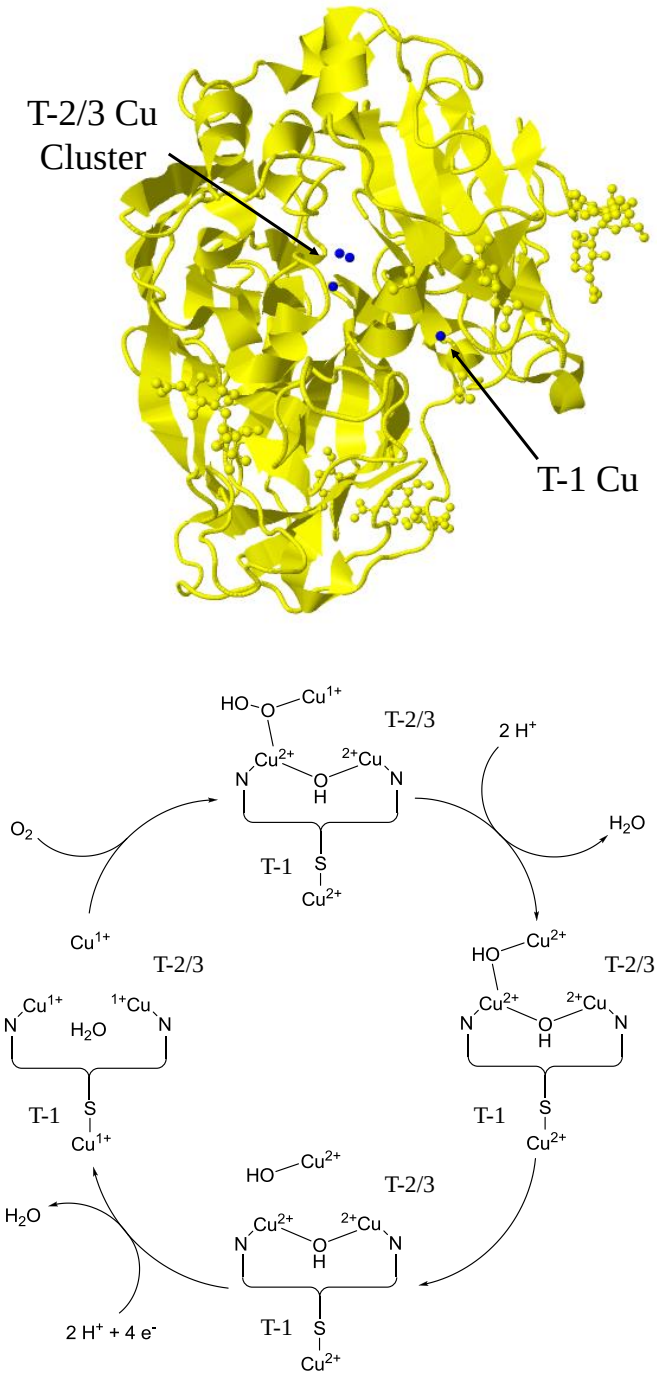

Figure **4.1**: Crystal structure of laccase from *Trametes versicolor* in its oxidized form, obtained from PDB (top), and its proposed mechanism for the reduction of O_2 to H_2O, adopted from Solomon *et al.*[10]

the amount of active enzyme that can be used is limited to a single monolayer. This limitation creates the necessity for elaborate electrode structures to achieve a practical amount of current. Even with high surface area materials, this induces a very practical limitation to the amount of current that can be generated. Alternatively, several studies have demonstrated the effective use of osmium redox mediators in hydrogel-immobilized laccase biocathodes.[19,70,72,112,146]

Osmium-modified redox polymers designed by Heller *et al.* are popular enzymatic electron mediators because they can be cross-linked to form a hydrogel that allows for effective of substrate diffusion and that is capable of high rates of electron diffusion.[70,95,112,147] Cathode materials utilizing poly(vinylpyridine) [Os(Me_2-bpy)$_2$(amino-Me_2bpy)] and laccase have achieved current densities as high as 1.0 mA/cm^2 at 37 °C.[17] However, much of the research on Os-mediated biocathodes has focused on the use of microelectrodes and has not yet been shown effective in larger scale electrode models. Additionally, the materials required to prepare various Os redox polymers can be very expensive and toxic.

The previous two chapters have demonstrate the use of a polymethylated ferrocene-modified linear poly(ethylenimine) (LPEI) redox polymer in multiple contexts as a bioanode.[8,9] The use of electron releasing methyl functionalities allowed for a decrease the redox potential to minimize the induced anodic overpotential, while maintaining exceptionally high rates of electron transfer, as discussed in **Chapter** 2. A similar strategy can be implemented to allow ferrocene to be used as a biocathode mediator. By substituting ferrocene with an electron withdrawing functionality, it has been shown that the redox potential of ferrocene can be increased while maintaining the capability of fast electron

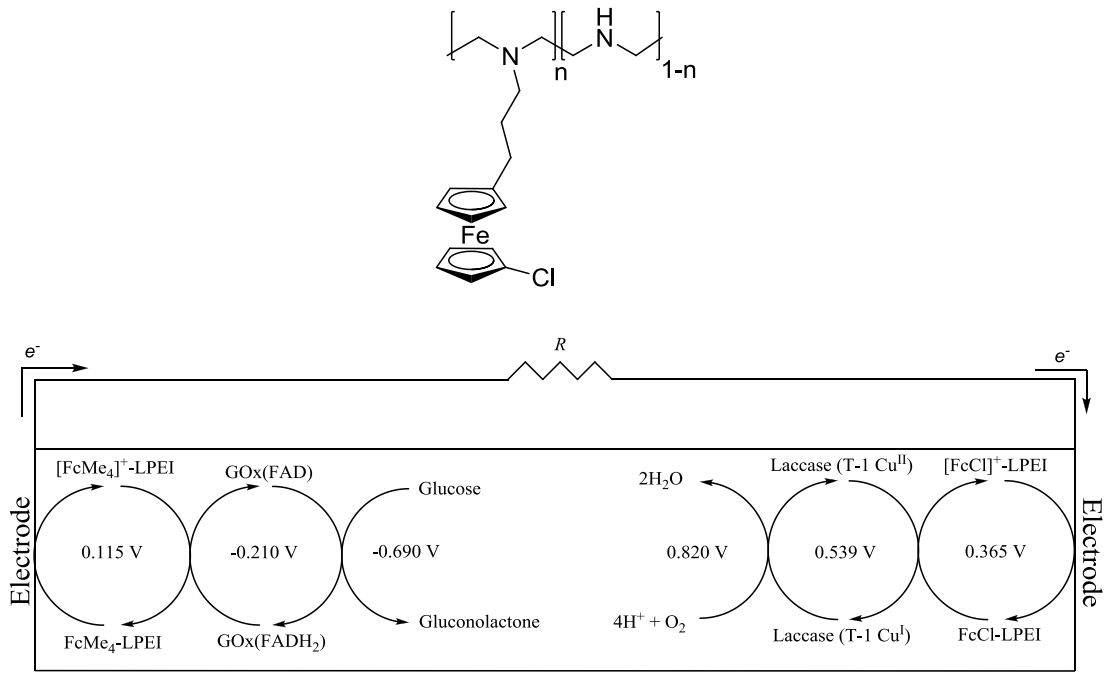

Figure **4.2**: Molecular diagram of FcCl-C_3-LPEI (top) and schematic diagram of a glucose/O_2 biofuel cell using a $FcMe_4$-C_3-LPEI/GOx anode and a FcCl-C_3-LPEI/laccase cathode(bottom).

diffusion.

In this chapter, a novel material, chloroferrocene-modified LPEI (FcCl-C_3-LPEI), is described for its use with laccase in an enzymatic biocathode. The use of a chloro-substituted ferrocene mediator is shown to have a redox potential that is ∼100 mV higher than its unsubstituted counterpart. Upon cross-linking FcCl-C_3-LPEI in the presence of laccase onto the surface of a carbon electrode, the resulting biocathode is able to achieve a maximum catalytic current density (J_{max}) of 3.54 mA/cm^2 at 25 °C. The FcCl-C_3-LPEI/laccase cathode is combined with the $FcMe_4$-C_3-LPEI/GOx anode, described in **Chapter** 2 and shown in **Figure 4.2**, to construct a glucose/O_2 biofuel cell that is capable of generating 260 μW/cm^2 and 830 μA/cm^2 at 25 °C. This is the first reported

example of an enzymatic biofuel cell that is mediated by a ferrocene species at both the anode and cathode.

4.2 Experimental

4.2.1 Chemicals and Solutions

Laccase from *Trametes versicolor* (EC 1.10.3.2., ≥10 U/mg), glucose oxidase from *Aspergillus niger* (EC 1.1.3.4, type X-S, 147 units/mg solid, 75% protein) and all chemicals were purchased from Sigma-Aldrich unless otherwise noted and used as received. Ethylene glycol diglycidyl ether (EGDGE) was purchased from Polysciences Inc., Warrington, PA. Stock solutions of 2 M glucose were allowed to mutarotate for 24 hr before use and subsequently kept refrigerated at 4 °C for biofuel cell experiments. Carbon felt electrodes (3.18 mm (0.1125 in) thick, 99.0%, Product Number 43199) were purchased from Alfa Aesar. $FcMe_4$-C_3-LPEI was synthesized as described in **Chapter** 2.[9,67]

4.2.2 Synthesis of Chloroferrocene

Chloroferrocene was prepared using a procedure by Nesmejanow *et al.*[148] $CuCl_2 \cdot 2\,H_2O$ (1.48 g, 8.70 mmol) was added to a stirring solution of ferrocene boronic acid (1.00 g, 4.35 mmol) in 30 mL H_2O at 50 - 60 °C. The reaction mixture was stirred for 24 h under N_2 at 60 °C. The solution was cooled to room temperature and the product was extracted twice with 30 mL aliquots of diethyl ether. The organic portion was dried over $MgSO_4$ and the concentrated under reduced pressure. The crude product was filtered through flash silica using hexanes to remove any starting material. The solvent was

removed under reduced pressure to obtain 0.717 g of chloroferrocene (75% yield). ^{1}H-NMR (300 MHz, $CDCl_3$): δ 3.95 (t, 2H, Fe-(CCl)-C**H**-CH), 4.16 (s, 5H, CpCl-Fe-Cp-**H**), 4.31 (s, 2H, Fe-CH-C**H**-CH).

4.2.3 Synthesis of (3-Bromopropionyl)chloroferrocene

3-Chloroferrocenepropanoyl bromide was prepared using a modified synthesis by Metay *et al.*.[94] 3-Bromopropionyl chloride (0.214 g, 1.25 mmol) was added dropwise to a stirring solution of aluminum chloride (0.167 g, 1.25 mmol) in dichloromethane (5 mL). The mixture was stirred for one hour at room temperature until the aluminum chloride was completely dissolved. The bromopropionyl chloride solution was added dropwise to a stirring solution of chloroferrocene (0.23 g, 1.05 mmol) in dichloromethane (10 mL) at 0 °C. The reaction mixture was stirred for 24 h at room temperature, then diluted with dichloromethane (10 mL) and poured over an equivalent volume of ice. The mixture was stirred until all of the ice was melted. The organic portion was washed with saturated $NaHCO_3$ (aq) and a brine solution. The organic portion was then dried through $MgSO_4$ and the product was concentrated under reduced pressure. The crude product was a red viscous liquid, and was used without further purification. A yield of 100% was assumed to ensure a sufficient amount of reductant was used in the subsequent step.

4.2.4 Synthesis of (3-Bromopropyl)chloroferrocene

A solution of borane *tert*-butylamine complex (0.364 g, 4.18 mmol) in dichloromethane (3 mL) was slowly added to a stirring solution of aluminum chloride (0.278 g, 2.09 mmol) at 0 °C. The mixture was allowed to warm to room temperature and stirred for one hour.

A solution of (3-bromopropionyl)chloroferrocene (0.371 g, 1.05 mmol) in dichloromethane (5 mL) was added to the stirring borane/aluminum chloride mixture. The reaction mixture was allowed to stir for 24 hours at room temperature. The reaction was quenched by slowly adding H_2O (25 mL) to the reaction mixture at 0 °C. The biphasic mixture was stirred for two hours at room temperature to ensure that the reaction was complete. The organic portion was dried over $MgSO_4$, and the product was concentrated under reduced pressure. The product was purified through a column of flash silica with a 10:1 mixture of hexanes/diethyl ether. Two significant fractions were collected; the first fraction was a light yellow band that was determined to be unreacted chloroferrocene; the second fraction was dark orange and was determined to be the desired product by ^{1}H-NMR spectroscopic analysis. The final product weight was 0.200 g (0.59 mmol, 56% yield over two steps). ^{1}H-NMR (300MHz, $CDCl_3$): δ 1.96-2.10 (p, J = 6.45 Hz, 2H, CH_2-C**H**$_2$-CH_2), 2.48-2.56 (t, J = 6.45 Hz, 2H, Fc-C**H**$_2$-CH_2), 3.37-3.43 (t, J = 6.45 Hz, 2H, CH_2-C**H**$_2$-Br), 4.03 (t, J = 1.76 Hz, 2H, Fe-(CCl)-C**H**-CH), 4.12 (d, J = 1.76 Hz, 2H, ClCp-Fe-CH-C**H**-CH), 4.15 (d, J = 1.75 Hz, 2H, ClCp-Fe-(C-CH_2)-C**H**-CH), 4.31 (t, J = 1.76 Hz, Fe-(CCl)-C**H**-CH).

4.2.5 Synthesis of FcCl-C_3-LPEI

LPEI (0.126 g, 2.93 mmol) was dissolved in a 10:1 mixture of acetonitrile/methanol (10 mL) at 60 °C. 3-Chloroferrocenepropyl bromide (0.126 g, 0.34 mmol) in acetonitrile (1 mL) was added to the stirring solution of LPEI. The reaction solution was heated to reflux the solvent and stirred for 24 hours at 90 °C. The solution was cooled to room temperature and the solvent was removed under reduced pressure. The solid

polymer was extracted with diethyl ether to remove any unreacted starting material. The organic portion was decanted and the excess solvent was removed under reduced pressure. ^{1}H-NMR (300 MHz, CD_3OD): δ 1.72 (broad, m, 2H, CH_2-C**H**$_2$-CH_2), 2.83 (broad, t, 2H, FcCl-C**H**$_2$-CH_2), 2.61 (broad, s, Fc(CH_2)$_2$-C**H**$_2$-N), 2.74 (broad, s, CH_2-C**H**$_2$-N(CH_2)$_2$), 2.94 (broad, s, CH_2-C**H**$_2$-NH), 4.08 (s, 2H, Fe-(CCl)-C**H**-CH), 4.16 (s, 4H, ClCp-Fe-CH_2Cp-**H**), 4.34 (s, 2H, Fe-(CCl)-C**H**-CH).

The degree of PEI backbone substitution was determined using a method described previously in which, the substitution percentage is described by **Equation 4.1**;

$$\%FcCl-C_3-LPEI substitution = \frac{4}{backbone\mathbf{H}integration - 2} \times 100 \qquad (\mathbf{4.1})$$

where the backbone **H** integration includes the three broad overlapping singlets from δ 2.5 - 3.0. FcCl-C_3-LPEI substitutions of 17% and 24% were used throughout this work, as there no measurable difference in their electrochemical properties.

4.2.6 Electrode Film Preparation

FcCl-C_3-LPEI/Laccase film solutions were prepared by combining 14 μL of FcCl-C_3-LPEI solution (12 mg/mL), 6 μL of laccase solution (16 mg/mL), and 0.75 μL of EGDGE solution (10 μL/45 μL H_2O). $FcMe_4$-C_3-LPEI/GOx bioanodes were prepared as reported in **Section** 2.2. Bioanode film solutions were prepared by combining 14 μL of $FcMe_4$-C_3-LPEI (12 mg/mL), 6 μL of GOx solution (13 mg/mL), and 0.75 μL of EGDGE solution (2 μL/45 μL H_2O). Both anode and cathode films were cast onto

3 mm glassy carbon electrodes, 5 mm rotating disc electrodes, or 0.25 cm $\times$ 0.25 cm carbon felt electrodes by spreading 3 μL, 5 μL, or 125 μL of film solution respectively onto the electrode surface, and allowing them to cure for 24 hours at room temperature.

4.2.7 Electrochemical Measurements

Constant potential experiments and cyclic voltammetry were performed with a CH Instruments Model 832 bipotentiostat. Unless otherwise noted, experiments utilizing the potentiostat were conducted using a three-electrode cell configuration with a saturated calomel reference electrode (SCE), and a platinum wire counter electrode using 0.05 M sodium citrate buffer (pH = 4.5) as the background electrolyte for FcCl-C_3-LPEI/laccase experiments unless otherwise noted. Constant temperature of 25 $\pm$ 1 °C (or 35 $\pm$ 1 °C in the case of high-temperature biofuel cell experiments) was maintained by using a water-jacketed electrochemical cell connected to a circulating water bath during the experiments. Cyclic voltammetry experiments were performed at 0.05 V/sec unless otherwise noted. Constant potential amperometric experiments were performed at -0.05 V relative to the peak reduction potential, E_{ipc}, of each film. Variable pH measurements were performed using solutions of 0.05 M citric acid that were tuned to the required pH by adding aliquots of a 1.0 M NaOH solution at 25 °C.

Biofuel cell experiments were performed using a CH Instruments Model 832 bipotentiostat. A "three-electrode cell" configuration was used in which, the cathode was used as the working electrode, and the anode was used as both the reference and auxiliary electrode. Linear sweep voltammetry experiments were performed on the fuel cell from the open circuit potential to 0.005 V at $1 - 2$ mV/sec. using 0.5 M citrate buffer (pH

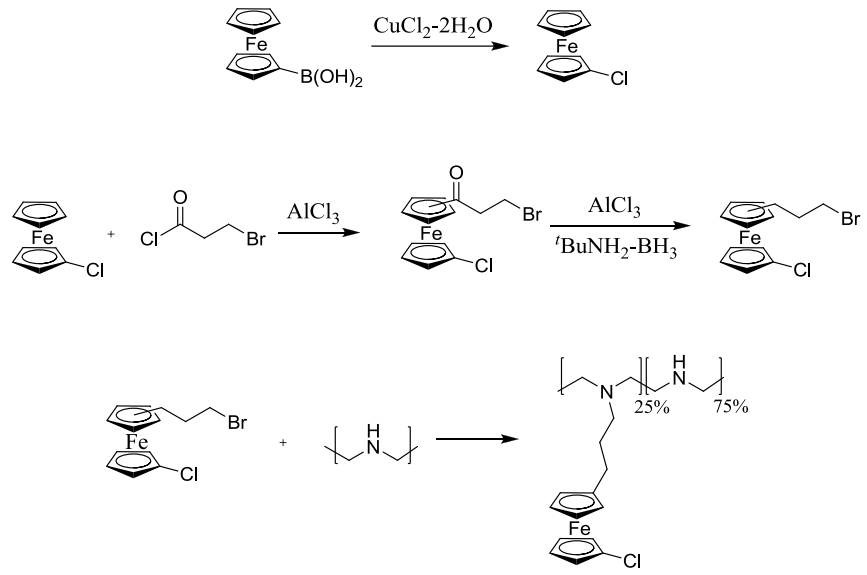

Figure **4.3**: Synthetic scheme of FcCl-C_3-LPEI.

= 5.2) at 25 °C (or 35 °C where noted).

4.3 Results and Discussion

4.3.1 Synthesis and Characterization of Chloroferrocene-Modified LPEI

Chloroferrocene was synthesized by a previously described method using ferrocene boronic acid and two equivalents of $CuCl_2 \cdot 2\,H_2O$.[148] A three-carbon spacer was attached via Friedel-Crafts acylation followed by a reduction using *tert*-butylamine borane as shown in **Figure 4.3**. The ferrocene species was used to covalently modify LPEI resulting in FcCl-C_3-LPEI with a substitution of 17 mol.%. To the best of our knowledge, this is the first use of a halogenated ferrocene species in a redox polymer for any use.

FcCl-C_3-LPEI was cross-linked with ethylene glycol diglycidyl ether (EGDGE) onto

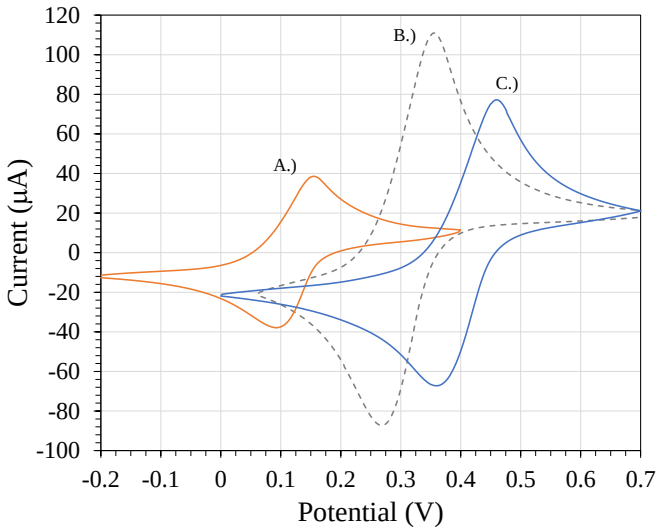

Figure **4.4**: CV comparison of $FcMe_4$-C_3-LPEI (A), Fc-C_3-LPEI (B) and FcCl-C_3-LPEI (C). Experiments were performed using a 0.05 M citrate buffer (pH 5.5) at 0.05 V/sec. and 25 °C

the surface of a carbon electrode to determine the effects of ferrocene halogenation on its electrochemical redox potential. The resulting FcCl-C_3-LPEI films have a redox potential of 0.42 V vs. SCE as compared to 0.32 V vs. SCE for Fc-C_3-LPEI and 0.12 V vs. SCE for $FcMe_4$-C_3-LPEI as shown in **Figure 4.4**. A decrease in peak current from Fc-C_3-LPEI to FcCl-C_3-LPEI can be observed despite both films containing approximately equal concentrations of respective ferrocene species. This is largely due to steric bulk imposed by the addition of a chloride group which slows the rate of electron diffusion as discussed previously.[9] Despite a small decrease in electron transport between ferrocene species, FcCl-C_3-LPEI films provided the desired effect of increasing the redox potential with respect to their unsubstituted counterpart by 100 mV.

Having achieved the desired increase in $E_{1/2}$, FcCl-C_3-LPEI was cross-linked in the presence of laccase onto a 3 mm glassy carbon electrode to construct a ferrocene-mediated biocathode hydrogel (FcCl-C_3-LPEI/laccase). Constant potential amperometry was

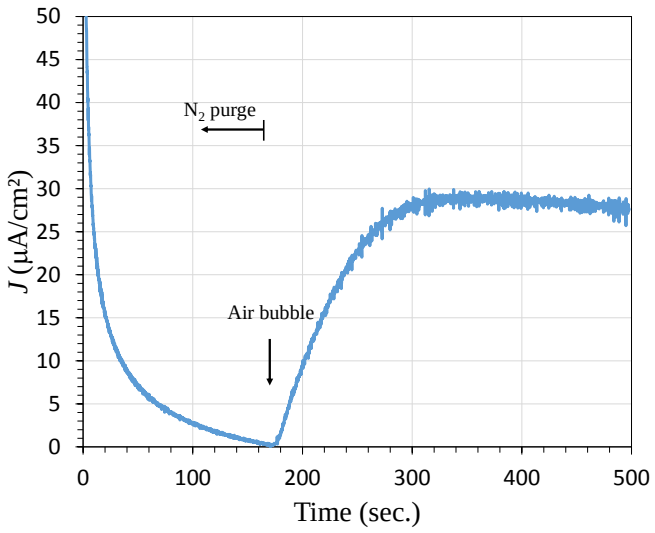

Figure **4.5**: Example of constant potential amperometric experiment used to determine J_{max} of FcCl-C_3-LPEI/laccase. Films were prepared with 12 mol% EGDGE and 60 wt% laccase on 3 mm glassy carbon electrodes. Experiments were performed at E_{ipc} - 0.05 V, using 0.05 M citrate buffer, pH = 4.5, at 25 °C .

used to determine the maximum catalytic current density (J_{max}) of the resulting films. The electrodes were held at a constant reducing potential using a deoxygenated 0.5 M citrate buffer (pH = 4.5); once a steady state background current had been established, an air flow was bubbled into the buffer solution while the change in current was monitored. **Figure 4.5** shows an example of such an experiment that results in a J_{max} = 29.6 μA/cm^2.

While the novel biocathode material did produce an electrocatalytic response to O_2, the resulting J_{max} was significantly lower than previously reported catalytic values for redox-mediated laccase biocathodes. Therefore, it became necessary to determine the highest possible J_{max} that the newly constructed FcCl-C_3-LPEI/laccase films could generate. Several methods detailed in **Chapter** 2 for optimizing J_{max}, such as varying the amount of EGDGE/laccase used to prepare biocathode films and altering the electrode

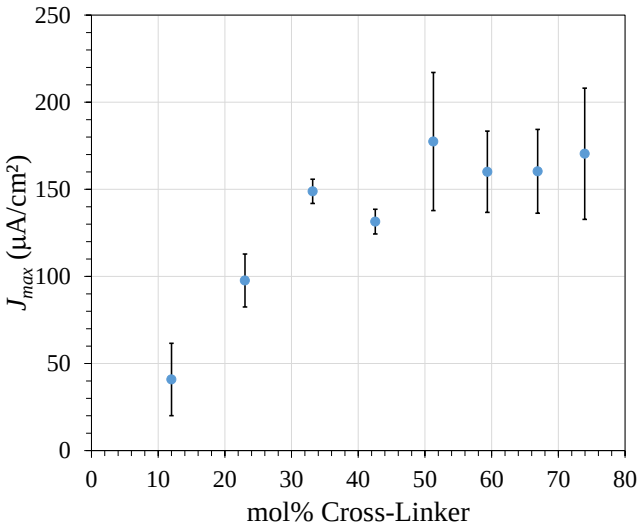

Figure **4.6**: Values of J_{max} for FcCl-C_3-LPEI/laccase as a function of the concentration of cross-linker, EGDGE. Films were prepared using 60 wt% laccase, and values for J_{max} were determined from constant potential amperometry on 3 mm glassy carbon electrodes, using 0.05 M citrate buffer (pH 4.5) at 25 °C under vigorous air bubbling.

geometry, were employed here.

4.3.2 Effects of Variable Cross-Linking

Previous studies have described that the degree of cross-linking in enzymatic redox polymers can have a large impact on the rate of substrate diffusion, as well as electron diffusion, throughout the polymer film.[1,20,49–51,60,86] The effects of varying EGDGE concentration on J_{max} for FcCl-C_3-LPEI/laccase films is shown in **Figure 4.6**. Values of J_{max} for the enzymatic electrode films increases with increased EGDGE concentration from 41 ± 21 μA/cm^2 with 12 mol% EGDGE to a peak J_{max} of 177 ± 40 μA/cm^2 with 51 mol% EGDGE at 25 °C. This trend was shown in $FcMe_4$-C_3-LPEI/GOx films to be the result of an increase in the electron diffusion caused by reduction in film swelling.

Figure 4.7 shows the effect of the degree of cross-linking on $cD_e^{1/2}$ and redox po-

tential ($E_{1/2}$) for FcCl-C_3-LPEI/laccase films. $E_{1/2}$ for FcCl-C_3-LPEI/laccase films increases slightly from 0.394 ± 0.002 V with 12 mol% EGDGE to 0.407 ± 0.002 V with 33 mol% EGDGE. These results are consistent with those described in **Chapter** 2 for $FcMe_4$-C_3-LPEI/GOx films. As the concentration of EGDGE is increased, the extent to which the films can swell is diminished. The decrease in film swelling results in the ferrocene moieties, on average, being in closer proximity to cationic ammonium sites on the PEI backbone, and the coulombic interactions from this cationic proximity cause $E_{1/2}$ to increase.[51,95] The decrease in film swelling also results in a smaller distance between redox sites, which can allow for an increase in the rate of electron transfer, provided that the decrease in swelling does not significantly limit segmental mobility.

As discussed previously, electron diffusion is reported as a function of concentration of the ferrocene species in the FcCl-C_3-LPEI film. Swelling of the redox films makes the concentration of the ferrocene species a dynamic variable that is dependent on the state of film swelling; which in turn is dependent on localized pH and the ratio of ferrocene/ferrocenium within the film. This makes exact determination of the redox site concentration very difficult, so the electron diffusion coefficient (D_e) is reported in terms of redox concentration by the proportionality, $i_p \propto cD_e^{1/2}$, as derived from the Randel-Sevcik equation.[103,104] FcCl-C_3-LPEI/laccase films show a small increase in $cD_e^{1/2}$ with increased EGDGE concentration, from $9.5 \times 10^{-9} \pm 0.9 \times 10^{-9}$ with 23 mol% EGDGE to $11.7 \times 10^{-9} \pm 0.8 \times 10^{-9}$ with 51 mol% EGDGE. While this increase represents a relatively small increase in $cD_e^{1/2}$, the lack of a downward trend is unique to ferrocene-modified LPEI films and counter to the trend observed in many previously reported redox polymers.[51] This result, combined with the observed increase in $E_{1/2}$,

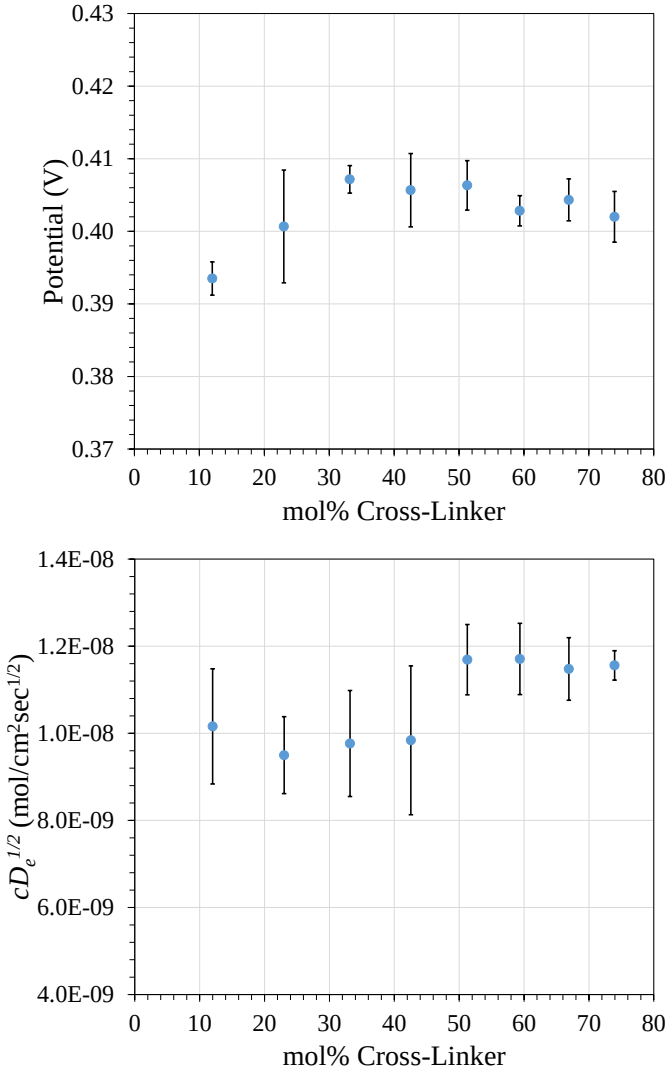

Figure **4.7**: Plots showing the effect of EGDGE concentration on $E_{1/2}$ (top) and $cD_e^{1/2}$ (bottom) of FcCl-C_3-LPEI/laccase films. Data was determined from CVs of films using 0.05 M citrate buffer (pH 4.5) at 25 °C and 0.05 V/sec.

indicates that increased EGDGE concentration results in a decrease in the films ability to swell, however not to the extent that would cause significant restriction to segmental mobility of the ferrocene moieties.

The cause for increased catalytic current density with EGDGE concentration from 12% EGDGE to 50% EGDGE is unclear. As mentioned above, there is a weak correlation between the rate of electron transfer and J_{max}, which could partially account for a lower J_{max} with smaller EGDGE concentration. However, it is also possible that films with a lower degree of cross-linking are not able to adhere completely to the film, thus causing enzymatic leaching into the buffer solution. Further studies are ongoing to determine the cause of the increase in J_{max} with EGDGE concentration. While J_{max} for films containing 51 mol% EGDGE to 74 mol% EGDGE were very statistically similar, 51 mol% EGDGE was selected as resulting in the "optimum" degree of cross-linking because it requires the least amount of EGDGE while achieving the peak J_{max}.

4.3.3 Effects of Laccase Loading

One of the primary benefits of using of redox polymers as enzymatic electrode scaffolds is that they provide a means to incorporate multiple layers of enzyme. The effects of variable laccase loading on J_{max} for FcCl-C_3-LPEI/laccase films, are shown in **Figure 4.8**. Our previous studies of $FcMe_4$-C_3-LPEI/GOx films showed that there is a physical limitation to the amount of enzyme that the film can hold, and the increase in J_{max} with GOx loading plateaus once this limitation is reached. However, FcCl-C_3-LPEI/laccase films do not follow this trend. J_{max} increases with higher laccase loading to a maximum catalytic current density of 217 $\mu A/cm^2$ with 40 wt% laccase, while

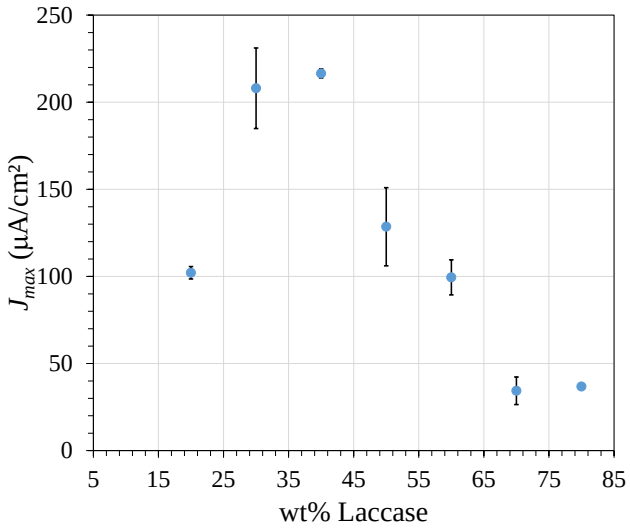

Figure **4.8**: Graph of J_{max} for variable laccase loadings in FcCl-C_3-LPEI/laccase films. Films were prepared with 50 mol% EGDGE on 3 mm glassy carbon electrodes. Maximum catalytic current density was determined using 0.05 M citrate buffer, pH 4.5, at room temperature under a flow of air.

loadings greater than 40% result in precipitously lower values for J_{max}. Additionally, it should be noted that a large amount of precipitate forms when aqueous solutions of the polymer and enzyme are mixed together, and the amount of precipitate increases as the ratio of laccase to FcCl-C_3-LPEI increases. This behavior could indicate that there is an interaction between FcCl-C_3-LPEI and laccase that is causing an inhibition of either the enzyme activity or the electron transfer throughout the film. While the enzyme activity can be difficult to monitor directly within the film, the electron diffusion kinetics can be determined using the Randles-Sevcik method described in **Chapter** 2.

The effects of laccase loading on $cD_e^{1/2}$ and the electrochemical potential of FcCl-C_3-LPEI/laccase films is shown in **Figure 4.9**. There is a significant decrease in both $cD_e^{1/2}$ and $E_{1/2}$ as the enzyme loading increases beyond 40 wt% laccase. Values of $cD_e^{1/2}$ decrease by 50% from $2.01 \times 10^{-8} \pm 1.74 \times 10^{-9}$ with 40 wt% laccase to 1.01×10^{-8}

$\pm$ 1.04×10^{-9} with 80 wt% laccase, while the redox potential shifts from 0.404 $\pm$ 0.005 V with 40 wt% laccase to 0.340 $\pm$ 0.002 V with 80 wt% laccase. This data correlates strongly to the observed decrease in catalytic current density for the same enzyme loadings, which indicates that inhibition of electron diffusion is at least a contributing factor to the loss of J_{max} at higher enzyme loading. One possible model to explain this inhibition is based on a strong molecular interaction between FcCl-C_3-LPEI and laccase.

LPEI has long been known to engage in strong ionic biomolecular interactions that are induced by the cationic nature of its backbone, and recent crystallography studies have shown that several ferrocene species are capable of forming an electrostatic complex with the active site of an enzyme.[149–154] So, it is not unreasonable to suspect that either ionic or electrostatic interactions are causing a complexation to occur between FcCl-C_3-LPEI and laccase that would result in the ferrocene moieties to be in close proximity to the enzyme, as shown in **Figure 4.10**. However, the effective molecular "wiring" of oxidoreductases with redox polymers depends on some concentration of the redox species near the active site of the enzyme and some concentration to be present intermittently between the enzyme and the electrode.[40,77,155] So, as laccase loading is increased, the complexed ferrocene concentration is increased while the non-complexed ferrocene concentration is decreased. This decrease in non-complexed ferrocene concentration limits the number of electron hopping pathways, and thus inhibits the overall electron diffusion throughout the films.

Ongoing studies are being performed to determine the nature of this interaction, and the current model is still highly speculative. However, the exact mechanism of inhibition is not necessary to determine that the optimum laccase loading occurs at 40 wt% to

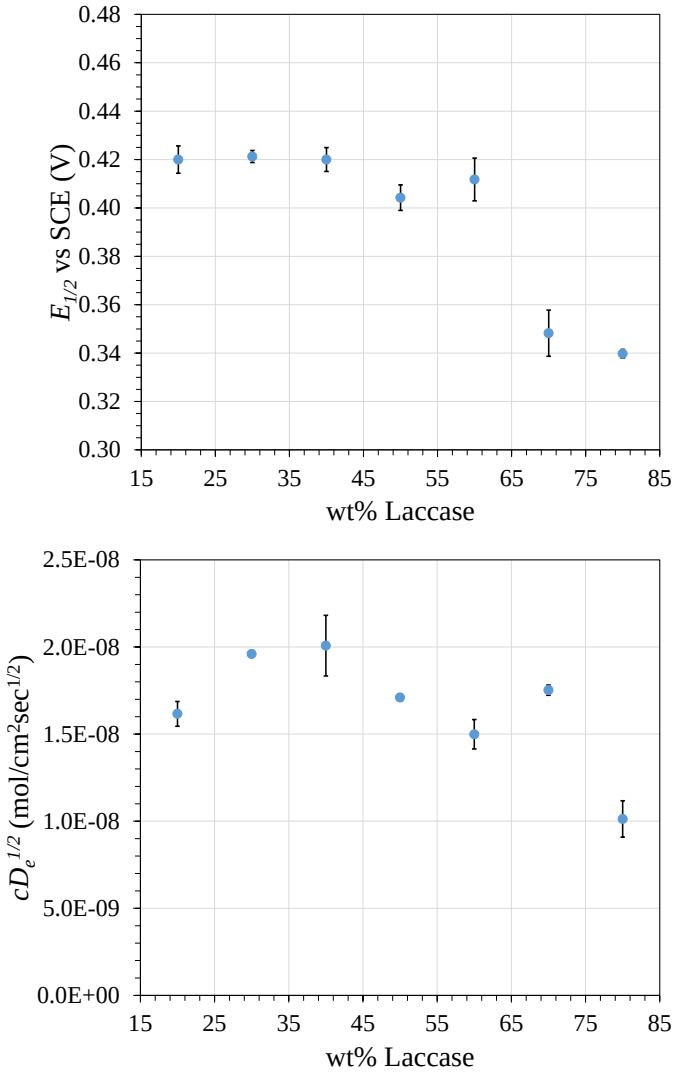

Figure **4.9**: Effects of laccase loading on $E_{1/2}$ (top) and $cD_e^{1/2}$ (bottom) on FcCl-C_3-LPEI/laccase films prepared with 50 mol% EGDGE on 3 mm glassy carbon electrodes. Experiments were performed using a 0.05 M citrate buffer, pH = 4.5, at 25 °C .

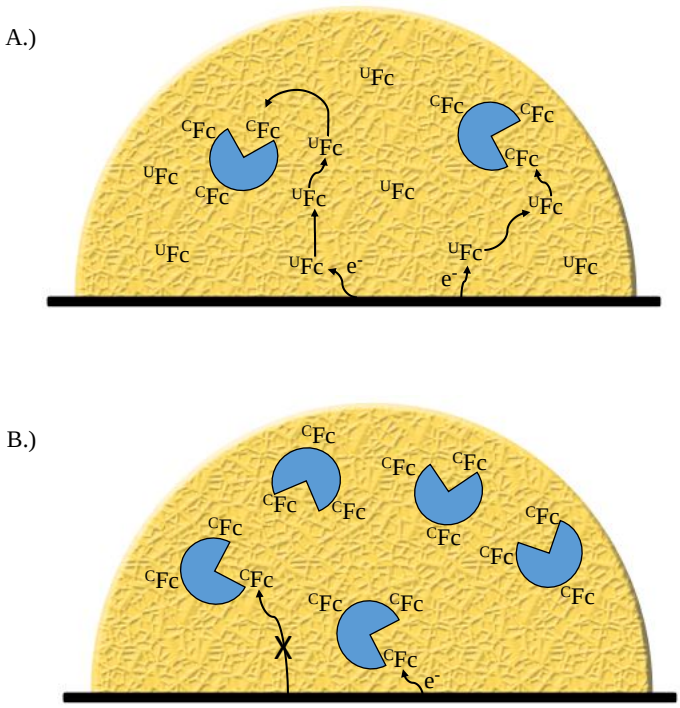

Figure **4.10**: Schematic of possible FcCl-C_3-LPEI/laccase model to account for the decrease in electron diffusion with increased laccase loading. At low laccase loading (top), there is enough uncomplexed ferrocene (^{U}Fc) to allow for efficient electron transfer. At high laccase loading (bottom), most of the ferrocene is complexed to laccase (^{C}Fc), and therefore there are not sufficient electron hopping pathways to facilitate efficient electron transfer.

generate a maximum catalytic current density of 217 μA/cm^2 on a 3 mm glassy carbon electrode surface.

4.3.4 O_2 Diffusion through Biocathode Films

For many enzymatic biocathodes, diffusion of molecular oxygen to the enzyme is the rate-limiting step. Diffusion limitations are caused by the low solubility of O_2 in aqueous solutions as well as slow O_2 diffusion through the electrode material.[19,51,70,156] Mass transport kinetics of for O_2 through FcCl-C_3-LPEI/laccase films were studied using amperometric experiments with rotating disc electrodes (RDEs). In such experiments, the RDE is attached to an electric motor that rotates the electrode at a regular speed which drags solvent across the electrode surface due to centrifugal force.[157] This causes a laminar flow that is normal to the rotating surface and dependent on the rate of rotation. This provides a means to control and enhance the rate of substrate diffusion across the electrode surface. The limiting catalytic current for RDEs is described by the Levich equation[157];

$$i_L = 7.91nFAC_{O_2}D_{O_2}^{2/3}\omega^{1/2}\nu^{-1/6} \qquad (\mathbf{4.2})$$

where i_L is the limiting current density, n is the number of electrons involved in the catalytic redox process, F is Faraday's constant, A is the area of the RDE, C_{O_2} is the analytical oxygen concentration (0.25 mM), D_{O_2} is the O_2 diffusion coefficient (1.41×10^{-5} cm^{2}sec^{-1})[158], ω is the rotation frequency in Hz, and ν is the kinematic viscosity of the electrolyte (1.02 cm^{2}sec^{-1})[158].[157,158] It should be noted that the prefactor constant,

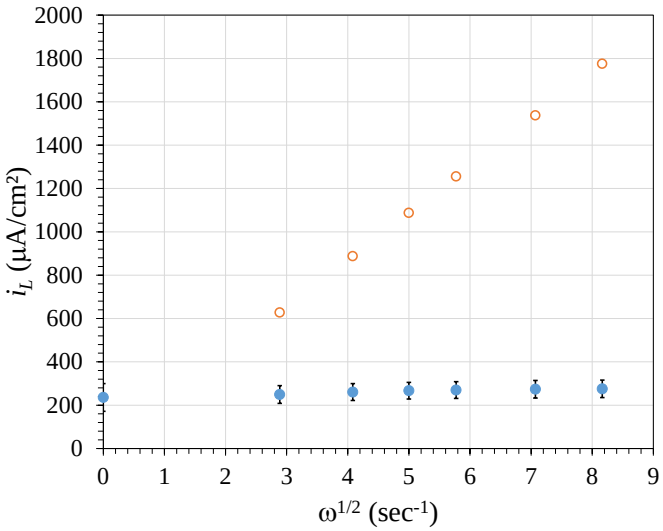

Figure **4.11**: Levich plot showing the effects of O_2 diffusion on the maximum catalytic current density of FcCl-C_3-LPEI/laccase electrodes. Values of i_L for FcCl-C_3-LPEI/laccase films (dark circles) were determined amperometrically, and theoretical diffusion-limited values of i_L were calculated using the Levich equation. FcCl-C_3-LPEI/laccase films were cross-linked with 50 mol% EGDGE and 40 wt% laccase onto a 5 mm rotating disk electrode. Experiments were performed using a 0.05 M citrate buffer, pH = 4.5, at 25 °C .

7.91, is specific for rotation frequency in units of sec^{-1}, and an alternative prefactor of 0.62 should be used if ω is in units of rad/sec. A plot of i_L and $\omega^{1/2}$ should be linear for a system that is entirely limited by convective diffusion, and significant deviation from linearity is an indication that the system is limited by a secondary kinetic parameter.

Amperometric RDE experiments were performed on optimized FcCl-C_3-LPEI/laccase films; the resulting Levich plot is shown in **Figure 4.11** along with the theoretical mass transport-limited i_L values (as calculated from the Levich equation). At 50 Hz, the Levich equation yields $i_L = 1.532$ mA/cm^2, which is considerably higher than any value observed experimentally. This likely indicates that optimized FcCl-C_3-LPEI/laccase films are not limited by O_2 diffusion on glassy carbon electrodes, but rather limited by the apparent catalytic activity of laccase within the film.[19,70] Having reached the optimal

laccase loading, further strategies must be developed to increase the catalytic density within the film. One possible solution is the use of laccase with a higher activity, and ongoing research is being done to this affect.

4.3.5 Effects of Film Loading on Carbon Felt Electrodes

Having shown that the optimized laccase loading in FcCl-C_3-LPEI/laccase films provides an upper limit to the amount of enzyme that can be effectively incorporated, an alternative strategy was necessary to enhance the catalytic output of the biocathode films. The use of a carbon felt material as an electrode scaffold was described in **Chapter** 2 as a means of dramatically increase the electrode surface density, and some previous reports have demonstrated its use in an air-breathing cathode material.[109] While the use of other carbon networks (such as carbon paper, carbon nanotubes, and graphite rods) as electrode scaffolds has been studied extensively as a means of achieving high surface density, the uniquely porous three-dimensional structure of carbon felt electrodes (CFEs) allows for much larger quantities of enzymatic film solution to be coated onto an electrode and allows for a much higher rate of substrate diffusion.[70,106,111,159,160]

Figure 4.12 shows the effect of variable FcCl-C_3-LPEI/laccase film loading on J_{max} under a vigorous bubbling of air. A clear positive correlation exists between the amount of FcCl-C_3-LPEI/laccase/EGDGE solution used to coat the felt electrodes and the magnitude of the corresponding J_{max}. The maximum catalytic current density increases from 45 μA/cm^2 with 5 μL/cm^2 to 2900 $\pm$ 500 μA/cm^2 with 400 μL of FcCl-C_3-LPEI/laccase film solution. An extrapolation of this trend indicates that much high catalytic current densities can be achieved, however the felt material is limited by the volume of liquid

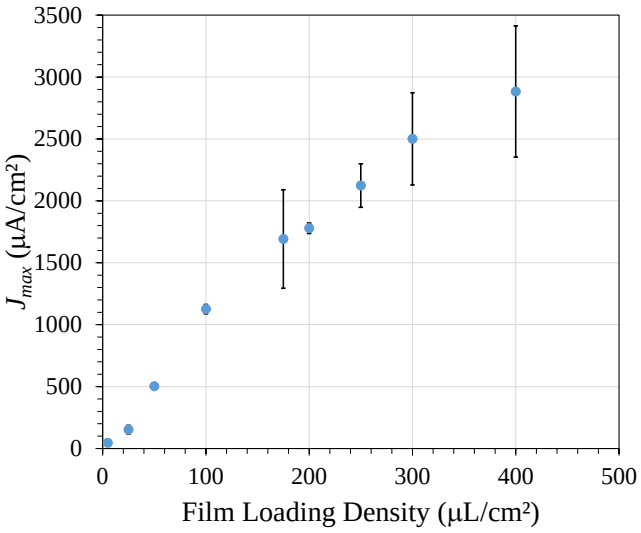

Figure **4.12**: Effects of variable FcCl-C_3-LPEI/laccase film loading on the maximum catalytic current density. Films were prepared with 50 mol% EGDGE and 40 wt% laccase on 0.25 cm × 0.25 cm carbon felt electrodes. Experiments were performed using 0.05 M citrate buffer, pH 4.5, at 25 °C. Error bars represent one standard deviation from the mean (n = 3).

that in can hold, and attempts at higher film solution loading consistently resulted in the excess volume of liquid dripping off of the electrode. A CFE with the dimensions of 1 cm × 1 cm × 0.318 cm CFE occupies a volume of 0.318 cm^3, which approximately corresponds to the maximum reproducible loading volume of 400 μL. While maximum finite loading capacity of the electrode materials present limitations on the volume of FcCl-C_3-LPEI/laccase film that can be coated onto an electrode, it may be possible to overcome some of these limitations by modifying the procedure used to coat the electrodes. Nevertheless, the use of CFEs allowed for FcCl-C_3-LPEI/laccase films to generate background-corrected current densities as high as 3540 $\mu A/cm^2$ at 25 °C which is among the highest current densities reported for an enzymatic biocathode of any type.

4.3.6 FcCl-C_3-LPEI/Laccase in a Ferrocene-Mediated Biofuel Cell

Once the FcCl-C_3-LPEI/laccase biocathode films had been optimized, our objective shifted towards implementing the material in a glucose/O_2 biofuel cell. The biocathode was poised against a $FcMe_4$-C_3-LPEI/GOx bioanode described in **Chapter** 2. It should be noted at the outset that previous studies have shown the optimum pH of *in situ* laccase is pH = 3, whereas the optimum pH of $FcMe_4$-C_3-LPEI/GOx films was shown to be >6.5.[161] The pH profiles of FcCl-C_3-LPEI/laccase and $FcMe_4$-C_3-LPEI/GOx are shown overlaid in **Figure 4.13**. Values of J_{max} were determined by measuring the current density response of films on 3 mm glassy carbon electrodes in saturating O_2 or glucose concentrations at 25 °C . The pH profile for FcCl-C_3-LPEI/laccase films shows a trend that is similar to previously published pH profiles of laccase *in situ*, so that the maximum apparent film activity occurs between pH = 3.0 and pH = 4.0 and the maximum pH limit occurs at pH = 7.0. Based on the overlaid plots, the optimum pH of a BFC using both electrodes should occur at pH = 5.0.

Biofuel cells were analyzed in a compartmentless cell using a 0.05 M citrate buffer with pH = 5.2, and at 25 °C . As expected, both the current and power outputs of $FcMe_4$-C_3-LPEI/GOx - FcCl-C_3-LPEI/laccase fuel cells were highly dependent on the surface area and geometry of the electrodes used to construct each cell. Comparative power and current density curves are shown in **Figure 4.14**.

The resulting biofuel cells were able to generate 37 ± 6 $\mu W/cm^2$ at 0.273 V on 3 mm glassy carbon electrodes, and 57 ± 6 $\mu W/cm^2$ at 0.256 V when the cathode was coated onto a 5 mm RDE and rotated at 3000rpm, both at 25 °C. The increase in power

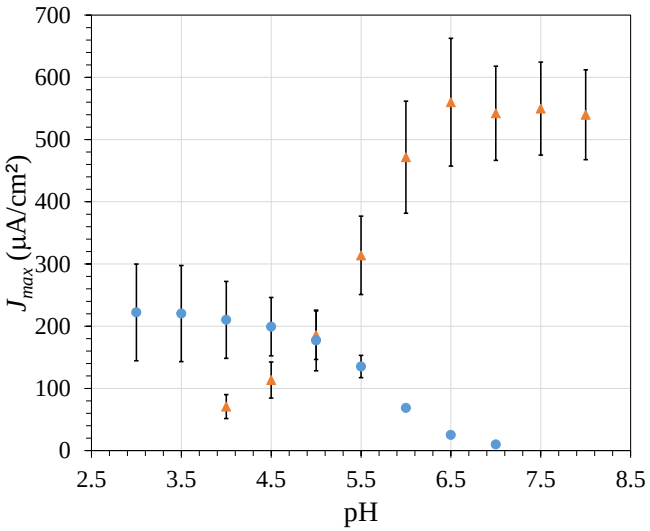

Figure **4.13**: Overlaid pH profiles of FcCl-C_3-LPEI/laccase (circles) and $FcMe_4$-C_3-LPEI/GOx (squares). Values of J_{max} for FcCl-modified and $FcMe_4$-modified films were tested at 25 °C using 0.05 M citrate buffer and 0.05 M phosphate, respectively, at varying values of pH. FcCl-C_3-LPEI/laccase films were prepared with 40 wt% laccase and 50 mol% EGDGE, while $FcMe_4$-C_3-LPEI/GOx films were prepared with 32 wt% GOx and 14 mol% EGDGE, both on 3 mm glassy carbon electrodes.

observed with a RDE cathode indicates that it is the limiting electrode. However, there is very little improvement in the mass transport-limited region of the current density curve between the stationary BFCs and the rotating-cathode BFCs. This lends further evidence that the apparent catalytic activity of laccase is rate-limiting. When both planar electrodes were replaced with carbon felt electrodes, the BFC was able to generate 501 ± 75 μW/cm^2 at 0.258 V. Analysis of the current density curve shows a significant decrease in the catalytically-limited current (current generated at high potential), and a significant increase in the diffusion-limited current (current plateaus at low potential). This indicates that, for fuel cells constructed with CFEs, the limitations are almost entirely limited by mass transport.

Figure 4.15 shows comparative power and current density curves for $FcMe_4$-C_3-

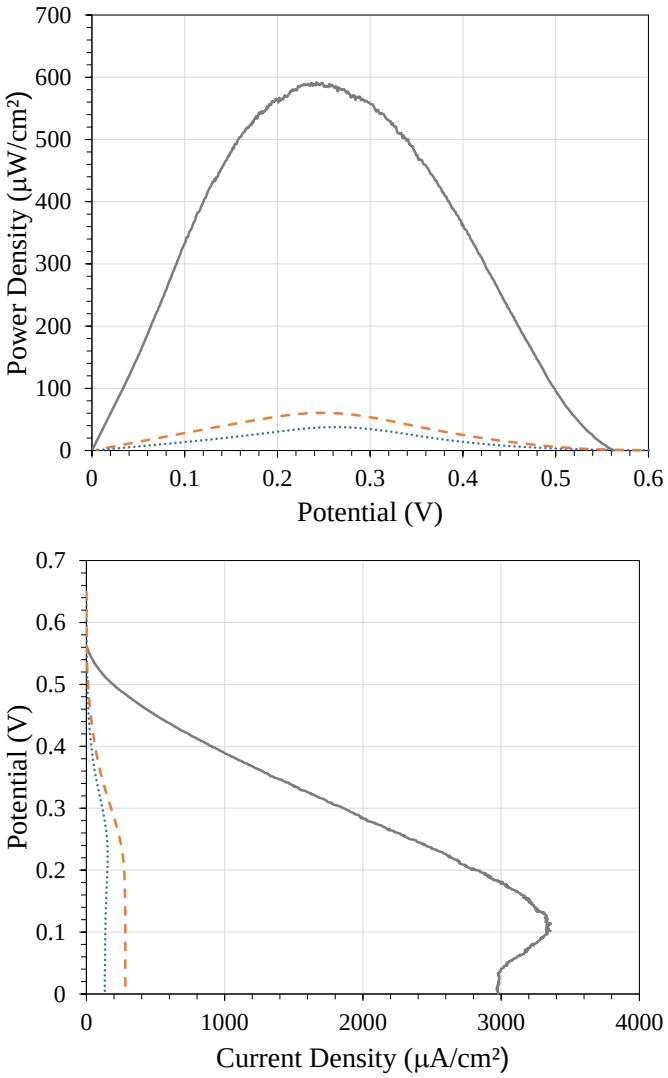

Figure **4.14**: Power curves (top) and current density curves (bottom) comparing $FcMe_4$-C_3-LPEI/GOx - FcCl-C_3-LPEI/laccase BFCs using different electrode materials. BFCs were made using 3 mm glassy carbon for both electrodes (dotted line), a 3 mm glassy carbon anode and a 5 mm RDE (dashed line), and 0.5 cm^2 carbon felt for both electrodes (solid line). FcCl-C_3-LPEI/laccase films were prepared with 40 wt% laccase and 50 mol% EGDGE, while $FcMe_4$-C_3-LPEI/GOx films were prepared with 32 wt% GOx and 14 mol% EGDGE. Experiments were performed usng 0.05 M citrate buffer, pH = 5.2, at 25 °C with 100 mM glucose.

Electrode Material	Temp. (°C)	E_{open} (V)	J_{max} (μA/cm^2)	Power Density (μA/cm^2)	$E_{max\ power}$ (V)
3 mm glassy carbon	25	0.637 ± 0.01	144 ± 32	37 ± 6	0.273 ± 0.01
5 mm RDE cathode	25	0.657 ± 0.01	256 ± 36	57 ± 7	0.256 ± 0.01
0.25 cm^2 CFE	25	0.588 ± 0.02	2733 ± 569	501 ± 75	0.258 ± 0.01
0.25 cm^2 CFE	37	0.616 ± 0.01	3427 ± 227	636 ± 36	0.256 ± 0.01

Table **4.1**: Summary of $FcMe_4$-C_3-LPEI/GOx - FcCl-C_3-LPEI/laccase glucose/O_2 BFC results. BFCs were prepared on 0.5 cm^2 carbon felt with 40 wt% laccase and 50 mol% EGDGE in the cathode, and 32 wt% GOx and 14 mol% EGDGE at the anode. Experiments were performed using 0.05 M citrate buffer, pH = 5.2.

LPEI/GOx - FcCl-C_3-LPEI/laccase BFCs constructed with CFEs at 25 °C and 37 °C . Fuel cells were able to generate 636 ± 36 μW/cm^2 at 0.339 ± 0.002 V with a maximum current density of 3427 ± 227 μA/cm^2 at 37 °C . This is among the highest reported power densities generated by an enzymatic biofuel cell. Previous studies have shown that, in catalytically limited systems, an increase in fuel cell temperature results in an increase in current output that is proportional to the increase in enzymatic activity.[8] So an increase in temperature from 25 °C to 37 °C of a BFC using GOx and laccase should see as much as a 100% increase in the observed power density. However, $FcMe_4$-C_3-LPEI/GOx - FcCl-C_3-LPEI/laccase cells using CFEs only exhibit an 25% increase in power from 501 μW/cm^2 to 636 μW/cm^2 . This increase is more closely proportional to the increase in convectional diffusion with temperature. Therefore, even at elevated temperatures, BFCs prepared on CFEs are not catalytically limited, but rather they are likely limited by O_2 diffusion. A compilation of all pertinent fuel cell data is shown in **Table 4.1**.

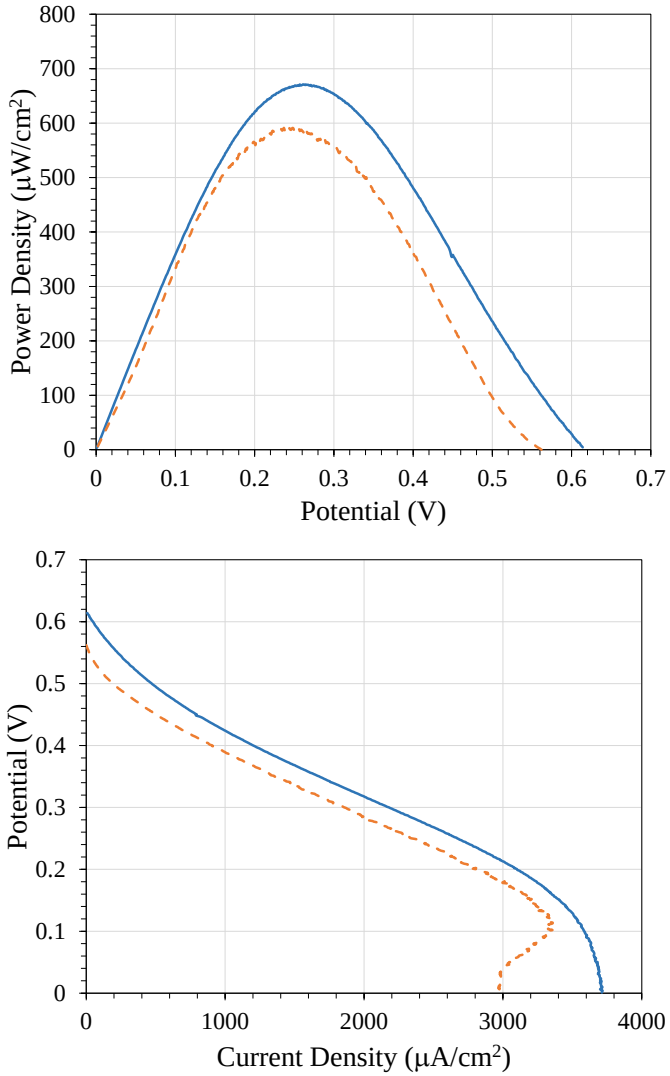

Figure **4.15**: Representative power (top) and current density (bottom) curves comparing the output of $FcMe_4$-C_3-LPEI/GOx - FcCl-C_3-LPEI/laccase BFCs at 25 °C (dashed lines) and 37 °C (solid lines). BFCs were prepared on 0.5 cm^2 carbon felt with 40 wt% laccase and 50 mol% EGDGE in the cathode, and 32 wt% GOx and 14 mol% EGDGE at the anode. Experiments were performed using 0.05 M citrate buffer, pH = 5.2.

4.4 Conclusion

A newly synthesized FcCl-C_3-LPEI polymer displayed a redox potential of 0.42 V vs SCE, which is ∼0.1 V higher than its non-chlorinated counterpart. FcCl-C_3-LPEI was cross-linked onto the surface of an electrode in the presence of laccase to form an enzymatic biocathode. Molecular oxygen was reduced by the novel biocathode material with a J_{max} of 304 μA/cm^2 on a RDE at 4000 rpm, and 3.54 mA/cm^2 on a 0.5 cm^2 carbon felt electrode, both at 25 °C .

The FcCl-C_3-LPEI/laccase cathode was combined with a $FcMe_4$-C_3-LPEI/GOx anode (described in **Chapter** 2) to make a glucose/O_2 biofuel cell capable of generating power densities as high as 501 μW/cm^2 with a maximum current density of 2733 μA/cm^2 at 25 °C, and 636 μW/cm^2 with a maximum current density of 3427 μA/cm^2 at 37 °C , which are among the highest reported values for a BFC of this type. BFCs prepared with CFEs were shown to be limited by mass transport at both 25 °C and 37 °C , which is highly suspected to have been caused by the low solubility of O_2 in aqueous solutions. Ongoing research is primarily focused on developing a more effective means of O_2 delivery to the biocathode.

Chapter 5

Conclusions and Future Directions

5.1 Conclusions

The contents of this work present the synthesis and versatile applications of two ferrocene-modified linear poly(ethylenimine) materials as redox scaffolds for enzymatic bioelectrocatalysis. The first, $FcMe_4$-C_3-LPEI, has been prepared in previously published work.[9] However, a more efficient synthetic route was developed that allowed for the preparation of much greater quantities of the material. $FcMe_4$-C_3-LPEI was cross-linked in the presence of glucose oxidase (GOx) onto the surface of an electrode to form a bioanode hydrogel. The resulting films were thoroughly characterized, and a mathematical model was adapted from Benito *et al.* to account for a previously uncharacterized electrochemical effect of film swelling as a result of changes in pH. Through optimization of cross-linker and GOx concentration, the maximum catalytic current density (J_{max}) of $FcMe_4$-C_3-LPEI/GOx was significantly increased previously reported values.

The utility of the $FcMe_4$-C_3-LPEI films was expanded by the incorporation of two additional enzymes, fructose dehydrogenase (FDH) and invertase (Inv), to catalyze the hydrolysis and subsequent oxidation of sucrose. Films utilizing all three enzymes (GOx/FDH/Inv) were capable of extracting four electrons per molecule of fuel, as compared to the two-electron oxidation of films with only GOx. Additionally, a previously unreported synergistic effect was shown to occur with GOx/FDH/Inv films. Both GOx and FDH are mutually necessary to prevent a form of product inhibition of Inv from oc-

curing. This type of reaction cascade provides a framework for the use of fuel substrates as targets that are upstream of the commonly used glucose and fructose.

Finally, a new redox material, FcCl-C_3-LPEI, was synthesized to be used as a biocathode redox mediator. The addition of an electron-withdrawing group to ferrocene had the effect of raising the electrochemical potential of the redox polymer, therefore making it a more suitable cathodic mediator. FcCl-C_3-LPEI was cross-linked in the presence of laccase to catalyze the complete reduction of O_2 to H_2O. A strong complexation between the ferrocene redox polymer and laccase, was shown to inhibit electrochemical communication between redox sites at high concentrations of laccase, therefore limiting the extent of enzyme loading within the film. Optimization of cross-linking and enzyme-loading parameters for FcCl-C_3-LPEI/laccase films resulted in significant increases in J_{max}. However, even under optimized conditions, the new biocathode material was catalytically limited.

Carbon felt electrodes were used to provide a three-dimensional network that allowed for a dramatic increase in film loading per geometric area. The optimized $FcMe_4$-C_3-LPEI/GOx bioanode and the newly prepared FcCl-C_3-LPEI/laccase biocathode were each prepared on carbon felt electrodes, and combined in the first glucose/O_2 fuel cell to be entirely mediated by ferrocene. The ferrocene-mediated fuel cells utilizing carbon felt electrodes were limited by O_2 diffusion through the aqueous buffer solution. However, these materials were capable of achieving some of the highest reported power densities of any glucose/O_2 fuel cell.

5.2 Future Work

The largest problem to be addressed in future work, will be the minimization of the overpotential at both the anode and the cathode while maintaining or even increasing the maximum current density that can be achieved by both electrodes. The maximum possible cell potential is fixed by the use of GOx and laccase as the anodic and cathodic catalysts, respectively. The oxidation potential of the flavin adenine dinucleotide (FAD) active site of GOx is -0.210 V vs SCE, and the reduction potential of the type-1 (T1) Cu center of laccase is 0.539 V vs SCE; which results in a maximum cell potential of 0.749 V vs SCE. However, the use of a redox mediator at either electrode induces an overpotential that decreases the electrochemical driving force of the fuel cell.

A GOx/laccase biofuel cell that is mediated by $FcMe_4$-C_3-LPEI ($E_{1/2}$ = 0.110 V vs SCE) and FcCl-C_3-LPEI ($E_{1/2}$ = 0.410 V vs SCE) respectively, will have a theoretical cell potential of 0.300 V. In order to generate 1 mW/cm^2 of power with E_{cell} = 0.300 V, a limiting catalytic current density of 3.3 mA/cm^2 must be achieved. This is over three times the limiting current densities generated in this work. However, generating the same power with an unmediated biofuel cell (E_{cell} = 0.749 V) only requires a limiting catalytic current density of 1.3 mA/cm^2, which is within the experimental error of the current densities achieved in **Chapter** 4. While the use of a direct electron transfer electrode can be a reasonable way to circumvent this problem, when the structure of the enzyme permits, it should be noted that the use of such electrodes establishes a theoretical maximum enzyme loading of a single molecular layer and thus limits the maximum current density that can be achieved. A more complete solution is to design

redox mediators so as to minimize the overpotential that they impose.

The next logical step from the work presented here would be the further methylation of ferrocene as an anodic mediator (ie octamethylferrocene or decamethylferrocene), and the further chlorination of ferrocene as a cathodic mediator (ie dichloroferrocene or decachloroferrocene). While synthetic routes to these structures are known, both sets of mediators present potential problems that must be addressed. As discussed in **Chapter** 2, ferrocene with higher degrees of methylation exhibits slower rates of electron transfer, because the methyl functionalities impose a significant amount of steric bulk. Additionally, the low oxidation potential of polymethylated ferrocenes (*eg.* octamethylferrocene) causes rapid mediator oxidation in aqueous solutions, thus making it thermodynamically unstable and practically difficult to prepare. Polychlorinated ferrocene contains similar problems with decreased electron transfer with enhanced steric bulk of the chlorine substituents. While the increased redox potential of polychlorinated ferrocene affords it better thermodynamic stability, the electrochemical stability of such compounds is reported to be very poor.

One alternative possibility for an anodic mediator is an aminated ferrocene substituent. Britton *et al.* previously reported on the anomalous electrochemical effects of aminoferrocene.[62] The substitution of one methyl group onto the cyclopentadiene (C_p) ring of ferrocene, lowers its redox potential by 0.075 V, whereas the substitution of one amine onto the C_p ring of ferrocene, lowers its redox potential by 0.370 V.[62] Therefore, the use of a 1-methyl-1'-aminoferrocene moiety could allow for a redox potential as low as -0.065 V without the steric bulk associated with highly methylated ferrocenes.

Another alternative is the use of organic mediators at both the anode and the cath-

ode. Compounds such as 2,2'-azinobis (3-ethylbenzothiazoline-6-sulfonate) (ABTS) and naphthoquinone have been recently been used as biocathode and bioanode mediators respectively.[1,46] These provide reasonably efficient electron transfer with low overpotentials, however fine-tuning the electrochemical properties of organic mediators can be very difficult. Additionally, the poor electrochemical stability of such compounds causes the lifetime of their associated biofuel cells to decrease to a timescale of a few hours rather than the several week lifetime of their organometallic counterparts.

Appropriate selection and modification of the redox mediator can significantly improve the overall cell potential. However, the most common factor limiting the maximum current density in biofuel cells is the low solubility and slow diffusion of O_2 in aqueous solutions. The mole fraction solubility of O_2 in water in is 2.3×10^4 at 25 °C, which is considerably lower than that of O_2 in benzene or hexane (8.1×10^4 and 12.3×10^4 respectively).[162–164] In the most extreme cases, the mole fraction of O_2 solubility can be as high as 24.2×10^4 in hexafluorobenzene and 53.4×10^4 in perfluorooctane.[164,165] A possible solution could be the incorporation of perfluorinated structures near the exterior of the cathodic film to enhance the permeability of dissolved gas bubbles across the solution-polymer interface. This area of research is largely unstudied in the context of enzymatic biofuel cells. In order to increase the current and power outputs of glucose/O_2 BFCs, it is essential to develop strategies for enhancing O_2 solubility and diffusion through aqueous solutions.

Finally, it is important that work be done to increase the lifetime of enzymatic biofuel cells. Electrode stability is not significantly discussed in the context of this work. However, it is a topic that must be addressed moving forward. Currently, the operational

lifetime of BFCs is on the timescale of several weeks. However, for the ultimate goal of utilizing BFCs as a means of *in vivo* power generation, the operational lifetime must be increased to several years. Recent results have indicated that the incorporation of dispersed carbon nanostructures may significantly improve the electrochemical lifetime of the enzymatic electrodes presented in this work. Additionally, the use of thermophilic enzymes has shown great promise in addressing the long term stability of BFCs. In conclusion, a combination of the strategies discussed here will be necessary for enzymatic biofuel cells to become a viable source of renewable energy.

Bibliography

[1] Palmore, G. T. R.; Kim, H.-H. *Journal of Electroanalytical Chemistry* **1999**, *464*, 110–117.

[2] Atanassov, P.; Apblett, C.; Banta, S.; Brozik, S.; Barton, S. C.; Cooney, M.; Liaw, B. Y.; Murkerjee, S.; Minteer, S. D. *The Electrochemical Society Interface* **2007**, *16*, 28–31.

[3] Bullen, R. A.; Arnot, T. C.; Lakeman, J. B.; Walsh, F. C. *Biosensors and Bioelectronics* **2006**, *21*, 2015–2045.

[4] Romero, E. *Powering Biomedical Devices*; Elsevier Inc.: Oxford, 2013.

[5] Heller, A. *The Journal of Physical Chemistry* **1992**, *96*, 3579–3587.

[6] Cracknell, J. A.; Vincent, K. A.; Armstrong, F. A. *Chemical Reviews* **2008**, *108*, 2439–2461.

[7] Smits, R. G.; Koper, G. J. M.; Mandel, M. *The Journal of Physical Chemistry* **1993**, *97*, 5745–5751.

[8] Meredith, M. T.; Kao, D.-Y.; Hickey, D.; Schmidtke, D. W.; Glatzhofer, D. T. *Journal of The Electrochemical Society* **2011**, *158*, B166–B174.

[9] Meredith, M. T.; Hickey, D. P.; Redemann, J. P.; Schmidtke, D. W.; Glatzhofer, D. T. *Electrochimica Acta* **2013**, *92*, 226–235.

[10] Solomon, E. I.; Sundaram, U. M.; Machonkin, T. E. *Chemical Reviews* **1996**, *96*, 2563–2606.

[11] Potter, M. C. *Proceedings of the Royal Society of London. Series B, Containing Papers of a Biological Character* **1911**, *84*, 260–276.

[12] Yahiro, A. T.; Lee, S. M.; Kimble, D. O. *Biochimica et Biophysica Acta (BBA) - Specialized Section on Biophysical Subjects* **1964**, *88*, 375–383.

[13] Wingard Jr, L. B.; Shaw, C. H.; Castner, J. F. *Enzyme and Microbial Technology* **1982**, *4*, 137–142.

[14] Du, Z.; Li, H.; Gu, T. *Biotechnology Advances* **2007**, *25*, 464–482.

[15] Logan, B. E.; Hamelers, B.; Rozendal, R.; Schrder, U.; Keller, J.; Freguia, S.; Aelterman, P.; Verstraete, W.; Rabaey, K. *Environmental Science and Technology* **2006**, *40*, 5181–5192.

[16] Logan, B. E.; Regan, J. M. *Environmental Science and Technology* **2006**, *40*, 5172–5180.

[17] Soukharev, V.; Mano, N.; Heller, A. *Journal of the American Chemical Society* **2004**, *126*, 8368–8369.

[18] Chen, T.; Barton, S. C.; Binyamin, G.; Gao, Z.; Zhang, Y.; Kim, H.-H.; Heller, A. *Journal of the American Chemical Society* **2001**, *123*, 8630–8631.

[19] Mano, N.; Fernandez, J. L.; Kim, Y.; Shin, W.; Bard, A. J.; Heller, A. *Journal of the American Chemical Society* **2003**, *125*, 15290–15291.

[20] Calabrese Barton, S.; Gallaway, J.; Atanassov, P. *Chemical Reviews* **2004**, *104*, 4867–4886.

[21] Habrioux, A.; Merle, G.; Servat, K.; Kokoh, K. B.; Innocent, C.; Cretin, M.; Tingry, S. *Journal of Electroanalytical Chemistry* **2008**, *622*, 97–102.

[22] Larminie, J.; Dicks, A. *Fuel Cell Systems Explained*, 2nd ed.; Wiley & Sons: New York, 2003.

[23] Willner, I.; Katz, E.; Patolsky, F.; F. Buckmann, A. *Journal of the Chemical Society, Perkin Transactions 2* **1998**, 1817–1822.

[24] Yan, Y.-M.; Yehezkeli, O.; Willner, I. *Chemistry A European Journal* **2007**, *13*, 10168–10175.

[25] Zhang, M.; Xu, S.; Minteer, S. D.; Baum, D. A. *Journal of the American Chemical Society* **2011**, *133*, 15890–15893.

[26] Tominaga, M.; Nomura, S.; Taniguchi, I. *Biosensors and Bioelectronics* **2009**, *24*, 1184–1188.

[27] Tsujimura, S.; Nishina, A.; Kamitaka, Y.; Kano, K. *Analytical Chemistry* **2009**, *81*, 9383–9387.

[28] Meredith, M. T.; Minson, M.; Hickey, D.; Artyushkova, K.; Glatzhofer, D. T.; Minteer, S. D. *ACS Catalysis* **2011**, *1*, 1683–1690.

[29] Ianniello, R. M.; Lindsay, T. J.; Yacynych, A. M. *Analytical Chemistry* **1982**, *54*, 1098–1101.

[30] Bogdanovskaya, V. A.; Tarasevich, M. R.; Hintsche, R.; Scheller, F. *Bioelectrochemistry and Bioenergetics* **1988**, *19*, 581–584.

[31] Falk, M.; Blum, Z.; Shleev, S. *Electrochimica Acta* **2012**, *82*, 191–202.

[32] Murata, K.; Suzuki, M.; Kajiya, K.; Nakamura, N.; Ohno, H. *Electrochemistry Communications* **2009**, *11*, 668–671.

[33] Deng, L.; Shang, L.; Wen, D.; Zhai, J.; Dong, S. *Biosensors and Bioelectronics* **2010**, *26*, 70–73.

[34] Xu, F. *Biochemistry* **1996**, *35*, 7608–7614.

[35] Minson, M.; Meredith, M. T.; Shrier, A.; Giroud, F.; Hickey, D.; Glatzhofer, D. T.; Minteer, S. D. *Journal of the Electrochemical Society* **2012**, *159*, G166–G170.

[36] Okuda, J.; Yamazaki, T.; Fukasawa, M.; Kakehi, N.; Sode, K. *Analytical Letters* **2007**, *40*, 431–440.

[37] Mano, N. *J Biotechnol* **2011**, *151*, 122–9, Using Smart Source Parsing Jan 10 doi: 10.1016/j.jbiotec.2010.10.077. Epub 2010 Oct 30.

[38] Milburn, C. C.; Lamble, H. J.; Theodossis, A.; Bull, S. D.; Hough, D. W.; Danson, M. J.; Taylor, G. L. *Journal of Biological Chemistry* **2006**, *281*, 14796–14804.

[39] Degani, Y.; Heller, A. *The Journal of Physical Chemistry* **1987**, *91*, 1285–1289.

[40] Heller, A. *Accounts of Chemical Research* **1990**, *23*, 128–134.

[41] Schuhmann, W.; Ohara, T. J.; Schmidt, H. L.; Heller, A. *Journal of the American Chemical Society* **1991**, *113*, 1394–1397.

[42] Dalton, E. F.; Surridge, N. A.; Jernigan, J. C.; Wilbourn, K. O.; Facci, J. S.; Murray, R. W. *Chemical Physics* **1990**, *141*, 143–157.

[43] Fei, J.; Song, H.-K.; Palmore, G. T. R. *Chemistry of Materials* **2007**, *19*, 1565–1570.

[44] Cardoso, F. P.; Aquino Neto, S.; Fenga, P. G.; Ciancaglini, P.; De andrade, A. R. *Electrochimica Acta* **2013**, *90*, 90–94.

[45] Tsujimura, S.; Tatsumi, H.; Ogawa, J.; Shimizu, S.; Kano, K.; Ikeda, T. *Journal of Electroanalytical Chemistry* **2001**, *496*, 69–75.

[46] Reuillard, B.; Le Goff, A.; Agnes, C.; Holzinger, M.; Zebda, A.; Gondran, C.; Elouarzaki, K.; Cosnier, S. *Physical Chemistry Chemical Physics* **2013**, *15*, 4892–4896.

[47] Zhu, Z.; Sun, F.; Zhang, X.; Zhang, Y. H. P. *Biosensors and Bioelectronics* **2012**, *36*, 110–115.

[48] Zhu, Z.; Kin Tam, T.; Sun, F.; You, C.; Percival Zhang, Y. H. *Nat Commun* **2014**, *5*, Supplementary information available for this article at http://www.nature.com/.

[49] Ohara, T. J.; Rajagopalan, R.; Heller, A. *Analytical Chemistry* **1993**, *65*, 3512–3517.

[50] Gallaway, J. W.; Calabrese Barton, S. A. *Journal of the American Chemical Society* **2008**, *130*, 8527–8536.

[51] Mao, F.; Mano, N.; Heller, A. *Journal of the American Chemical Society* **2003**, *125*, 4951–4957.

[52] Koide, S.; Yokoyama, K. *Journal of Electroanalytical Chemistry* **1999**, *468*, 193–201.

[53] Bunte, C.; Rhe, J. *Macromolecular Rapid Communications* **2009**, *30*, 1817–1822.

[54] Bunte, C.; Prucker, O.; Konig, T.; Ruhe, J. *Langmuir* **2009**, *26*, 6019–6027.

[55] Bunte, C.; Hussein, L.; Urban, G. A. *Journal of Power Sources* **2014**, *247*, 579–586.

[56] Kealy, T. J.; Pauson, P. L. *Nature* **1951**, *168*, 1039–1040, 10.1038/1681039b0.

[57] Liaudet, E.; Battaglini, F.; Calvo, E. J. *Journal of Electroanalytical Chemistry and Interfacial Electrochemistry* **1990**, *293*, 55–68.

[58] Perseghini, M.; Togni, A. In *Science of Synthesis*; Houben-Weyl,, Ed.; Thieme Medical Publishers, Vol. 1; pp 889–929.

[59] Merchant, S. A.; Meredith, M. T.; Tran, T. O.; Brunski, D. B.; Johnson, M. B.; Glatzhofer, D. T.; Schmidtke, D. W. *The Journal of Physical Chemistry C* **2010**, *114*, 11627–11634.

[60] Merchant, S. A.; Glatzhofer, D. T.; Schmidtke, D. W. *Langmuir* **2007**, *23*, 11295–11302.

[61] Tauhardt, L.; Kempe, K.; Knop, K.; Altunta, E.; Jger, M.; Schubert, S.; Fischer, D.; Schubert, U. S. *Macromolecular Chemistry and Physics* **2011**, *212*, 1918–1924.

[62] Britton, W. E.; Kashyap, R.; El-Hashash, M.; El-Kady, M.; Herberhold, M. *Organometallics* **1986**, *5*, 1029–1031.

[63] N.P.R.A. Silva, M. E.; Pombeiro, A. J. L.; Frasto da Silva, J. J. R.; Herrmann, R.; Deus, N.; E.Bozak, R. *Journal of Organometallic Chemistry* **1994**, *480*, 81–90.

[64] Emlia, M.; Silva, N. P. R. A.; Pombeiro, A. J. L.; da Silva, J. J. R. F.; Herrmann, R.; Deus, N.; Castilho, T. J.; Silva, M. F. C. G. *Journal of Organometallic Chemistry* **1991**, *421*, 75–90.

[65] Jego-Evanno, P.; Hurvois, J. P.; Moinet, C. *Journal of Electroanalytical Chemistry* **2001**, *507*, 270–274.

[66] Kazarinov, V. E.; Levi, M. D.; Skundin, A. M.; Vorotyntsev, M. A. *Journal of Electroanalytical Chemistry and Interfacial Electrochemistry* **1989**, *271*, 193–211.

[67] Hickey, D. P.; Giroud, F.; Schmidtke, D. W.; Glatzhofer, D. T.; Minteer, S. D. *ACS Catalysis* **2013**, *3*, 2729–2737.

[68] Davis, G.; Hill, H. A. O.; Aston, W. J.; John Higgins, I.; Turner, A. P. F. *Enzyme and Microbial Technology* **1983**, *5*, 383–388.

[69] Persson, B.; Gorton, L.; Johansson, G.; Torstensson, A. *Enzyme and Microbial Technology* **1985**, *7*, 549–552.

[70] Barton, S. C.; Kim, H.-H.; Binyamin, G.; Zhang, Y.; Heller, A. *The Journal of Physical Chemistry B* **2001**, *105*, 11917–11921.

[71] Heller, A.; Feldman, B. *Chemical Reviews* **2008**, *108*, 2482–2505.

[72] Heller, A. *Current Opinion in Chemical Biology* **2006**, *10*, 664–672.

[73] Ballarin, B.; Cassani, M. C.; Mazzoni, R.; Scavetta, E.; Tonelli, D. *Biosensors and Bioelectronics* **2007**, *22*, 1317–1322.

[74] Cass, A. E. G.; Davis, G.; Francis, G. D.; Hill, H. A. O.; Aston, W. J.; Higgins, I. J.; Plotkin, E. V.; Scott, L. D. L.; Turner, A. P. F. *Analytical Chemistry* **1984**, *56*, 667–671.

[75] Sui, X.; Feng, X.; Hempenius, M. A.; Vancso, G. J. *Journal of Materials Chemistry B* **2013**, *1*, 1658–1672.

[76] Cinquin, P.; Gondran, C.; Giroud, F.; Mazabrard, S.; Pellissier, A.; Boucher, F.; Alcaraz, J.-P.; Gorgy, K.; Lenouvel, F.; Math, S.; Porcu, P.; Cosnier, S. *PLoS ONE* **2010**, *5*, e10476.

[77] Degani, Y.; Heller, A. *Journal of the American Chemical Society* **1989**, *111*, 2357–2358.

[78] Lau, C.; Adkins, E. R.; Ramasamy, R. P.; Luckarift, H. R.; Johnson, G. R.; Atanassov, P. *Advanced Energy Materials* **2012**, *2*, 162–168.

[79] Stepnicka, P. *Ferrocenes*; John Wiley & Sons, Ltd, 2008; pp 177–204.

[80] Liu, A.; Anzai, J.-i. *Langmuir* **2003**, *19*, 4043–4046.

[81] Hradsky, A.; Bildstein, B.; Schuler, N.; Schottenberger, H.; Jaitner, P.; Ongania, K.-H.; Wurst, K.; Launay, J.-P. *Organometallics* **1997**, *16*, 392–402.

[82] Zou, C.; Wrighton, M. S. *Journal of the American Chemical Society* **1990**, *112*, 7578–7584.

[83] Bildstein, B.; Hradsky, A.; Kopacka, H.; Malleier, R.; Ongania, K.-H. *Journal of Organometallic Chemistry* **1997**, *540*, 127–145.

[84] Bashkin, J. K.; Kinlen, P. J. *Inorganic Chemistry* **1990**, *29*, 4507–4509.

[85] Marcus, R. A. *The Journal of Chemical Physics* **1956**, *24*, 966–978.

[86] Andrieux, C. P.; Savant, J. M. *Journal of Electroanalytical Chemistry and Interfacial Electrochemistry* **1980**, *111*, 377–381.

[87] Marcus, R. A.; Sutin, N. *Biochimica et Biophysica Acta (BBA) - Reviews on Bioenergetics* **1985**, *811*, 265–322.

[88] Moser, C. C.; Keske, J. M.; Warncke, K.; Farid, R. S.; Dutton, P. L. *Nature* **1992**, *355*, 796–802, 10.1038/355796a0.

[89] Crofts, A. R.; Rose, S. *Biochimica et Biophysica Acta (BBA) - Bioenergetics* **2007**, *1767*, 1228–1232.

[90] Voityuk, A. A. *Physical Chemistry Chemical Physics* **2012**, *14*, 13789–13793.

[91] Lousada, C. M.; Pinto, S. S.; Canongia Lopes, J. N.; Minas da Piedade, M. F.; Diogo, H. P.; Minas da Piedade, M. E. *The Journal of Physical Chemistry A* **2008**, *112*, 2977–2987.

[92] Struchkov, Y. T.; Andrianov, V. G.; Sal'nikova, T. N.; Lyatifov, I. R.; Materikova, R. B. *Journal of Organometallic Chemistry* **1978**, *145*, 213–223.

[93] Rose, S.; Crofts, A. Electron transfer rate calculation. 2012.

[94] Mtay, E.; Duclos, M. C.; Pellet-Rostaing, S.; Lemaire, M.; Schulz, J.; Kannappan, R.; Bucher, C.; Saint-Aman, E.; Chaix, C. *European Journal of Organic Chemistry* **2008**, *2008*, 4304–4312.

[95] Aoki, A.; Heller, A. *The Journal of Physical Chemistry* **1993**, *97*, 11014–11019.

[96] Aoki, A.; Rajagopalan, R.; Heller, A. *The Journal of Physical Chemistry* **1995**, *99*, 5102–5110.

[97] Franks, F. *Water: A Comprehensive Treatise*; Aqueous Solutions of Simple Electrolytes; Plenum Press: New York City, 1973; Vol. 3.

[98] Marcus, Y. *Chemical Reviews* **1988**, *88*, 1475–1498.

[99] Benito, A.; Martinez-Manez, R.; Soto, J.; Tendero, M. J. L. *Journal of the Chemical Society, Faraday Transactions* **1997**, *93*, 2175–2180.

[100] Gregg, B. A.; Heller, A. *Analytical Chemistry* **1990**, *62*, 258–263.

[101] Fritsch-Faules, I.; Faulkner, L. R. *Journal of Electroanalytical Chemistry and Interfacial Electrochemistry* **1989**, *263*, 237–255.

[102] Lyons, M. E. G.; Fay, H. G.; Vos, J. G.; Kelly, A. J. *Journal of Electroanalytical Chemistry and Interfacial Electrochemistry* **1988**, *250*, 207–211.

[103] Aoki, K.; Tokuda, K.; Matsuda, H. *Journal of Electroanalytical Chemistry and Interfacial Electrochemistry* **1983**, *146*, 417–424.

[104] Aoki, K.; Tokuda, K.; Matsuda, H. *Journal of Electroanalytical Chemistry and Interfacial Electrochemistry* **1984**, *160*, 33–45.

[105] Bourdillon, C.; Demaille, C.; Moiroux, J.; Saveant, J. M. *Journal of the American Chemical Society* **1993**, *115*, 1–10.

[106] Carta, R.; Palmas, S.; Polcaro, A. M.; Tola, G. *Journal of Applied Electrochemistry* **1991**, *21*, 793–798.

[107] Ayranci, E.; Conway, B. E. *Journal of Applied Electrochemistry* **2001**, *31*, 257–266.

[108] Geneste, F.; Cadoret, M.; Moinet, C.; Jezequel, G. *New Journal of Chemistry* **2002**, *26*, 1261–1266.

[109] Clauwaert, P.; van der Ha, D.; Boon, N.; Verbeken, K.; Verhaege, M.; Rabaey, K.; Verstraete, W. *Environmental Science & Technology* **2007**, *41*, 7564–7569.

[110] Zhang, Y.; Sun, J.; Hu, Y.; Li, S.; Xu, Q. *International Journal of Hydrogen Energy* **2012**, *37*, 16935–16942.

[111] Gonzalez-Garcia, J.; Bonete, P.; Exposito, E.; Montiel, V.; Aldaz, A.; Torregrosa-Macia, R. *Journal of Materials Chemistry* **1999**, *9*, 419–426.

[112] Mano, N.; Kim, H.-H.; Heller, A. *The Journal of Physical Chemistry B* **2002**, *106*, 8842–8848.

[113] Binyamin, G.; Heller, A. *Journal of The Electrochemical Society* **1999**, *146*, 2965–2967.

[114] Palmore, G. T. R.; Bertschy, H.; Bergens, S. H.; Whitesides, G. M. *Journal of Electroanalytical Chemistry* **1998**, *443*, 155–161.

[115] Rashidi, R.; Dincer, I.; Naterer, G. F.; Berg, P. *Journal of Power Sources* **2009**, *187*, 509–516.

[116] Gibson, Q. H.; Swoboda, B. E. P.; Massey, V. *Journal of Biological Chemistry* **1964**, *239*, 3927 – 3934.

[117] Sokic-Lazic, D.; Minteer, S. D. *Electrochemical and Solid-State Letters* **2009**, *12*, F26–F28.

[118] Moehlenbrock, M. J.; Toby, T. K.; Pelster, L. N.; Minteer, S. D. *ChemCatChem* **2011**, *3*, 561–570.

[119] de Oliveira, R. F.; de Moraes, M. L.; Oliveira, O. N.; Ferreira, M. *The Journal of Physical Chemistry C* **2011**, *115*, 19136–19140.

[120] Arechederra, R. L.; Treu, B. L.; Minteer, S. D. *Journal of Power Sources* **2007**, *173*, 156–161.

[121] Arechederra, R. L.; Minteer, S. D. *Fuel Cells* **2009**, *9*, 63–69.

[122] Kar, P.; Wen, H.; Li, H.; Minteer, S. D.; Barton, S. C. *Journal of The Electrochemical Society* **2011**, *158*, B580–B586.

[123] Akers, N. L.; Moore, C. M.; Minteer, S. D. *Electrochimica Acta* **2005**, *50*, 2521–2525.

[124] Addo, P.; Arechederra, R.; Minteer, S. *Electroanalysis* **2010**, *22*, 807–812.

[125] Shao, M.; Nadeem Zafar, M.; Sygmund, C.; Guschin, D. A.; Ludwig, R.; Peterbauer, C. K.; Schuhmann, W.; Gorton, L. *Biosensors and Bioelectronics* **2013**, *40*, 308–314.

[126] Xu, S.; Minteer, S. D. *ACS Catalysis* **2011**, *2*, 91–94.

[127] Majer-Baranyi, K.; Adnyi, N.; Vradi, M. *European Food Research and Technology* **2008**, *228*, 139–144.

[128] Soldatkin, O. O.; Kucherenko, I. S.; Pyeshkova, V. M.; Kukla, A. L.; Jaffrezic-Renault, N.; El'skaya, A. V.; Dzyadevych, S. V.; Soldatkin, A. P. *Bioelectrochemistry* **2012**, *83*, 25–30.

[129] Moehlenbrock, M. J.; Meredith, M. T.; Minteer, S. D. *MRS Communications* **2011**, *1*, 37–40.

[130] Merchant, S. A.; Tran, T. O.; Meredith, M. T.; Cline, T. C.; Glatzhofer, D. T.; Schmidtke, D. W. *Langmuir* **2009**, *25*, 7736–7742.

[131] Johnson, K. A.; Goody, R. S. *Biochemistry* **2011**, *50*, 8264–8269.

[132] Kurganov, B. I.; Lobanov, A. V.; Borisov, I. A.; Reshetilov, A. N. *Analytica Chimica Acta* **2001**, *427*, 11–19.

[133] Kern, G.; Schlke, N.; Jaenicke, R.; Schmid, F. X. *Protein Science* **1992**, *1*, 120–131.

[134] Cui, Q.; Karplus, M. *Protein Science* **2008**, *17*, 1295–1307.

[135] Bergmeyer, H.; Bergmeyer, J.; Grassl, M. *Methods of enzymatic analysis*; Verlag Chemie, 1986.

[136] Tk, J.; Votiar, I.; turdk, E.; Gemeiner, P.; Mastihuba, V.; Annus, J. *Analytica Chimica Acta* **2001**, *439*, 39–46.

[137] Bohmhammel, K.; Httl, R.; Pritzkat, K.; Wolf, G. *Thermochimica Acta* **1993**, *217*, 9–18.

[138] Vrbel, P.; Polakovi, M.; tefuca, V.; Ble, V. *Enzyme and Microbial Technology* **1997**, *20*, 348–354.

[139] Hui, H.; Huang, D.; McArthur, D.; Nissen, N.; Boros, L. G.; Heaney, A. P. *Pancreas* **2009**, *38*, 706–12, Hui, Hongxiang Huang, Danshan McArthur, David Nissen, Nicholas Boros, Laszlo G Heaney, Anthony P R01 CA123273-01A2/CA/NCI NIH HHS/United States R01 CA12327301/CA/NCI NIH HHS/United States Comparative Study Evaluation Studies Research Support, N.I.H., Extramural Research Support, Non-U.S. Gov't United States Pancreas Pancreas. 2009 Aug;38(6):706-12. doi: 10.1097/MPA.0b013e3181a7c6e5.

[140] Courjean, O.; Mano, N. *Journal of Biotechnology* **2011**, *151*, 122–129.

[141] Sanjay, G.; Sugunan, S. *Food Chemistry* **2006**, *94*, 573–579.

[142] Anthony, G.-E.; Chenghong, L.; Ray, H. B. *Nanotechnology* **2002**, *13*, 559.

[143] Katz, E.; Willner, I.; Kotlyar, A. B. *Journal of Electroanalytical Chemistry* **1999**, *479*, 64–68.

[144] Kamitaka, Y.; Tsujimura, S.; Setoyama, N.; Kajino, T.; Kano, K. *Physical Chemistry Chemical Physics* **2007**, *9*, 1793–1801.

[145] Shleev, S.; Tkac, J.; Christenson, A.; Ruzgas, T.; Yaropolov, A. I.; Whittaker, J. W.; Gorton, L. *Biosensors and Bioelectronics* **2005**, *20*, 2517–2554.

[146] Barton, S. C.; Pickard, M.; Vazquez-Duhalt, R.; Heller, A. *Biosensors and Bioelectronics* **2002**, *17*, 1071–1074.

[147] Rajagopalan, R.; Aoki, A.; Heller, A. *The Journal of Physical Chemistry* **1996**, *100*, 3719–3727.

[148] Nesmejanow, A. N.; Ssasonowa, W. A.; Drosd, V. N. *Chemische Berichte* **1960**, *93*, 2717–2729.

[149] Atkinson, A.; Jack, G. W. *Biochimica et Biophysica Acta (BBA) - Nucleic Acids and Protein Synthesis* **1973**, *308*, 41–52.

[150] Kichler, A.; Leborgne, C.; Coeytaux, E.; Danos, O. *The Journal of Gene Medicine* **2001**, *3*, 135–144.

[151] Dai, J.; Zou, S.; Pei, Y.; Cheng, D.; Ai, H.; Shuai, X. *Biomaterials* **2011**, *32*, 1694–1705.

[152] Heine, A.; Stura, E. A.; Yli-Kauhaluoma, J. T.; Gao, C.; Deng, Q.; Beno, B. R.; Houk, K. N.; Janda, K. D.; Wilson, I. A. *Science* **1998**, *279*, 1934–1940.

[153] Nakashima, S.; Ichikawa, N.; Komatsu, H.; Yamada, K.; Okuda, T. *Polyhedron* **2000**, *19*, 205–210.

[154] Salmon, A. J.; Williams, M. L.; Hofmann, A.; Poulsen, S.-A. *Chemical Communications* **2012**, *48*, 2328–2330.

[155] Taylor, C.; Kenausis, G.; Katakis, I.; Heller, A. *Journal of Electroanalytical Chemistry* **1995**, *396*, 511–515.

[156] Calabrese Barton, S. *Electrochimica Acta* **2005**, *50*, 2145–2153.

[157] Bard, A. J.; Faulkner, L. R. *Electrochemical Methods - Fundamentals and Applications*; John Wiley & Sons: New York, 1980.

[158] Scodeller, P.; Carballo, R.; Szamocki, R.; Levin, L.; Forchiassin, F.; Calvo, E. J. *Journal of the American Chemical Society* **2010**, *132*, 11132–11140.

[159] Davis, J. J.; Coles, R. J.; Allen, H.; Hill, O. *Journal of Electroanalytical Chemistry* **1997**, *440*, 279–282.

[160] Campbell, J. K.; Sun, L.; Crooks, R. M. *Journal of the American Chemical Society* **1999**, *121*, 3779–3780.

[161] Delanoy, G.; Li, Q.; Yu, J. *International Journal of Biological Macromolecules* **2005**, *35*, 89–95.

[162] Wilhelm, E.; Battino, R. *The Journal of Chemical Thermodynamics* **1973**, *5*, 117–120.

[163] Benson, B.; Krause, J., Daniel; Peterson, M. *Journal of Solution Chemistry* **1979**, *8*, 655–690.

[164] Battino, R.; Rettich, T. R.; Tominaga, T. *Journal of Physical and Chemical Reference Data* **1983**, *12*, 163–178.

[165] Wesseler, E. P.; Iltis, R.; Clark Jr, L. C. *Journal of Fluorine Chemistry* **1977**, *9*, 137–146.

Appendix A

NMR Data

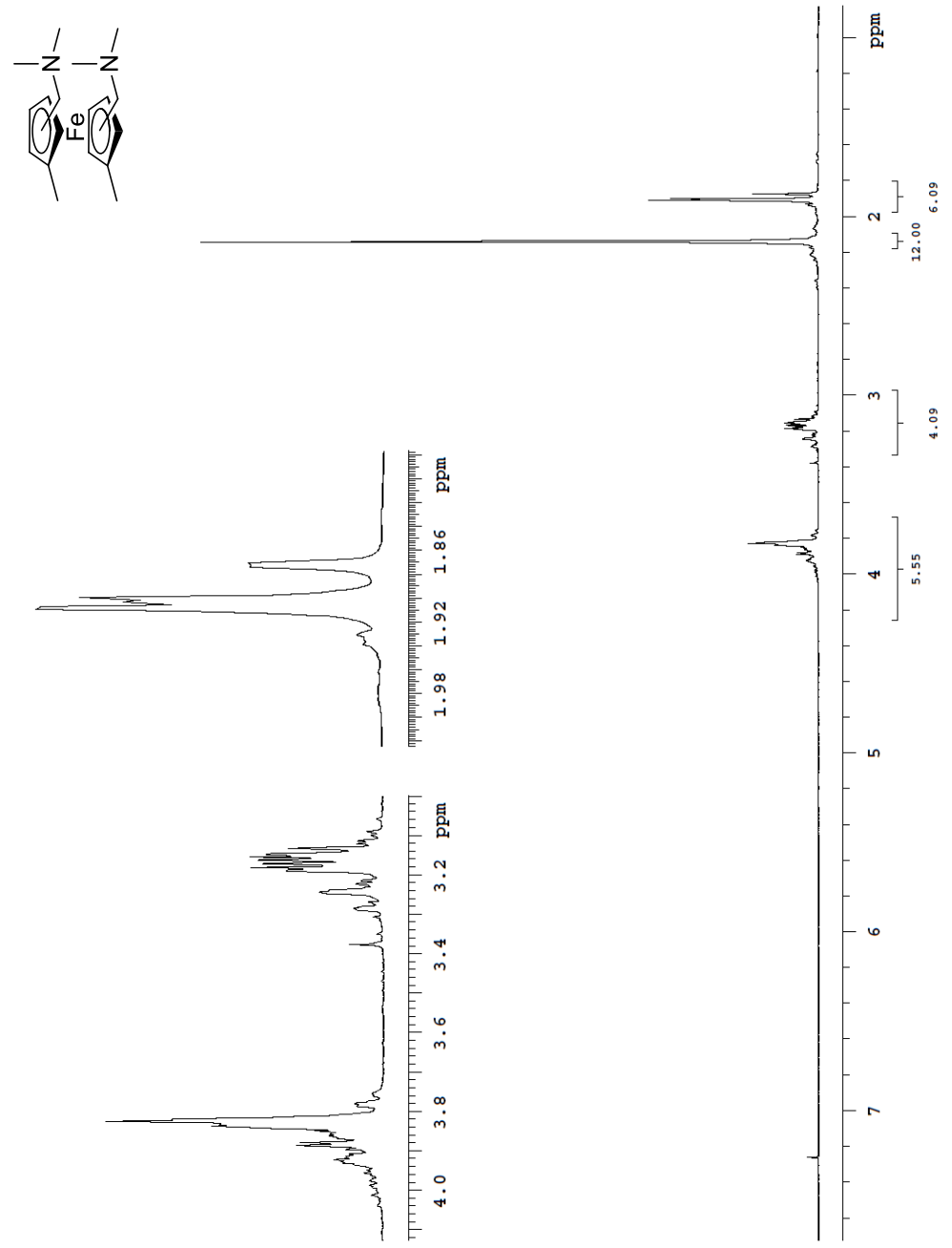

Figure **A.1**: 1,1'-*bis*-(Dimethylaminomethyl)-Dimethylferrocenes ($CDCl_3$)

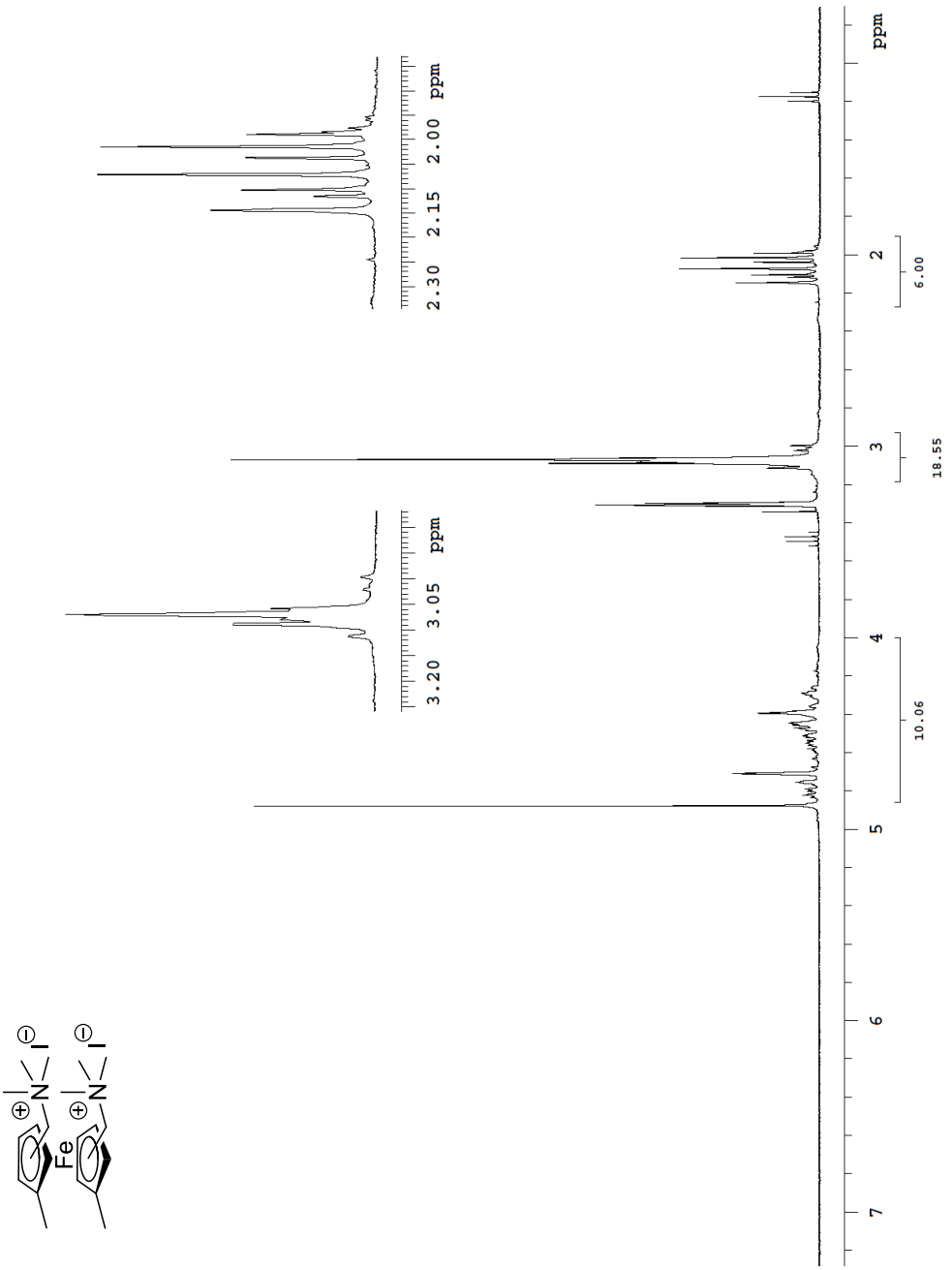

Figure **A.2**: 1,1'-*bis*-(Dimethylaminomethyl)-Dimethylferrocene Dimethiodide (CD_3OD)

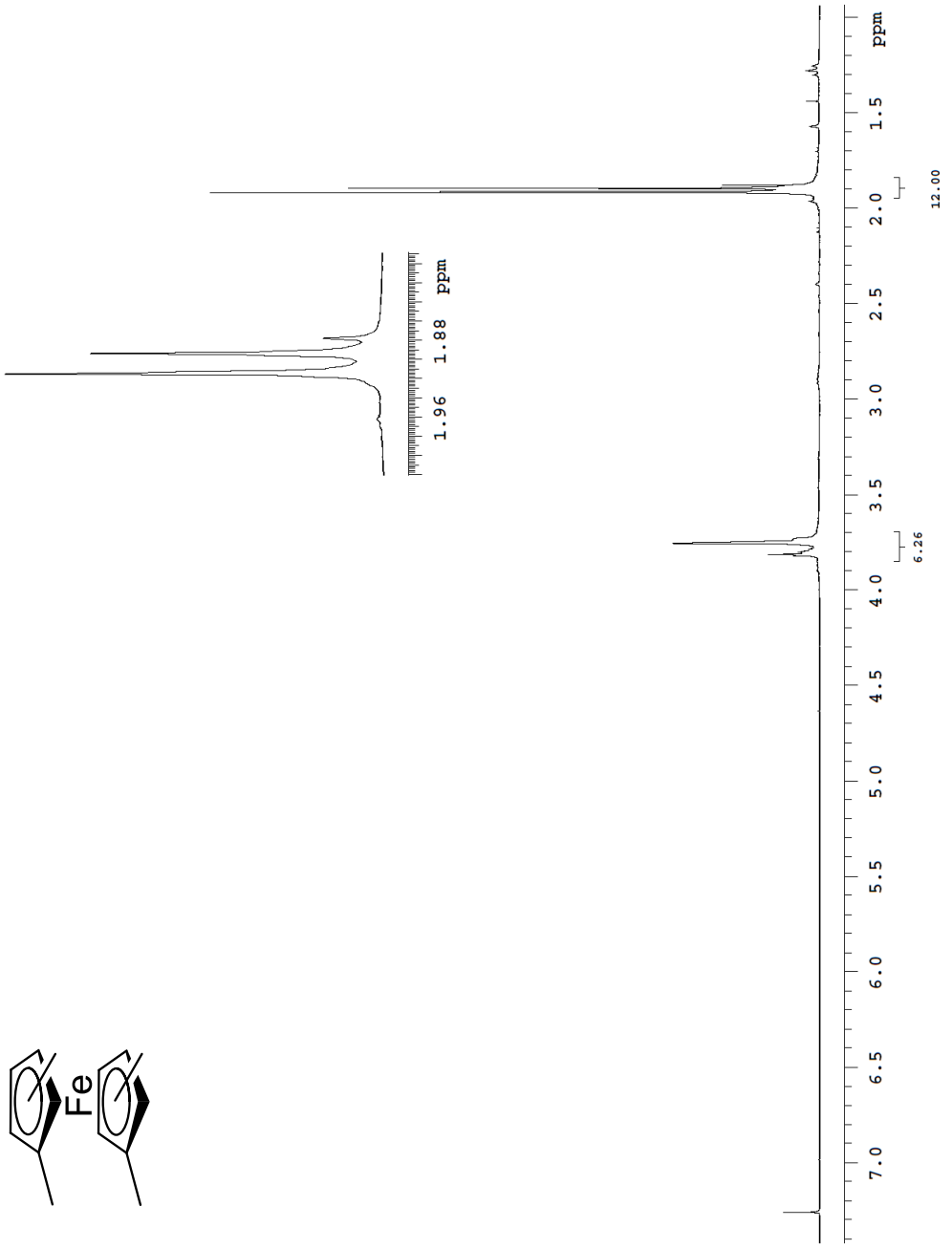

Figure **A.3**: Tetramethylferrocenes ($CDCl_3$)

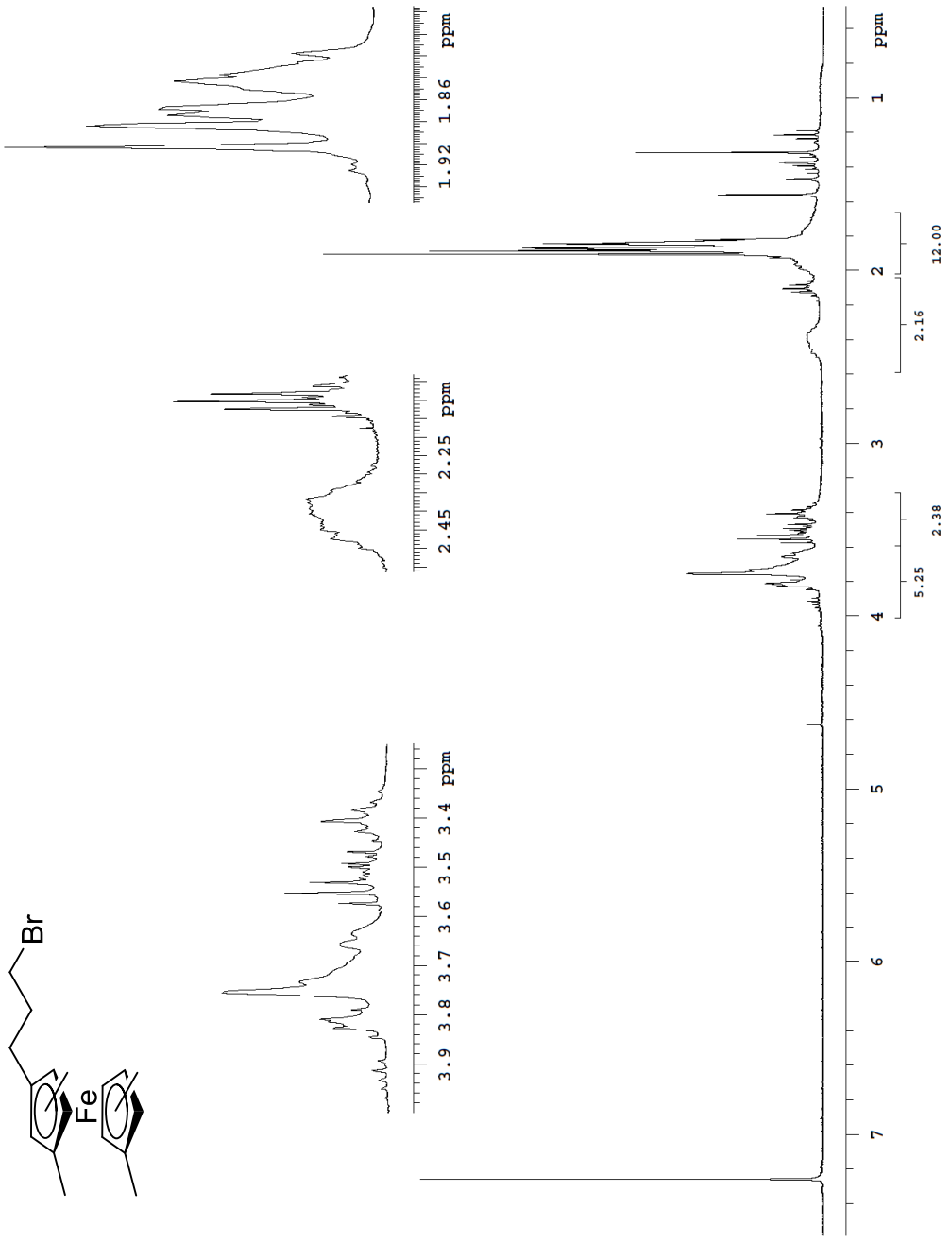

Figure **A.4**: 3-(Bromopropyl)tetramethylferrocenes ($CDCl_3$)

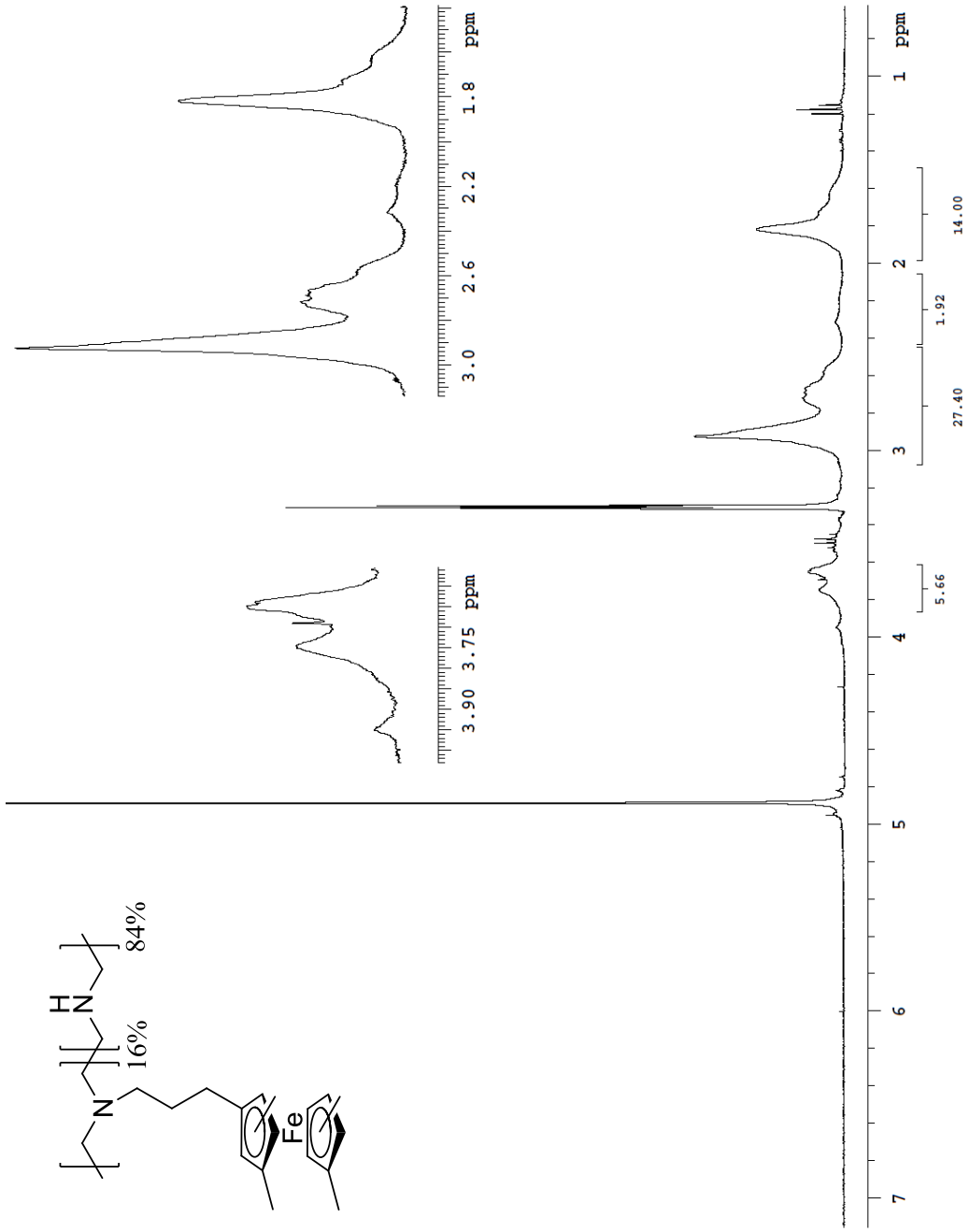

Figure **A.5**: $FcMe_4$-C_3-LPEI (CD_3OD)

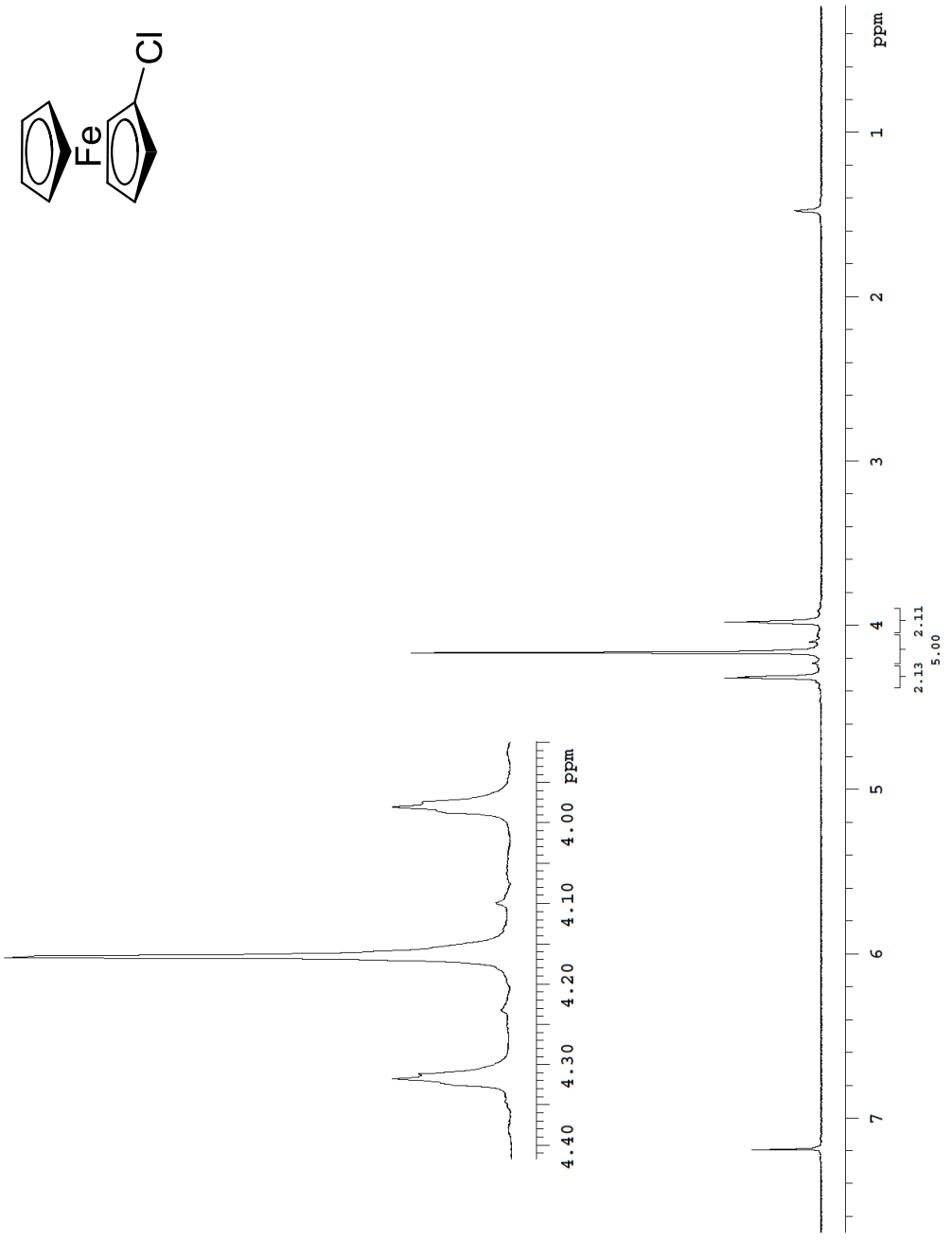

Figure **A.6**: Chloroferrocene ($CDCl_3$)

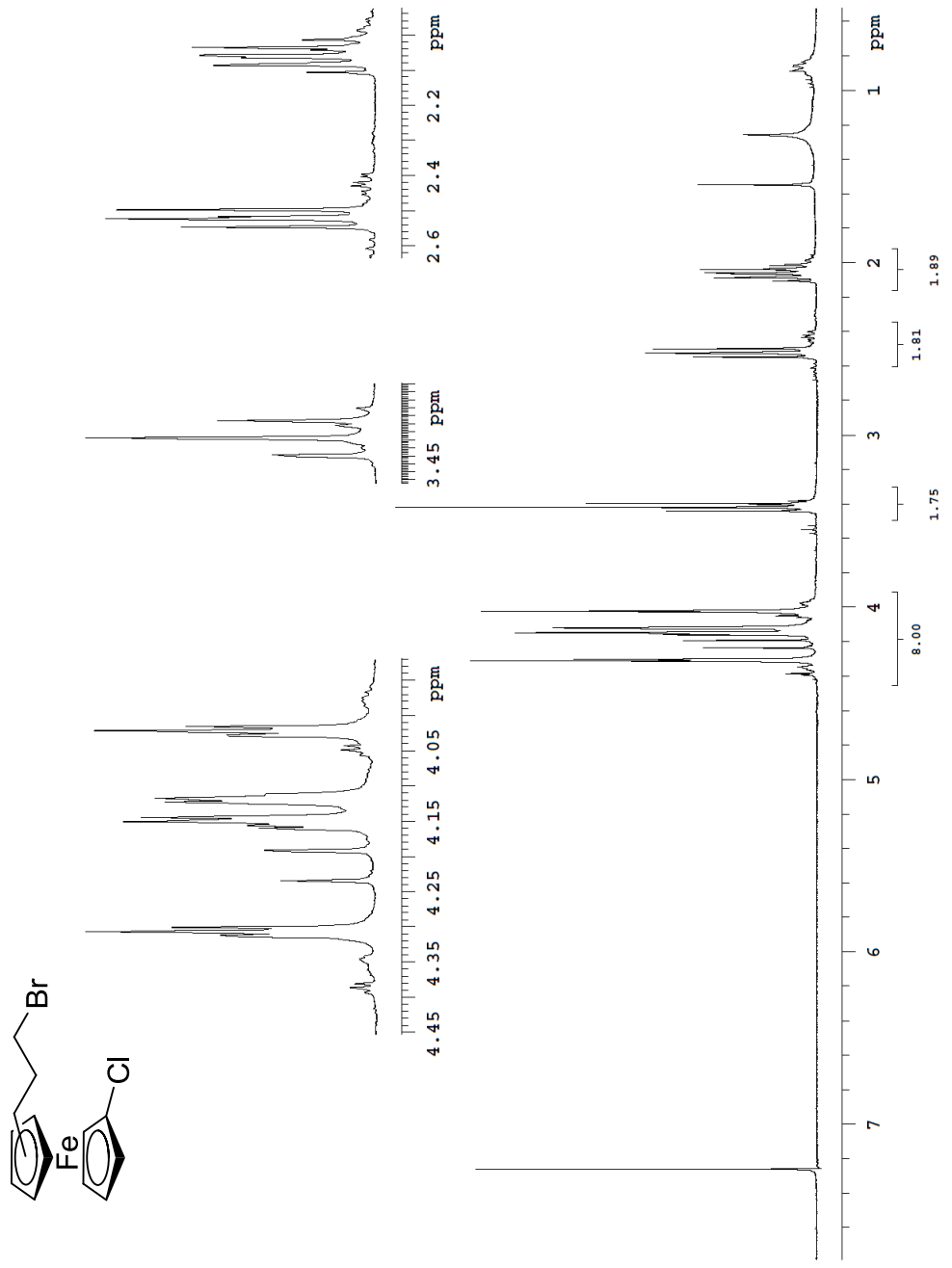

Figure **A.7**: (3-Bromopropyl)chloroferrocene ($CDCl_3$)

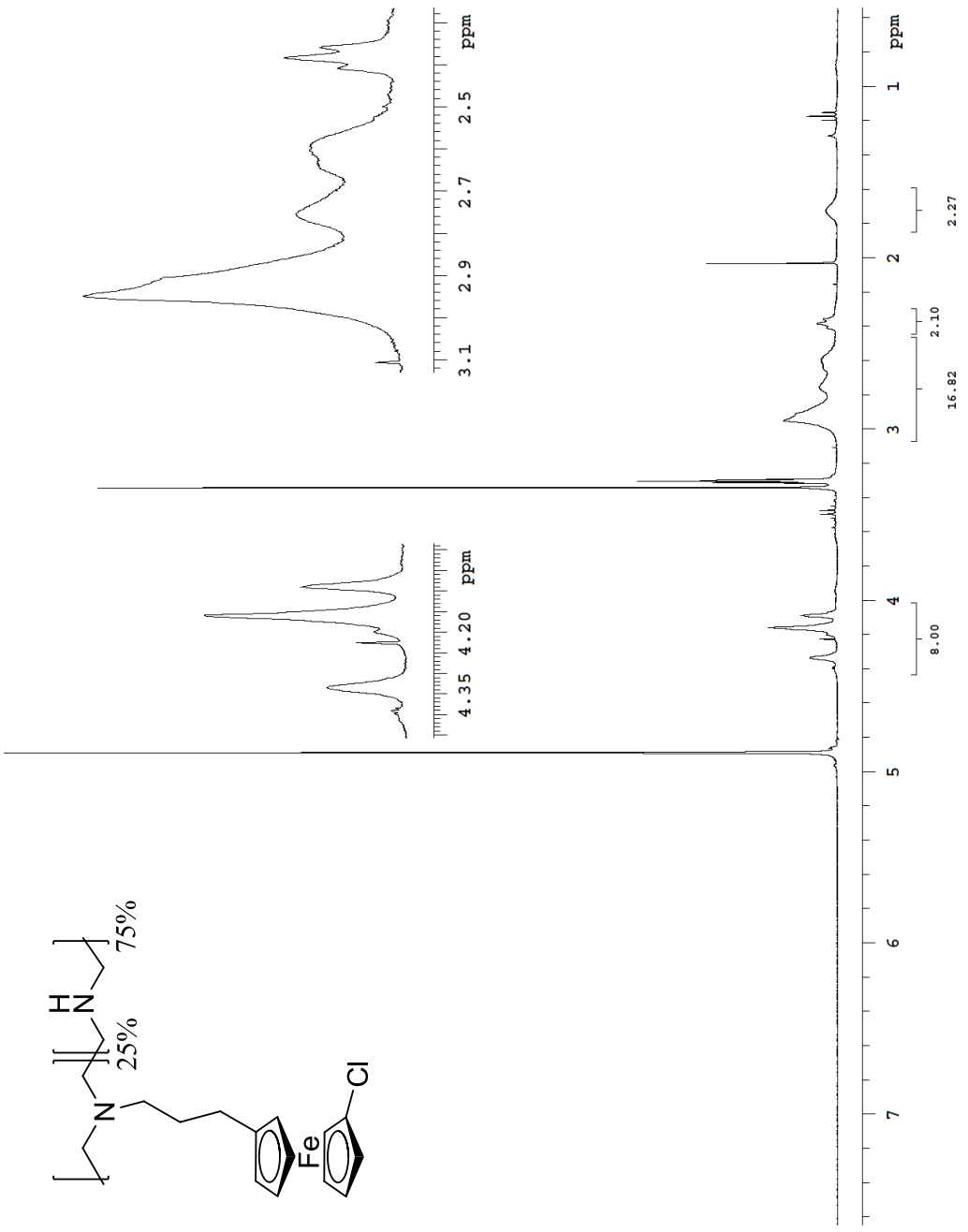

Figure **A.8**: FcCl-C_3-LPEI (CD_3OD)